Dynamics and stress field of the Eurasian plate: a combined lithosphere-mantle approach

Karin Warners-Ruckstuhl

UTRECHT STUDIES IN EARTH SCIENCES
No. 011

Members of the dissertation committee:

Prof. dr. S. A. P. L. Cloetingh
Department of Earth Sciences, Universiteit Utrecht
Utrecht, The Netherlands

Prof. dr L. Fleitout
Laboratoire de Géologie, Ecole normale supérieure
Paris, France

Prof. dr. L. Flesh
Department of Earth and Atmospheric Sciences, Purdue University
West Lafayette, USA

Prof. dr. G. A. Houseman
School of Earth and Environment, University of Leeds
Leeds, UK

Prof. dr. W. Spakman
Department of Earth Sciences, Universiteit Utrecht
Utrecht, The Netherlands

The research in this thesis was carried out at:

Tectonophysics group
Department of Earth Sciences
Faculty of Geosciences
Universiteit Utrecht
Utrecht, The Netherlands

ISBN: 978-90-6266-292-0

Cover illustration: World seismicity map centred over Eurasia indicating plate tectonic boundaries.

Dynamics and stress field of the Eurasian plate: a combined lithosphere-mantle approach

Dynamica en spanningsveld van de Euraziatische plaat: een gecombineerde lithosfeer-mantel aanpak
(met een samenvatting in het Nederlands)

Proefschrift

ter verkrijging van de graad van doctor aan de Universiteit Utrecht op gezag van de rector magnificus, prof.dr. G.J. van der Zwaan, ingevolge het besluit van het college voor promoties in het openbaar te verdedigen op vrijdag 24 februari 2012 des middags te 2.30 uur

door

Karin Nathalie Ruckstuhl

geboren op 2 november 1980
te Baden, Zwitserland

Promotor:	Prof. dr. M.J.R. Wortel
Co-promotor:	Dr. R. Govers

The research described in this thesis was financially supported by the Nederlands Organisation for Scientific Research (NWO).

For my father
who aroused my curiosity for the world

and my mother
who always encourages me

Contents

Chapter 1

Introduction

1.1 Scope of the thesis

The theory of plate tectonics states that the earth's outermost layer, the lithosphere, is fragmented into large more or less rigid plates that are moving atop hotter and weaker mantle material, the asthenosphere. Oceanic lithosphere is continuously renewed, being formed at mid-oceanic ridges and subducted at ocean trenches. Plate tectonics provides a general framework for many observed geological and geophysical processes on the earth's surface like continental drift, mountain building, seismicity and volcanism. Although it is a highly successful model, it is a kinematic parameterization which requires an explanation of the forces driving plate motion. This explanation is found deeper in the earth. A combination of secular cooling of the earth's hot interior and heat produced by radioactive decay in mantle rocks drives thermal convection in the earth's gravitational field due to thermal expansion and contraction. Material at the top of the mantle is cooled and becomes denser and gravitationally unstable. As a result it will ultimately start to sink. At the base of the mantle, the material will heat up, become lighter and start to ascend. The top of the mantle consists of the cold thermal boundary layer of the convecting system that, together with the overlying crust, forms the lithosphere.

The relation between plate tectonics and mantle convection has been recognized since the onset of the plate tectonics concept in the 1960's (see overview in Schubert et al. (2001)). It has thus long been realized that the lithosphere and underlying mantle are intrinsically coupled parts of the dynamic earth. The nature of the coupling between the two parts, however, has remained a subject of debate. Early studies on plate dynamics assumed that tectonic plates are mainly driven by the cooling and sinking of oceanic lithosphere. In that case, plates drive themselves and stir the underlying mantle as they go. Forces at their base result from passive resistance of the underlying mantle against plate motion (Forsyth and Uyeda, 1975; Harper, 1975; Richardson et al., 1979). More recently, studies focusing on mantle flow have demonstrated that mantle convection induced by density anomalies throughout the mantle can drive plates from below with active forward tractions (Ricard and Vigny, 1989; Lithgow-Bertelloni and Richards, 1998; Becker and O'Connell, 2001). How the actual lithosphere-mantle interaction results from a combination of the above two contributions is still debated today

and is intrinsically linked to the issue of plate driving forces (Becker and Faccenna, 2009).

A complete understanding of the forces that drive tectonic plates ideally arises from a coupled and self-consistent model of both plate motion and mantle convection. The rheological complexity of the system, however, has thus far prohibited such an integral approach. Studies focusing on plate driving forces therefore generally adopt either a lithosphere-based or a mantle-convection-based perspective. Both approaches have advantages and disadvantages. Lithosphere-based studies quantify lithospheric gravitational forces (like ridge push and slab pull, see section 1.2) using physical models. Forces due to plate interaction are modeled explicitly and constrained on the basis of mechanical equilibrium of tectonic plates either on a global (Forsyth and Uyeda, 1975; Chapple and Tullis, 1977; Hager and O'Connell, 1981) or single plate scale (Wortel et al., 1991; Meijer and Wortel, 1992; Govers and Meijer, 2001; Liu and Bird, 2002; Copley et al., 2010). The representation of the lithosphere-mantle interaction is based on the assumption of the lithosphere moving over a stagnant mantle and is the main weak point of this approach. Mantle flow based studies include gravitational forces in- and outside the lithosphere and account for tractions at the base of the lithosphere resulting from an actively convecting mantle. They solve for viscous plate coupling between the lithosphere and the underlying mantle by finding plate velocities that minimize the net-torque on the plates (Ricard and Vigny, 1989; Lithgow-Bertelloni and Richards, 1998; Zhong, 2001). Forces due to plate interaction are a weak point in this approach. They are often neglected or are controlled by rheological definitions of plate boundaries which are ill-constrained (i.e. Iaffaldano and Bunge (2009)). Furthermore, gravitational forces from subducting slabs are implemented as suction forces and act symmetrically on both the subducting and the overriding plate, neglecting stress guiding through the slab (review article by Becker and Faccenna (2009)).

In this thesis I aim to analyze the dynamics of tectonic plates focusing on both the lithosphere and the underlying mantle. To this end, I merge the strong points of the two classical modeling approaches into a new, combined approach. This approach incorporates tractions from convective mantle flow modeling into a detailed analysis of the forces acting on a single tectonic plate. Combination of lithospheric and mantle modeling has thus far only been performed at a global scale (Becker and O'Connell, 2001; Conrad and Lithgow-Bertelloni, 2002; Iaffaldano and Bunge, 2009). Edge forces could not be resolved on that scale because of strong trade-offs between the different edge force types (Becker and O'Connell, 2001). By focusing on a single plate my analysis allows for a more detailed resolution of edge forces.

The combined modeling approach presented in this thesis may be applied to all tec-

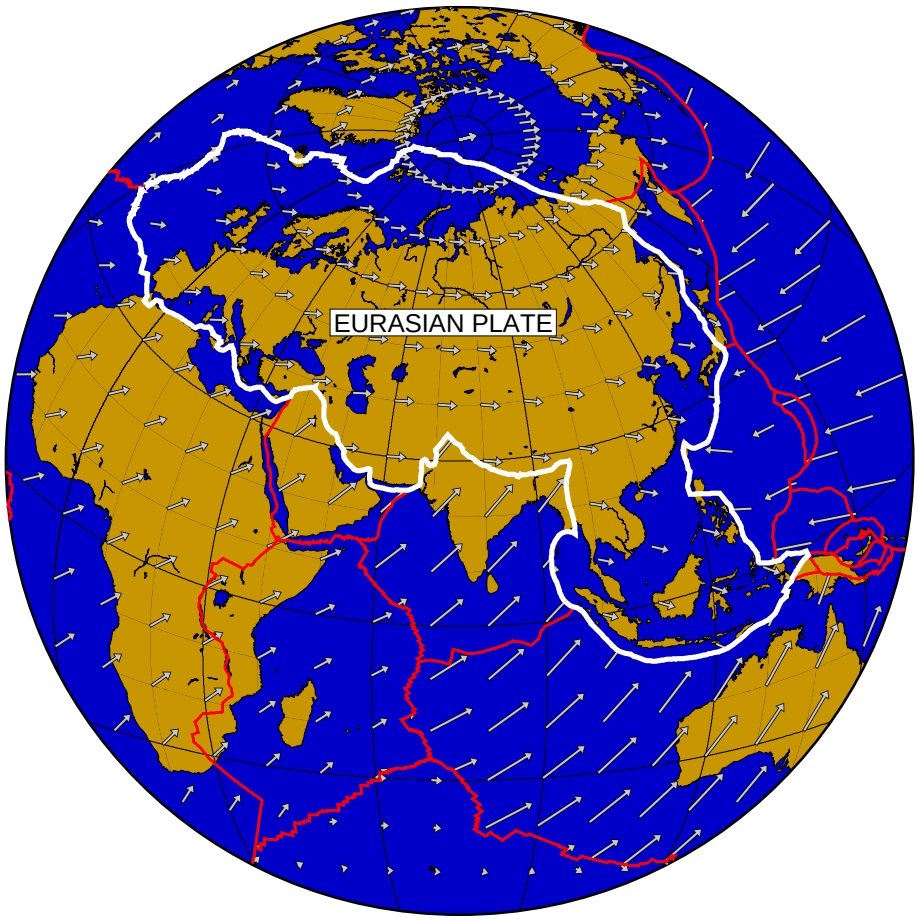

Figure 1.1: Boundaries of the Eurasian plate adopted in this thesis (white lines) and representation of plate velocities with respect to a stable lower mantle (arrows, given in a no-net-rotation reference frame) . Other major tectonic plate boundaries are indicated by red lines. Plate boundaries are after Bird (2003).

tonic plates. I focus, however, on the Eurasian plate (Fig. 1.1). Eurasia is a particularly challenging plate for a number of reasons. First, there is hardly any subducting lithosphere attached to the plate. Therefore, slab pull, which is usually a dominant plate driving force, is practically absent. This results in a high sensitivity of Eurasia's dynamics to the other less well understood forces. Secondly, it has a large variety in the nature of its boundaries, suggesting significant interaction with neighboring plates. And thirdly, the plate has a relatively large surface area and a low velocity with respect to the a stable lower mantle reference frame (absolute velocity, Fig. 1.1) so that the actively convective mantle possibly plays an important role in its dynamics. The most prominent expressions of an active mantle are the Iceland hotspot and a concentration of down-wellings in southeast Asia. Together, the above characteristics of Eurasia suggest that its dynamics can not be approximated by concentrating on either the mantle or the lithosphere, but is governed by a combination of the two. This makes Eurasia an ideal plate to study the relative importance of plate driving forces and the related issue of the nature of lithosphere-mantle coupling.

1.2 Forces acting on tectonic plates

In order to asses the relative importance of the various types of forces to the dynamics of Eurasia I analyze them in this thesis using numerical modeling. A short description of the forces and their implementation in modeling studies is therefore given below. Figure 1.2 schematically illustrates various forces acting on tectonic plates. They can be divided in three categories: 1) gravitational forces inside the lithosphere, referred to as lithospheric body forces (LBFs), 2) edge forces on the lateral boundaries of the plate resulting from interaction with neighboring plates and 3) tractions at the bottom of the plate due to interaction with the underlying mantle. The nature of the first two types of forces is implicit in their origin: LBFs are a direct result of gravity and actively contribute to drive tectonic plates whereas edge forces represent transmission of forces from one plate to another and are a consequence of plate motion. As explained previously, the nature of mantle tractions is not straightforward and is one of the questions addressed in this thesis.

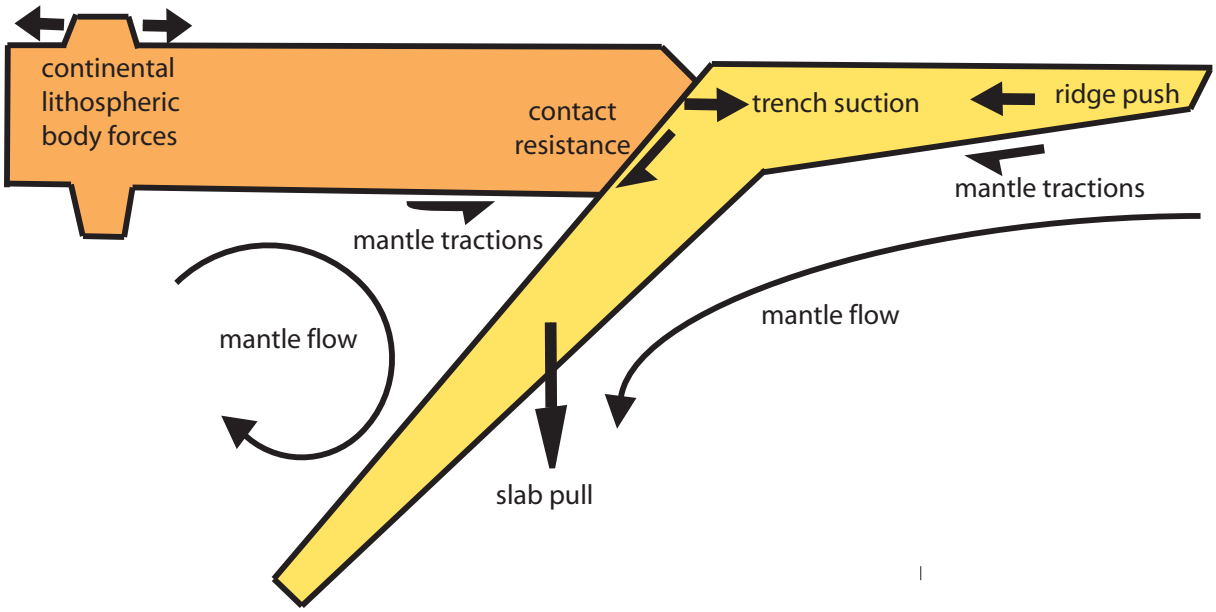

Figure 1.2: Schematic illustration of forces acting on tectonic plates.

Lithospheric body forces

Lateral mass variations generate forces under the influence of gravity. Typically two major types of LBFs act on a tectonic plate: 1) slab pull and 2) forces due to lateral variations in topography and lithospheric density structure. Slab pull is the mechanical pull onto the horizontal part of a tectonic plate exerted by gravitationally unstable oceanic lithosphere sinking into the underlying mantle (Jacoby, 1970). This force is generally

thought to play an important role in driving tectonic plates (Forsyth and Uyeda, 1975; Chapple and Tullis, 1977; Conrad and Lithgow-Bertelloni, 2002) but is insignificant on the Eurasian plate that has no major slabs attached to it. Forces due to lateral variations in topography and density structure are caused by horizontal gradients in the integrated vertical stress of the lithosphere (Artyushkov, 1973). They are distributed over the entire plate and can be divided into the relatively well constrained contribution due to cooling and contraction of oceanic lithosphere with age, referred to as ridge push (Lister, 1975) and the contribution of continental topography. Ridge push is sometimes incorrectly modeled as a line force acting at the ridge, but is a distributed force that acts in the direction of the age gradient of oceanic lithosphere. This direction is an imprint of spreading history and is roughly oriented from the ridge to the passive margin. Ridge push integrates to a substantial net force and has been recognized as an important plate driving force (Richardson, 1992). LBFs in continents contain larger uncertainties because crustal and lithospheric structures are not always well constrained. They generally do not align over large wavelength because topography variations are irregular. Although LBFs may locally be larger on continents than in oceans, the net contribution of continental LBFs to driving tectonic plates is therefore typically of second order to slab pull and ridge push. In this thesis, I evaluate forces resulting from different models for the density structure of the lithosphere, including both ridge push and continental LBFs. I find that despite the presence of a considerable ocean (the northeast Atlantic and the Artic Sea) and the largest topographical feature on Earth (Tibetan plateau), the net-contribution of LBFs to the dynamics of Eurasia is inferior to that of edge forces and mantle tractions. In the absence of slab pull, gravitational forces inside the lithosphere thus do not seem to be the main driving force.

Edge forces

The boundaries of tectonic plates are subject to forces from interaction with neighboring plates. Because edge forces are a consequence of plate motion driven by gravitational forces, they ideally arise self-consistently in global models that include LBFs and mantle buoyancy forces. However, because transmission of forces between plates depends on the still poorly understood rheological properties of plate boundaries, it is in practice not yet feasible to included realistic plate interaction in such models (Steinberger et al., 2001; Lithgow-Bertelloni and Silver, 1998). I therefore follow an other option, which is to model edge forces explicitly. Assuming that normal and shear stresses are transferred equally from one plate to the other, the direction of edge forces can be estimated based on the well-constrained direction of relative plate motion. Edge force magnitudes, however, are unknown. It is therefore common to subdivide edge forces

in categories and to attribute a constant force magnitude to each force type (Forsyth and Uyeda, 1975). These force magnitudes represent the average forcing per force type and need to be *a postiori* constrained based on mechanical equilibrium of tectonic plates (see section 1.3).

I subdivide the forces along Eurasia's boundary based on the tectonic setting and distinguish between oceanic transform faults, collision belts and margins overriding retreating and non-retreating subducting oceanic lithosphere. On transform and continental collision boundaries, forcing is assumed to be resistance to relative motion of the adjacent plate and is modeled in that direction. On overriding plate margins several forces may be at work (Fig. 1.2). The plate contact is subject to resistive forces due to relative motion (contact resistance). However, in case the margin is characterized by trench roll-back the retreating subducting plate also exerts an outward directed suction perpendicular to the boundary (trench suction). I therefore distinguish between overriding margins that experience considerable roll-back, were trench suction is expected to be the dominant force process, and margins where roll-back is non-existent or limited and contact resistance likely dominates. On each type of overriding margin, I consider the net contribution of the two forcing processes and approximate the direction of forcing based on the dominant force mechanism. Overall, my categorization of edge forces represents an approximation which does not consider variations in forcing on length-scales shorter than a few $100\ km$. Such a simplification is warranted in the plate-scale approach followed in this thesis but it implies that caution is required for interpretation of my results on a local scale.

Mantle tractions

Interaction between tectonic plates and the underlying mantle can be considered to arise from two processes (Lithgow-Bertelloni and Silver, 1998; Steinberger et al., 2001): 1) passive resistance of the mantle to motion of the plates and 2) active drive on the plates from flow generated by buoyancy forces inside the mantle. With the first process in mind, lithospheric based studies treating the dynamics of tectonic plates usually approximate interaction with the underlying mantle by a uniform force parallel to the direction of motion of the plate with respect to the underlying mantle (Forsyth and Uyeda, 1975; Wortel et al., 1991; Meijer and Wortel, 1992; Govers and Meijer, 2001; Liu and Bird, 2002; Copley et al., 2010). Although this force, referred to as basal drag, was classically seen as resistive to plate motion, it is sometimes found to be a driving force representing a net drive from the mantle. In chapter 1.4 of this thesis I evaluate this implementation of mantle tractions and conclude that it does not give a good representation of mantle forces on the Eurasian plate.

A more complete representation of lithosphere-mantle interaction is given by models that focus on convective flow in the earth mantle. These models solve the conservation equations (mass and momentum) for a viscous (Stokes) fluid in order to compute flow velocities throughout the mantle. The lithosphere is typically included as an outer layer of high viscosity. Convective flow is driven by density anomalies throughout the mantle that arise from variations in either thermal or chemical properties of the mantle. For the present day, density anomalies can be deduced from either tomography or the history of subduction. Tomographic imaging is based on travel times of seismic waves and inversely solves for regions of higher or lower than average seismic velocities. Velocity anomalies can subsequently be converted to density anomalies by making assumptions on their origin, which may be either chemical or thermal. Studies modeling mantle flow based on tomographic anomalies were successful in several global mantle convection applications like reconstructing plate velocities (Zhong, 2001; Becker and O'Connell, 2001), lithospheric stresses (Steinberger et al., 2001; Lithgow-Bertelloni and Guynn, 2004; Forte et al., 2010; Naliboff et al., 2009) and strain rate (Ghosh et al., 2008). Slab reconstruction models are an alternative to tomographic models and are derived from the history of subduction (Lithgow-Bertelloni and Richards, 1998). Implicitly, they miss contributions from upwelling material but have nonetheless been shown to successfully reproduce plate motion (Lithgow-Bertelloni and Richards, 1998; Becker and O'Connell, 2001; Steiner and Conrad, 2007).
I compute mantle tractions through the graphical user interface SEATREE (Milner et al., 2009) that calculates instantaneous flow velocities (and thus tractions) based on a semi-analytic propagator matrix approach (Hager and O'Connell, 1981). This time efficient method of flow computation can be used for radially varying mantle viscosity structures to which I restrict myself in this thesis. I drive flow by a combination of mantle buoyancy forces (derived from either tomography or subduction-history models) and observed plate velocities. The generated tractions at the base of lithosphere are then a combination of resistance to plate motion and drive from an actively convecting mantle.

1.3 Mechanical and observational constraints

I evaluate my numerical models on the basis of three constraints. The first and most basic constraint is the one of mechanical equilibrium of tectonic plates, which arises from the fact that tectonic plates do not accelerate significantly on short time scales. For practical purposes, this means that the net torque of the forces acting on the model plate is required to vanish (Forsyth and Uyeda, 1975; Chapple and Tullis, 1977).
The second constraint is the direction of Eurasia's absolute motion. This motion rela-

tive to a stable lower mantle reference frame arises from the sum torque of all forces driving the plate. Unfortunately, although the motions of plates relative to one another can be observed directly and are well known, absolute plate motion is uncertain because the net rotation of the lithosphere with respect to the underlying mantle is not well constrained. Uncertainties in the direction of absolute motion are particularly pronounced for the Eurasian plate because it moves relatively slowly. The net-rotation of the lithosphere is usually estimated from volcanic tracks from hotspots (plumes of hot upwelling mantle material) (Gripp and Gordon, 2002; Müller et al., 1993; Duncan and Richards, 1991). Results vary considerably, however, indicating that hotspots are not fixed with respect to the mantle (O'Neill et al., 2005; Torsvik et al., 2008). Recently, the net-rotation of the lithosphere has also been computed using sophisticated numerical models (Becker, 2006; Conrad and Behn, 2010). Uncertainties then arise from choices regarding the viscosity structure of the mantle. Mantle flow models without lateral viscosity variations implicitly can not generate a net rotation of the lithosphere (O'Connell et al., 1991). For practical purposes an absolute motion model based on a zero net-rotation of the lithosphere has therefore been proposed (Argus and Gordon, 1991).

In this thesis, I use the absolute motion direction of Eurasia in two different ways. In a first class of lithosphere-based models, I use this direction as an approximation for the direction of mantle tractions. In that case, I consider a range of absolute motion models. In a second more elaborate class of models, based on the combined lithosphere-mantle approach introduced in this thesis, I incorporate mantle tractions from mantle flow modeling and use the absolute motion direction of Eurasia as an external constraint to evaluate the force models. Because my models contain tractions from mantle flow models without lateral viscosity variations, they do not excite net rotation of the lithosphere. It is therefore natural to evaluate my models based on the absolute motion of Eurasia in a no-net-rotation reference frame (Fig. 1.1).

The third observational constraint I use is the intra-plate stress field, which is the result of the forces acting on the lithosphere. Because the stress field is sensitive to the distribution of forcing, it forms the strongest test for my force models. Stress data are gathered globally in the World Stress Map database (Fig. 1.3, Heidbach et al. (2008)), which combines numerous observations from various sources including earthquake focal mechanisms, borehole breakouts and geological field observations of recent and active faulting. The data coverage for Eurasia is uneven, with extensive parts of central Asia lacking any indicators due to seismic quiescence. Nevertheless there are noticeable features in the Eurasian stress field. The India-Eurasia collision zone shows a fan-like pattern of most compressional stress directions (S_{Hmax}), with thrust tectonics

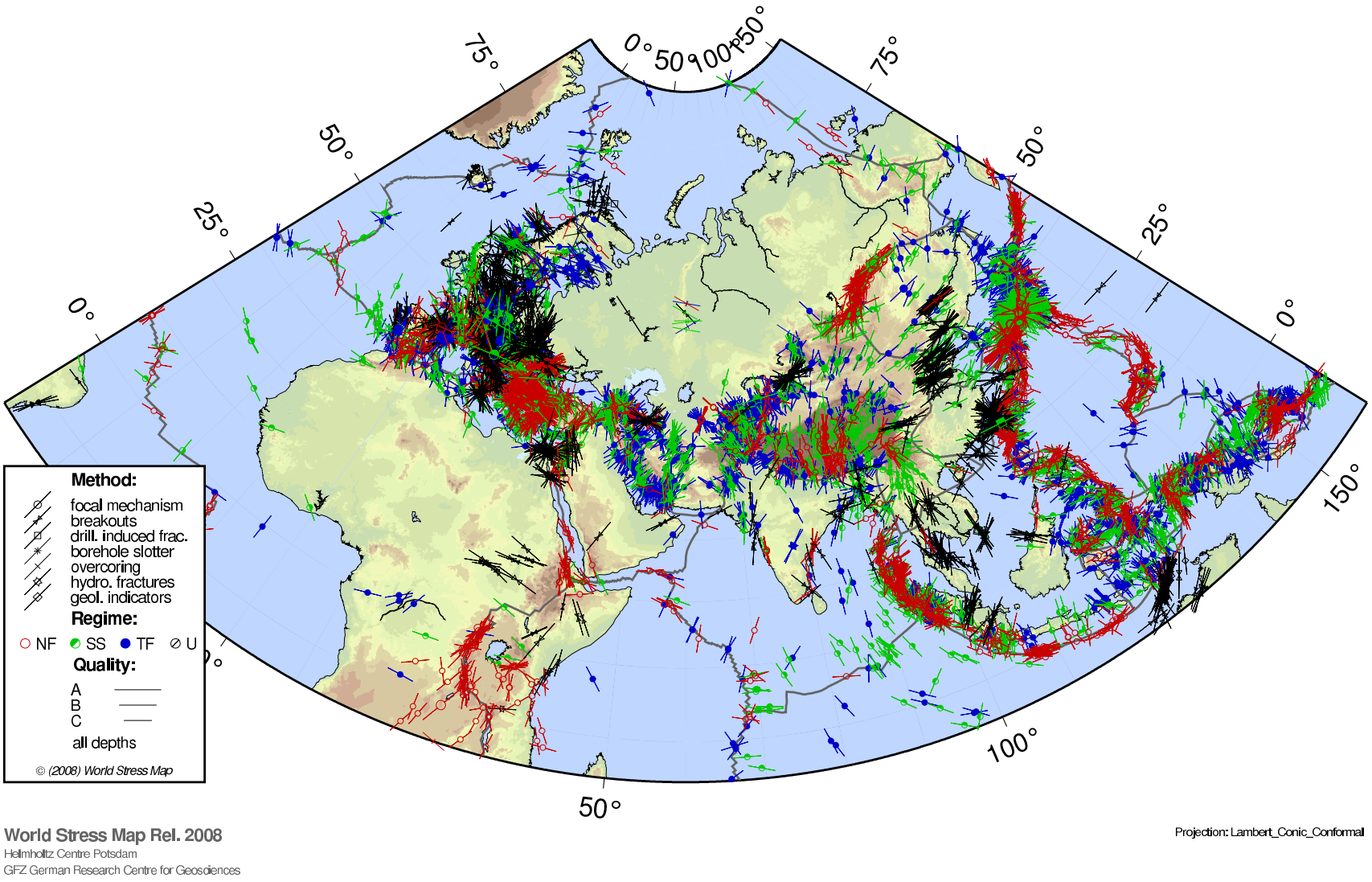

Figure 1.3: Present-day stress observations globally gathered in the World Stress Map Project (Release 2008, Heidbach et al. (2008)). Stripes indicate the direction of maximum compressional stress. Stress regimes are indicated by the color of the symbol; red represents normal faulting, green strike-slip faulting, blue thrust faulting and black is used when the regime is unknown (mainly borehole breakouts).

close to the collision zone and transition to strike-slip faulting further away. The Baikal region is characterized by northwest-southeast extension. Most stress information is available for Europe. S_{Hmax} shows a well constrained northwest-southeast orientations in western Europe and rotates towards westnorthwest-eastsoutheast in Scandinavia. The Aegean Sea and western Anatolia are characterized by nearly northsouth extension.

1.4 Thesis outline

In the next chapters of my thesis, I investigate the dynamics of the Eurasian plate step by step by evaluating force models using the above hierarchy of constraints.

In chapter 1.4, I evaluate lithospheric forces and their uncertainties and use the constraint of torque balance to estimate the net contribution of mantle tractions to the dynamics of the Eurasian plate. I conclude that the approximation of uniform shear (anti)-parallel to absolute plate motion does not give a good average of lithosphere-mantle interaction under Eurasia. Incorporation of active mantle flow in a direction other than absolute plate motion is thus indispensable for mechanical equilibrium of the Eurasian plate.

In chapter 3, I extend my analysis of Eurasian dynamics by evaluating mantle tractions from convective mantle flow models. I find that only mantle flow models based on shear-wave tomography can successfully be combined with models of lithospheric body and edge forces to mechanically balance Eurasia. Successful mantle flow models generate tractions on the base of the lithosphere that are approximately equally governed by active mantle flow and resistance to plate motion. I compare the net contribution of my model forces with the direction of absolute plate motion direction to identify the forces driving Eurasia. I find that forces arising from collision of Africa, Arabia and India substantially deviate the direction of motion generated by the gravitational forces. A comparison of the contribution of the different forces to the dynamics of Eurasia shows that edge forces dominate and generate a torque that is comparable to the combined contribution of mantle tractions and LBFs.

Finally, in chapter 4 I build upon the results of the previous chapters and evaluate force models that mechanically balance the Eurasian plate based on their ability to reproduce observed stress directions. I find that the stress field is predominantly sensitive to the magnitude of the collisional forces on the plate's southern boundary, which are responsible for mountain ranges like the Himalayas, the Zagros mountains and the Alps. Stress observations require collision forces on the India-Eurasia plate boundary of about $10\,TN/m$.

This thesis presents a new combined lithosphere-mantle modeling approach to the dynamics of a tectonic plate. This approach requires internal consistency between the model representation of both lithosphere dynamics and mantle flow. As such, it provides the opportunity to constrain remaining uncertainties, in particular concerning the nature and extent of coupling between the lithosphere and the underlying mantle. In this thesis, I focus on the Eurasian plate and find that it is approximately equally influenced by the actively convecting mantle and by resistance to plate motion. By its methodological nature, the presented modeling approach can also be applied to other tectonic plates. For other plates, the nature of lithosphere-mantle coupling may differ from that for Eurasia. Because Eurasia moves relatively slowly, most other plates are expected to experience stronger mantle resistance to plate motion. If tractions from the actively convecting mantle are assumed to be of comparable intensity globally, resistance to plate motion may be dominant under fast moving plates. This could explain why the classical approximation of mantle shear in the direction of absolute plate motion gives satisfying results for some plates (Pacific: Wortel et al. (1991), India: Copley et al. (2010)), despite being rejected in case of the Eurasian plate.

Chapter 2

A lithosphere-dynamics constraint on mantle flow: analysis of the Eurasian plate

Abstract

We present a method to estimate the poorly understood mechanical coupling between lithosphere and underlying mantle, and apply it to the Eurasian plate. Mechanical equilibrium of tectonic plates requires the torque from mantle tractions ($\overline{T}_M$) to be balanced by the torques from edge forces ($\overline{T}_E$) and lithospheric body forces ($\overline{T}_B$). The direction of $\overline{T}_E$ proves tightly constrained by plate boundary nature but $\overline{T}_B$ is affected by uncertainties in the density structure of continents. We consistently find that the non-zero torque required from mantle tractions does not agree with the orientation of any published absolute motion model. We conclude that mechanical balance of the Eurasian plate requires an actively convecting mantle, which should result in a torque on the Eurasian plate located in the southwest Pacific.

2.1 Introduction

In recent years it is increasingly being realized that the lithosphere and underlying deeper mantle are intrinsically coupled parts of the dynamic Earth which should be jointly addressed (Becker and Faccenna, 2009). Nevertheless, with only a few exceptions (e.g.(Ghosh et al., 2008; Iaffaldano and Bunge, 2009) model analyses of forces driving plate motion or producing the lithospheric stress field generally adopt either a lithosphere-based or a mantle-flow-based perspective. In the former the coupling with the underlying mantle is taken into account through boundary conditions, often in a simplified manner, e.g. through uniform basal drag (Forsyth and Uyeda, 1975; Meijer et al., 1997; Liu and Bird, 2002; Copley et al., 2010). In the latter approach the lithospheric plates are usually taken to be rigid with simplified plate boundaries (review article: Becker and Faccenna (2009)).

In this study we aim to interface the two modeling approaches by using a detailed anal-

This chapter has been published as:

Warners-Ruckstuhl, K. N., Meijer, P. T., Govers, R., Wortel, M. J. R., 2010, A lithosphere-dynamics constraint on mantle flow: Analysis of the Eurasian plate, Geophysical Research Letters 37, doi:10.1029/2010GL044431.

ysis of forces acting on the lithosphere as a basis for determining a dynamic constraint on the tractions exerted by the convecting mantle onto the lithosphere.
Our analysis is based on mechanical equilibrium, which requires that the sum of all torques on a tectonic plate vanishes (Forsyth and Uyeda, 1975). The forces acting on a plate can be divided in three categories: 1) edge forces due to interaction with neighboring plates ($\overline{F}_E$), 2) lithospheric body forces ($\overline{F}_B$) and 3) mantle tractions at the bottom of the plate ($\overline{F}_M$). For a total force-set including N_E edge force types ${}_i\overline{F}_E$ (with $i = 1, ..N_E$) and similarily N_B lithospheric body force types ${}_i\overline{F}_B$:

$$\sum_{i=1}^{N_E} \int_S \overline{r} \times \ {}_i\overline{F}_E \ dS + \sum_{i=1}^{N_B} \int_V \overline{r} \times \ {}_i\overline{F}_B \ dV + \int_A \overline{r} \times \overline{F}_M \ dA = \overline{0} \tag{2.1}$$

where the integration is over the boundary area S, the bottom area A, or the volume V, while $\overline{r}$ is the position vector from the center of the earth.
In this study we carefully assess the orientation, and when possible the magnitude of the first two terms of eq. 2.1. This provides constraints on the balancing torque arising from mantle tractions. We focus on the Eurasian plate. Due to its large size the ratio between total basal area and total boundary length is high, making it likely that mantle flow is a major contributor to the plate's dynamics.

2.2 Eurasian plate model boundaries

Torque calculations are performed on a spherical thin shell representing the Eurasian plate (Fig.2.1). Our model boundaries follow the major plate boundaries (Bird, 2003) where ${}_i\overline{F}_E$ are more clearly defined. The model domain includes several regions exhibiting non-rigid behavior, e.g., SE Asia, Okinawa, Birma, Aegean and Anatolia. This does not affect our torque calculations : Eurasia can be considered a closed system in which forces across internal faults oppose each other and do not contribute to the torque.
We determine the type of $\overline{F}_E$ based on tectonic setting (Fig.2.1). Focusing on the overall dynamics of the Eurasian plate, features smaller than a few hundred kilometers are neglected. We distinguish five categories representing the average boundary characteristics: 1) ridge and transform (red line), 2) continental collision (black triangles), 3) trench roll-back subduction (Schellart et al., 2008) (purple triangles), 4) non-roll-back subduction (orange triangles). 5) unknown boundary (black boundary segment); the boundary between continental North America and Eurasia is unclear both in location and nature due to the absence of seismicity and recent tectonic features; relative velocities are negligible.

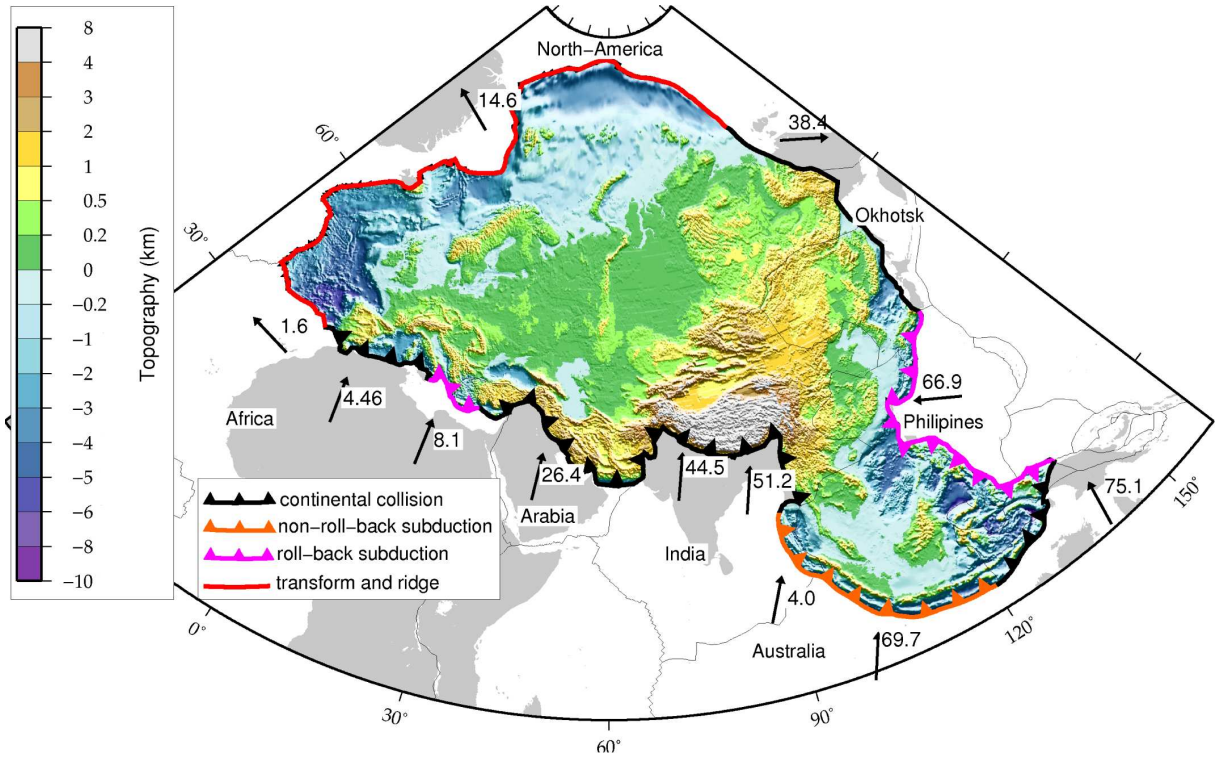

Figure 2.1: Topography and boundary types of our model Eurasian plate. Arrows denote relative motion of adjacent plate with respect to Eurasia according to NUVEL-1a, rate of motion is indicated in mm/yr. Thin black lines outline major tectonic units.

2.3 Torque analysis of edge forces

Directions of $\overline{F}_E$'s can be estimated with some confidence but their magnitudes are unknown, prohibiting full quantification of $\overline{T}_E$. However, we can constrain its orientation using the geometrical distribution and orientation of the various ${}_i\overline{F}_E$. Each boundary force is factorized into a constant magnitude per unit length of boundary, ${}_iF_E$, and a unit orientation vector $\overline{e}_i$ (Forsyth and Uyeda, 1975). ${}_iF_E$ represents the average contribution of processes beyond the boundary domain averaged along each boundary segment;

$$ {}_i\overline{T}_E = \int_S \overline{r} \times {}_i\overline{F}_E(\overline{r}) \; dS = {}_iF_E \int_S \overline{r} \times \overline{e}_i(\overline{r}) \; dS = {}_iF_E \, {}_i\overline{T}'_E \tag{2.2} $$

${}_i\overline{T}'_E$ will be referred to as geometrical torque.

Transform fault resistance, continental collision and forces at non-roll-back subduction segments arise from friction at the plate contact and are modeled anti-parallel to the direction of motion relative to the adjacent plate (NUVEL-1a (DeMets et al., 1994)). The force at subduction roll-back segments is expected to be dominated by suction of the

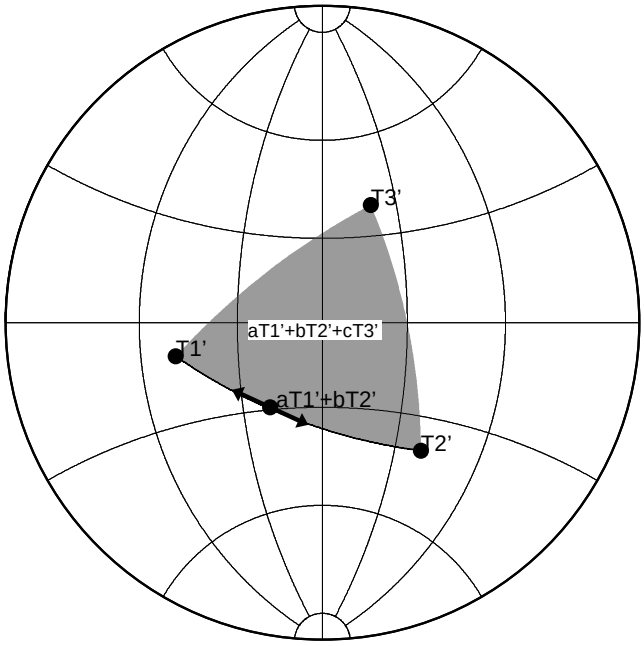

Figure 2.2: Illustration of the summation of geometrical torques. Positive torque vectors are represented by the intersection of the globe by a corresponding semi-line in an upper hemisphere stereographic projection. $a\overline{T}_1$ is parallel to $\overline{T}'_1$. For positive scaling factors a and b $a\overline{T}'_1 + b\overline{T}'_2$ lies on the connecting great-circle. Sum vector $a\overline{T}'_1 + b\overline{T}'_2 + c\overline{T}'_3$ lies inside the area (grey zone) enclosed by the connecting great circles.

retreating slab and is modeled outward and perpendicular to the boundary. No force is applied on the unknown North-America Eurasia boundary segment.

We use the various ${}_i\overline{T}'_E$ to constrain the orientation of the total torque $\overline{T}_E$. Figure 2.2 illustrates the geometrical properties of the vector sum of torques by representing torque orientations as the location where a semi-line of that direction intersects the globe. For positive scalar magnitudes, the sum of any number of torques is confined to the area enclosed by the connecting great circles.

The calculated ${}_i\overline{T}'_E$ are represented by black dots in Figure 2.3. As a continuous variation of the (positive) scalars ${}_iF_E$ is possible, $\overline{T}_E$ may lie anywhere inside the red line. This region can be refined by imposing constraints on the relative magnitudes of the ${}_i\overline{F}_E$. Based on the larger contact area per meter boundary we require 1) continental collision boundaries to have a larger resistance per meter boundary than transform fault boundaries and, 2) continental collision resistance to be strongest on the contact segment with the Indian plate. Within these two constraints a continuous variation of the relative force magnitudes remains possible, which limits $\overline{T}'_E$ to the red zone in Figure 2.3.

The robustness of the solution space for $\overline{T}'_E$ is decisive for the robustness of the resulting constraint on lithosphere-mantle interaction. Overall, torque directions are well constrained by plate boundary geometry and relative motion. We tested the sensitivity of $\overline{T}'_E$ to boundary conditions on the unknown North-America Eurasia boundary segment by treating it as a continental collision boundary and found the effect limited. Force directions oppose along this segment so that its torque contributon remains

small and does not influence our findings regarding $\overline{T}'_E$.

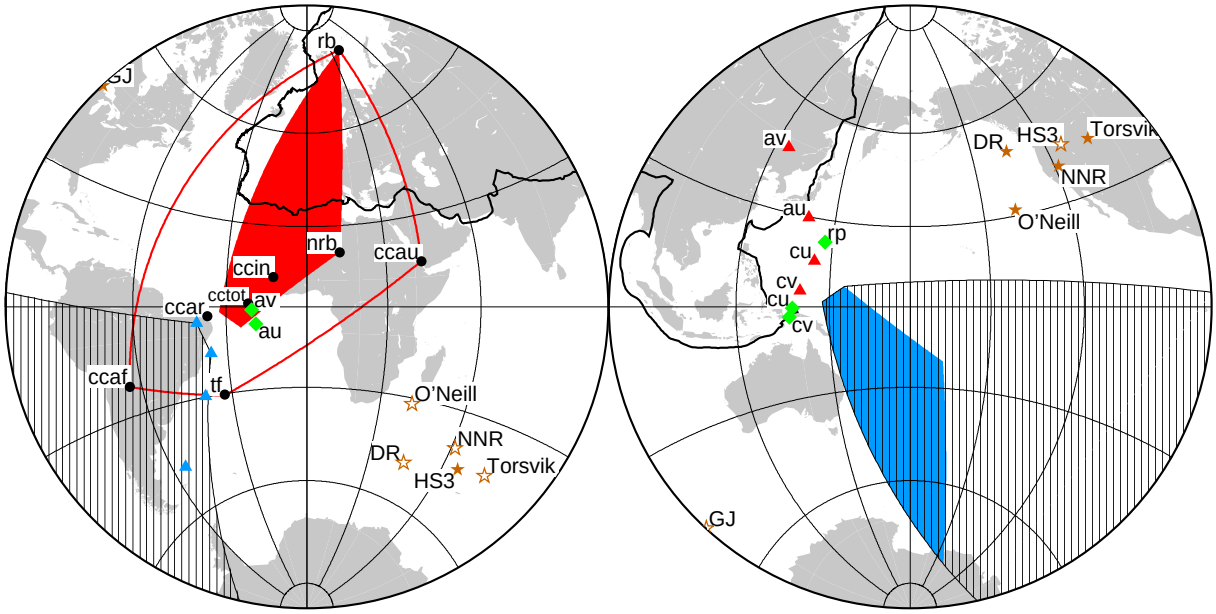

Figure 2.3: Analysis of torques acting on the Eurasian plate. Symbols represent the positive end of outward torques. Black circles represent ${}_i\overline{T}'_E$. Red line encircles theoretical solution space for the sum-torque $\overline{T}_E$. Red zone represents physically acceptable range for this torque. Green diamonds give torque orientations of ridge push and the various models for topography force, red triangles are the corresponding $\overline{T}_B$'s. The antipode of $\overline{T}_E$ is confined to the blue zone, and antipodes of the $\overline{T}_B$'s are represented by blue triangles. They confine the orientation of $\overline{T}_M$ to the shaded area (see text). Brown stars represent basal drag torques, labeled according to used absolute velocity model. Closed/open stars correspond to driving/resistive drag. Key: tf: transform fault resistance, $ccaf$: continental collision (cc) Africa, $ccar$: cc Arabia, $ccin$: cc India, $ccau$: cc Australia, $cctot$: total cc in case of equal forcing along entire continental collisional boundary, rb: force at roll-back trenches, nrb: force at non-roll-back trenches, rp: ridge push, au: crustal Airy model, av: Airy model homogenous thickening entire lithosphere, cu: crust2.0 model with uniform lithospheric thickness, cv: crust2.0 model with variable lithospheric thickness, $HS3$: HS3-NUVEL-1a model Gripp and Gordon (2002), NNR: No-net-rotation reference frame Argus and Gordon (1991), DR: Duncan and Richards (1991), GJ: Gordon and Jurdy (1986), $O'Neill$:O'Neill et al. (2005) in combination with NUVEL-1a, $Torsvik$: global moving hotspot frame Torsvik et al. (2008) in combination with NUVEL-1a.

2.4 Torque analysis of lithospheric body forces

$\overline{F}_B$'s result from gradients in gravitational potential energy (GPE) (Artyushkov, 1973). In oceanic domains, $\overline{F}_B$'s consist of slab pull, which is insignificant on the Eurasian plate, and ridge push, which can be quantified for a given thermal cooling model and age distribution (Lister, 1975). We use the boundary layer model with constant basal heat flux (Crough, 1975) and oceanic age distribution from Müller et al. (1997). The

ridge push torque is well constrained in both orientation and magnitude.

$\overline{F}_B$'s arising in the continents and passive margins (hereafter referred to as topography force) are more difficult to assess because the vertical density distribution of the lithosphere is not generally known. Warranted by the large horizontal scale of our model we make the assumption of isostatic equilibrium, which we use to infer the depth of major density interfaces from topography. However, as both crustal thickness and lithospheric depth vary laterally, additional assumptions are necessary. These turn out to have a dominant imprint on the topography force. We bound the plausible range of the topography torque by using different lithospheric density models that represent the extremes of what can be expected.

We consider two classes of density models, one where we calculate crustal thicknesses, and one based on observed crustal thicknesses. In the first class, we assume Airy compensation through crustal thickness variations inside a lithosphere of uniform (100km) thickness (model *Airyuni*), or Airy isostatic compensation of homogeneous (i,e. uniform) thickened/thinned crust and lithospheric mantle at the base of the lithosphere (model *Airyvar*). In the second class of models we use crustal thicknesses from CRUST2.0 (Bassin et al., 2000). Isostatic compensation follows by assuming either density variations in the lithospheric mantle above 100km (model *Crust2.0uni*), or thickness variations of the lithospheric mantle (model *Crust2.0var*).

We calculate the topographic force for regions above 1000m bathymetric depth to include the contribution of continental margins, but to exclude areas where ridge push acts and trenches where flexure dominates. Although plausible variations of the different parameters (e.g. densities, compensation depth) affect the magnitude of the forces, torque orientations are stable within a few degrees.

Force distributions for the four models (Fig. 2.4) are dominated by an outward pattern around the Tibetan plateau. However, whereas the *Airy* models show low forcing outside the main mountain areas, the *crust2.0* models induce horizontal forces in regions where crustal thickness variations are not reflected by topography. These crustal thickness variations have a long wavelength component (Siberian craton) that contributes significantly to the torque. This results in larger and almost anti-podal torques for the *crust2.0* models compared to the *Airy* models (Fig. 2.3). The figure also shows that torque orientations within each model class agree well. We find that torque magnitudes, however, are affected by the choice of lithospheric mantle properties, and can vary by up to a factor four.

We conclude that the topography torque of Eurasia is poorly constrained. However, the total $\overline{T}_B$ is less variable due to the large stable ridge push contribution. The red triangles in Figure 2.3 show $\overline{T}_B$ for our four models. Differences in their orientations

demonstrates the uncertainty in $\overline{T}_B$.

2.5 Implications for mantle contribution

The constraints on $\overline{T}_E$ and $\overline{T}_B$ allow us to limit the orientation of $\overline{T}_M$, which, from eq. 2.1, is the sum of the antipodes of the two:

$$\overline{T}_M = (-\overline{T}_E) + (-\overline{T}_B) \tag{2.3}$$

$\overline{T}_M$ represents the total effect of the mantle consisting of two contributions: 1) horizontal shear 2) the effect of normal pressure at the base of the lithosphere due to active mantle flow, which will alter GPE based on isostatic equilibrium.
In Fig. 2.3, the antipode of $\overline{T}_E$ is confined to the blue zone, and antipodes of the $\overline{T}_B$'s are represented by blue triangles. As magnitudes ${}_i\overline{F}_E$ are unknown, the solution space for $\overline{T}_M$ follows from a linear combination of the blue zone with any one $\overline{T}_B$ (as in Figure 2.2). Considering the solution spaces derived with the different $\overline{T}_B$'s, we confine the orientation of $\overline{T}_M$ to the shaded area of Figure 2.3.
Aditional assumptions regarding relative magnitudes of the involved torques can considerably tighten the solution space. Previous studies have globally found $\overline{T}_M$ to be of the same order as, or stronger than $\overline{T}_B$ (Bird et al., 2008). This restricts $\overline{T}_M$ to the southwest Pacific part of the shaded area, in or just outside the blue zone. The overall effect of the mantle then forces Eurasia's center southward.
A common simplification in lithospheric based studies is to model mantle tractions (anti)-parallel to the direction of absolute motion (Forsyth and Uyeda, 1975; Meijer et al., 1997; Liu and Bird, 2002; Copley et al., 2010). We evaluate this approach in the light of our torque analysis. Absolute motion of Eurasia is low and directions vary considerably depending on the chosen reference frame. We therefore use different velocity models to calculate the resulting geometrical torque for uniform basal shear (Fig.2.3). Although it is often seen as resistive to plate motion, its nature, being either resistive or driving, is ambiguous and we consider both options. The torques fall well outside the shaded area implying that uniform shear (anti)-parallel to absolute plate motion does not give a good average of lithosphere-mantle interaction under Eurasia. Due to the strong dominance of continental lithosphere, results obtained with a shear stress contrast between oceans and continents are very similar and do not alter this finding. Incorporation of active mantle flow in a direction other than absolute plate motion proves indispendable for equilibrium of the Eurasian plate. As the mantle does not force Eurasia towards or against its direction of motion it can not be seen as a truly driving or resistive force.

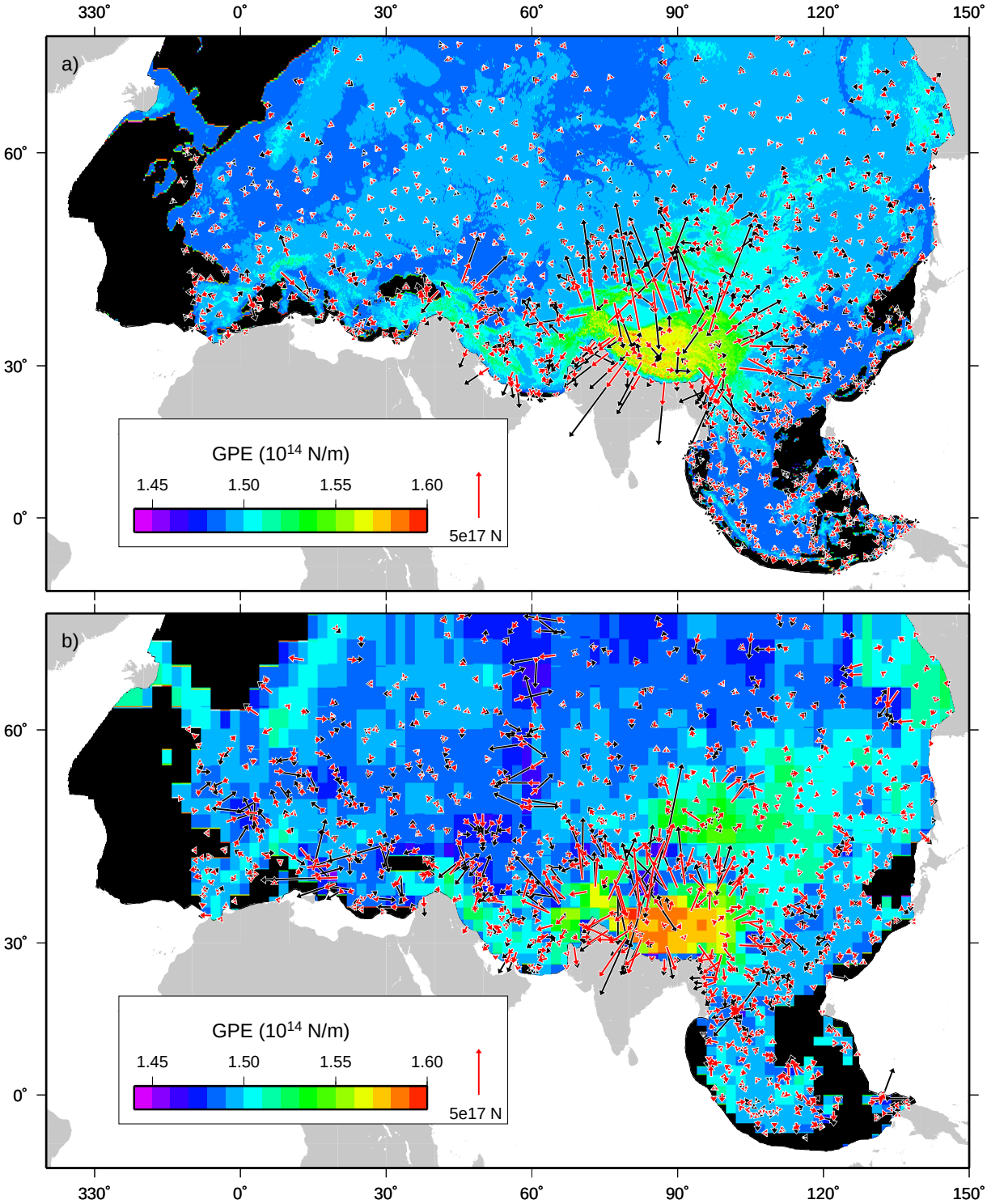

Figure 2.4: Distribution of topography force for *a)* $Airyvar$ (black arrows) and $Airyuni$ (red arrows) *b)* $crust2.0var$ (black arrows) and $crust2.0uni$ (red arrows). Contour data show GPE for the models with constant lithospheric thickness (100km). Areas below 1000m bathymetric depth are not included in topography force calculations to exclude areas where ridge push acts and trenches where flexure dominates.

2.6 Discussion

Our result for $\overline{T}_M$ is independent of the magnitudes ${}_iF_E$, on which we have not made assumptions, and considers GPE uncertainties. Although $\overline{F}_B$ are often thought to be well determined, systematic assessment of isostatic models for the lithospheric density structure shows that they are, in truth, poorly constrained on continents.
Our analysis concentrates on torque orientations and does not quantify $\overline{T}_M$. The fact that none of the $\overline{T}_B$'s falls into the antipodal area of $\overline{T}_E$, however, illustrates that $\overline{F}_B$ and $\overline{F}_E$ alone do not balance the Eurasian plate and a net contribution from the mantle is required. Calculations of plate velocities from mantle flow models are commonly based on the assumption of balance of torques arising from two sets of tractions: 1) shear due to relative motion of the plates over the passive mantle, and 2) tractions due to active mantle flow. This assumption is inconsistent with our findings: the sum of the two torques should be non-zero.
For other large continental plates (South-America (Meijer et al., 1997), India (Copley et al., 2010)), basal shear in the absolute plate motion direction, or opposite to it, does allow for mechanical balance. Our conclusion that, on average, lithosphere-mantle coupling must act in a different direction is therefore either unique to the Eurasian plate, or is made possible by a more tightly constrained $\overline{T}_M$.

2.7 Conclusions

Through mechanical equilibrium of the Eurasian plate, analysis of lithospheric forces has brought us insight on the net effect of mantle tractions. We find that:

1. The orientation of the mantle torque required to balance the Eurasian plate is constrained to the southwest Pacific.

2. A first-order representation of mantle tractions as uniform shear (anti-)parallel to absolute plate motion is inadequate for the Eurasian plate. Therefore active mantle flow should be taken into account when modeling lithosphere-mantle interaction.

Acknowledgments

Constructive reviews by two anonymous reviewers are greatly appreciated. Figures were produced with the GMT software by Wessel and Smith (1991). Work supported in part by the EUROMARGINS Programme of the European Science Foundation, project 01-LEC-EMA22F WESTMED.

Chapter 3

Lithosphere-mantle coupling and the dynamics of the Eurasian plate

Abstract

Mechanical equilibrium of tectonic plates implies that lithospheric edge and body forces are balanced by forces arising from interaction with the underlying mantle. We use this quantitative physical relation to integrate existing modelling approaches of lithosphere dynamics and mantle flow into a new combined approach applied to the Eurasian plate. By combining a thorough analysis of lithospheric forces with the requirement of torque balance we constrain the orientation of the torque on Eurasia arising from mantle tractions. We use this constraint to evaluate convective mantle flow models driven by tomographic or subduction history model anomalies and observed plate motion. Mantle forcing is considered through both shear at the bottom of the plate and induced dynamic topography. We find that instantaneous semi-analytic flow models without lateral viscosity variations generate tractions that meet the constraint from Eurasian lithosphere-dynamics, but only for specific ranges of mantle flow parameters. Of the explored set of mantle anomaly models, only mantle flow models based on S-wave tomography anomalies can balance Eurasia for realistic viscosity profiles and velocity-density scaling. Choices in mantle density forcing and viscosity are crucial in that they govern the relative magnitude of tractions due to convective mantle flow ("active tractions") and resistive tractions due to plate motion ("passive tractions"). We find mechanical balance is only achieved for similar torque magnitudes of active and passive shear. The two shear contributions do however in no case balance each other and a considerable, dominant, net torque from edge forces is required to balance total mantle tractions and lithospheric body forces. Our analysis provides a range of mechanically consistent total force sets acting on the Eurasian plate. Using this result we find that mantle buoyancy forces and lithospheric body forces acting on Eurasia itself are important driving forces but do not drive Eurasia in the observed direction. Continental collision at Eurasia's southern boundary significantly deviates Eurasia northward. Our combined torque balance approach, in which mantle tractions from convective mantle flow modelling are combined with explicitly applied edge forces, thus emphasizes the role of plate interactions to the dynamics of tectonic plates.

This chapter is in review at Geophysical Journal International as:
Warners-Ruckstuhl, K. N., Govers, R., Wortel, M. J. R., 2012, Lithosphere-mantle coupling and the dynamics of the Eurasian plate.

3.1 Introduction

The nature of mechanical coupling between the lithosphere and underlying mantle has been extensively debated since the advent of plate tectonics but is still poorly understood. Intrinsically linked to understanding lithosphere-mantle coupling is the question of which forces are the motor behind plate motion. Early studies on lithospheric driving forces, modelling coupling with the underlying mantle as passive drag against plate motion, identified slab pull and ridge push as the main plate driving forces (Forsyth and Uyeda, 1975; Harper, 1975; Richardson et al., 1979). More recently, mantle flow studies have demonstrated the importance of active mantle flow induced by density anomalies throughout the mantle in driving tectonic plates (Ricard and Vigny, 1989; Lithgow-Bertelloni and Richards, 1998; Becker and O'Connell, 2001). How actual lithosphere-mantle interaction results from the above two contributions depends on mantle parameters like viscosity distribution and density anomalies driving the flow (Conrad and Lithgow-Bertelloni, 2002, 2004; Becker, 2006), which remain the subject of ongoing investigation (Simmons et al., 2009; Steinberger and Calderwood, 2006) (review article: Becker and Faccenna (2009)).

In this study, we aim to evaluate lithosphere-mantle coupling for the Eurasian plate by combining lithospheric and mantle dynamics. Our analysis is based on mechanical equilibrium of tectonic plates which implies that, through torque balance, lithospheric edge and body forces must be counterbalanced by external forces arising from interaction with the underlying mantle (Forsyth and Uyeda, 1975; Chapple and Tullis, 1977). We build upon results presented by Warners-Ruckstuhl et al. (2010) (hereafter WR10, chapter 1.4 of this thesis), who analysed the lithospheric forces on the Eurasian plate to constrain the orientation of the torque resulting from mantle tractions at the base of the plate. This lithosphere-dynamic constraint on mantle tractions offers a simple test for models describing mantle flow. Interestingly, WR10 found that mantle tractions based on the classical approximation of uniform shear (anti)-parallel to absolute plate motion do not meet this constraint for Eurasia. Here, we evaluate whether tractions from convective global mantle flow models do mechanically balance Eurasia.

The constraint of torque balance can be seen as the basis in a hierarchy of constraints that should be met by models describing total sets of tectonic forces. Only models fulfilling torque balance can meaningfully be evaluated further based on observational constraints. Observed plate-motions form a natural second step in constraining tectonic forces because they are sensitive to the integral of forces. Quantities that are sensitive to the exact distribution of the force field (e.g. stresses) form a third level of constraints . In this study, we focus on integrated quantities. In a following study, we

will proceed to evaluate successful models based on the observed stress field.

We model the present mantle flow field by instantaneous flow in a viscous mantle driven by density anomalies based on various tomographic or geodynamic subduction-history models (Hager et al., 1985). Studies following this approach have shown successful results in several global mantle convection applications like reconstructing plate velocities (Lithgow-Bertelloni and Richards, 1998; Zhong, 2001; Becker and O'Connell, 2001), lithospheric stresses (Steinberger et al., 2001; Lithgow-Bertelloni and Guynn, 2004; Forte et al., 2010; Naliboff et al., 2009) and strain rate (Ghosh et al., 2008). In order to obtain realistic tractions at the base of Eurasia, we impose observed plate velocities as boundary conditions in the mantle flow field. Resulting tractions at the base of the lithosphere are the sum of two contributions (Ricard and Vigny, 1989; Lithgow-Bertelloni and Silver, 1998; Steinberger et al., 2001): 1) convective tractions generated by buoyancy forces inside the mantle (hereafter referred to as 'active tractions') and 2) resistance due to motion of the plates ('passive tractions'). The relative magnitude of both contributions indicates whether lithosphere-mantle coupling is dominated by drive from the mantle or from the plates and thus forms a good indication for the nature of the coupling. Because the ratio of active and passive tractions varies significantly depending on the assumed mantle buoyancy forcing and viscosity field it is not well constrained by mantle modelling alone. Here, we infer this ratio by making use of the external constraint of torque balance on the Eurasian plate.

Torque balance has extensively been used to constrain tectonic forces previously. Studies doing so have generally focused either on the lithosphere, over-simplifying interaction with the underlying mantle (Forsyth and Uyeda, 1975; Chapple and Tullis, 1977; Wortel et al., 1991; Meijer and Wortel, 1992; Govers and Meijer, 2001; Liu and Bird, 2002; Copley et al., 2010), or on the convecting mantle, neglecting edge forces due to plate interaction or implementing them through simplified rheological properties of plate boundaries (Ricard and Vigny, 1989; Lithgow-Bertelloni and Richards, 1998; Zhong, 2001; Steinberger et al., 2001; Lithgow-Bertelloni and Guynn, 2004; Ghosh et al., 2008). Both approaches yield a different application of the torque balance constraint. In the convecting mantle approach, in which plate velocities are solved for, torque balance is imposed on each plate taking into account passive tractions, active tractions and (in most cases) lithospheric body forces. Edge forces result self-consistently from plate motion driven by gravitational forces, but are not considered in the torque balance calculations. Implicitly, a zero net torque due to edge forces is therefore assumed on each plate (Steinberger et al., 2001), a restriction which has no physical grounds. In the lithosphere-based approach, both edge forces and basal (mantle) tractions are parameterized based on observed plate motion. This introduces forcing which is not directly

gravitational and requires that directions of boundary conditions be specified explicitly. Magnitudes of the parameterized forces are solved for such that torque balance occurs between mantle tractions, lithospheric body forces and edge forces. Typically, net edge force torques are considerable.

In recent years, a few global scale studies have merged both approaches and emphasized the need to simultaneously address the lithospheric and mantle system. Becker and O'Connell (2001) introduced parameterized edge forces (including slab pull) in a convecting mantle approach, but found that they could not significantly improve modelled plate motions due to their strong (anti-) correlation on the global scale. Conrad and Lithgow-Bertelloni (2002) concluded that adding a direct mechanical pull due to slabs in a mantle flow study considerably improves the match to observed plate motion. Bird et al. (2008) solved for basal shear stresses generating observed plate velocities in a lithospheric model in which edge forces arise self-consistently and are governed by friction coefficients on plate boundaries. They found that torques due to basal tractions, lithospheric body forces and edge forces are of comparable magnitude on most plates. Iaffaldano and Bunge (2009) coupled a geodynamic convection model to the lithospheric model of Bird et al. (2008) and showed that edge forces can be of significant magnitude relative to driving mantle buoyancy forces and can considerably affect plate motion.

In this study, we interface lithospheric and mantle modelling on a single-plate scale. We opt for a torque balance approach in which edge forces are modelled explicitly (and therefore may yield a non-zero net torque), and mantle tractions arise from mantle flow modelling. The plate-scale approach allows us to solve for the forces transmitted from adjacent plates without the need to make assumptions regarding the ill-constrained rheology of plate boundaries. It also allows for a more detailed resolution of edge forces than has been possible using a global-scale approach (Becker and O'Connell, 2001). In our new single-plate approach, the interaction of the plate with the underlying mantle is exclusively represented by tractions from mantle flow models that contain active and passive tractions. The variability of these tractions is controlled by the uncertainty range of mantle flow parameters. A previous lithospheric-based single-plate model that incorporated active mantle tractions in a study of the North-American plate (Humphreys and Coblentz, 2007) concluded that mantle flow modelling results needed to be down-scaled and complemented with a uniform shear in order to balance the plate and fit the observed stress field. In this study, we find that results from mantle flow modelling and lithospheric dynamics can be reconciled without the need to scale or add tractions.

We focus on the Eurasian plate. Although for most tectonic plates the lithosphere-

based torque balance method has produced force sets that were quite successful in reproducing the large scale stress field, this is not the case for Eurasia (Goes et al., 2000). Convective mantle based studies reproducing plate velocities or the first-order stress field on a global scale, did generally not produce particularly good results for the Eurasian part of their model (Steinberger et al., 2001; Lithgow-Bertelloni and Guynn, 2004; Ghosh et al., 2008). The difficulty of capturing the forces controlling Eurasia seems to indicate that its dynamics can not be approximated by concentrating on either the mantle or the lithosphere, but is governed by a combination of the two. This makes Eurasia an ideal plate to study lithosphere-mantle coupling and the related issue of plate driving forces.

The novelty of what we present does not lie in the individual assessment of the forces, for which we use existing modelling approaches, but in the way we merge these results. By linking mantle flow tractions at the base of the lithosphere with a detailed analysis of lithospheric body and edge forces we require consistency between results from mantle- and lithosphere-dynamics modelling. The requirement of torque balance then creates the possibility to constrain remaining model uncertainties. It enables us to confine the nature of lithosphere-mantle coupling by solving for the ratio of active versus passive tractions required to balance the lithospheric forces on the Eurasian plate. Subsequently, we use this result to analyse plate driving forces. Our analysis provides a range of mechanically consistent force sets acting on the Eurasian plate in which mantle tractions, lithospheric body forces as well as edge forces play an important role. We evaluate the relative contributions of the three types of forces to the dynamics of Eurasia. Finally, by evaluating the force sets in the light of observed motion of Eurasia we identify which role the different tectonic forces play in driving Eurasia.

3.2 Lithosphere-dynamics constraint on mantle flow

3.2.1 Torque balance

Three types of forces act on tectonic plates: 1) edge forces due to interaction of a plate with neighbouring plates 2) lithospheric body forces (LBFs) resulting from horizontal pressure gradients inside the lithosphere, caused by lateral variations in topography and density structure inside the lithosphere and 3) tractions at the bottom of the plate due to interaction with the underlying mantle. Mechanical equilibrium of tectonic plates implies that the sum of all torques on a plate vanishes (Forsyth and Uyeda, 1975; Chapple and Tullis, 1977). For a force distribution including N_E edge force types ${}_i\overline{F}_E$ (with $i = 1, ..N_E$), N_B lithospheric body force types ${}_i\overline{F}_B$ and mantle tractions $\overline{F}_M$:

$$\sum_{i=1}^{N_E} \int_S \overline{r} \times \ {}_i\overline{F}_E \ dS + \sum_{i=1}^{N_B} \int_V \overline{r} \times \ {}_i\overline{F}_B \ dV + \int_A \overline{r} \times \overline{F}_M \ dA = \overline{0} \tag{3.1}$$

where the integration is over the boundary area S, the bottom area A or the volume V of the plate, while $\overline{r}$ is the position vector from the centre of the earth.

Mantle tractions on the base of the lithosphere have shear and normal components, which both affect torque balance. The shear component directly contributes to the torque through the third integral of (3.1). The normal component induces dynamic topography that influences the gravitational potential energy (GPE) of the lithosphere (Hager et al., 1985; Lithgow-Bertelloni and Silver, 1998). Lateral variations in GPE of the lithosphere result from topography and density variations inside the lithosphere, and induce LBFs (Artyushkov, 1973; Fleitout and Froidevaux, 1982; Molnar and Lyon-Cean, 1988). Forces arising from the normal component of mantle tractions are therefore coupled to forces caused by the density structure of the lithosphere and enter eq. (3.1) via the second integral.

Edge forces result from mechanical interaction with neighbouring plates. We model their directions explicitly, so that they are independent of modelled mantle tractions. WR10 analysed edge forces on the Eurasian plate and confined the direction of the total edge force torque (first term of eq. (3.1)) on Eurasia. This result is based on the direction of forcing, inferred from the nature and geometry of the plate boundaries, and is independent of the poorly-known magnitude of the edge forces. The orientation of the total edge force torque constrains the sum of the remaining, mantle-flow-dependent, terms of (3.1) and forms the basis for our evaluation of mantle tractions. Below, we therefore present a summary of the analysis of edge forces previously outlined by WR10.

Pull due to down-going slabs has been treated in different ways in the past. Essentially a LBF, in mantle flow models slabs are part of mantle buoyancies driving the flow and affect both down-going and overriding plate through induced viscous flow. This treatment, however, does not directly incorporate the mechanical pull exerted by the slab on the surface part of the down-going plate (Becker and O'Connell, 2001; Conrad and Lithgow-Bertelloni, 2002). In lithospheric torque balance models, slab pull has been incorporated as a quantified edge force. The only slab attached to the Eurasian plate is the narrow section showing slab reversal in Taiwan and we choose to approximate its effect by incorporating it as part of the locally acting edge force.

3.2.2 Edge force torque

Following Forsyth and Uyeda (1975), edge forces are subdivided into categories based on tectonic setting (Fig. 3.1). Each edge force ${}_i\overline{F}_E$ is parameterized as a constant mag-

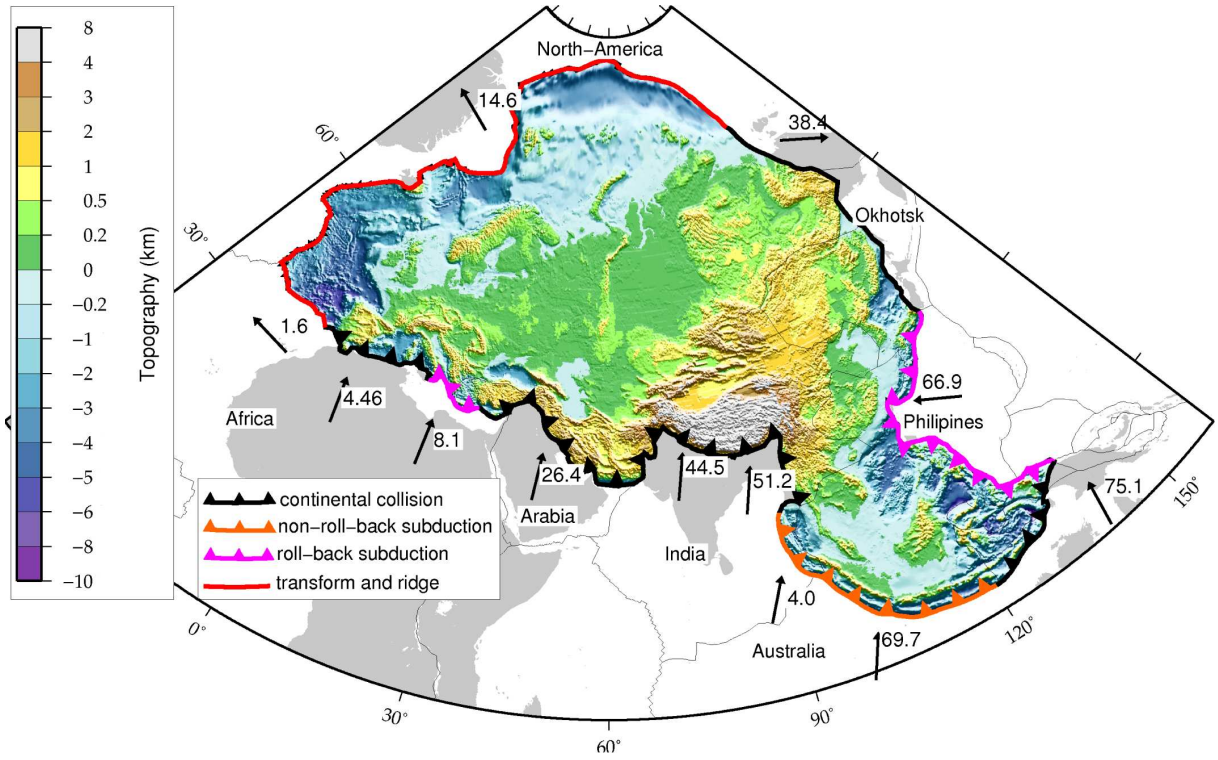

Figure 3.1: Topography and boundary types of Eurasian plate model, after WR10. Arrows denote motion of adjacent plate with respect to Eurasia according to NUVEL-1a, rate of motion is indicated in mm/yr. Plate boundaries after Bird (2003). Our model Eurasian plate follows major plate boundaries were edge forces are most easily defined.

nitude per unit length of boundary ${}_iF_E$ that represents the average contribution of processes beyond the boundary domain, and a unit vector $\overline{e}_i$ representing the relative motion direction. The torque contribution ${}_i\overline{T}_E$ by edge force ${}_i\overline{F}_E$ thus becomes:

$$ {}_i\overline{T}_E = \int_S \overline{r} \times \ {}_i\overline{F}_E(\overline{r}) \ dS = \ {}_iF_E \int_S \overline{r} \times \overline{e}_i(\overline{r}) \ dS = \ {}_iF_E \ {}_i\overline{T}'_E \tag{3.2} $$

${}_i\overline{T}'_E$ is an unscaled torque parallel to ${}_i\overline{T}_E$

Our model boundary for the Eurasian plate follows the major plate boundaries (Bird, 2003) where edge forces are most clearly defined (Fig. 3.1). We neglect features smaller than a few hundred kilometres and focus on the overall dynamics of Eurasia. By opting for a simple division of edge forces based on tectonic setting, we aim to represent the average force contribution of processes beyond our boundary domain. We distinguish five different edge force types (Fig. 3.1): 1) transform fault resistance on the ridge and transform boundary (red line), 2) continental collision force on the segments colliding with Africa, Arabia, India and Australia (black triangles), 3) forces at trench roll-back margins (purple triangles), 4) forces at non-roll-back margins (orange triangles) and

5) free boundary between continental North-America and Eurasia, where the exact boundary location is unclear both in location and nature due to negligible relative velocities and the absence of seismicity or recent tectonic features (black line). Assuming normal and shear stresses are transmitted equally from one plate to another, resistive forces (transform fault resistance, continental collision and forces at non-roll-back subduction margins) are modelled anti-parallel to the direction of motion relative to the adjacent plate (NUVEL-1a (DeMets et al., 1994)). The force at subduction roll-back segments is expected to be dominated by suction of the retreating slab and is modelled outward and perpendicular to the trench. Edge force magnitudes ${}_iF_E$ are poorly known and not imposed *a-priori*.

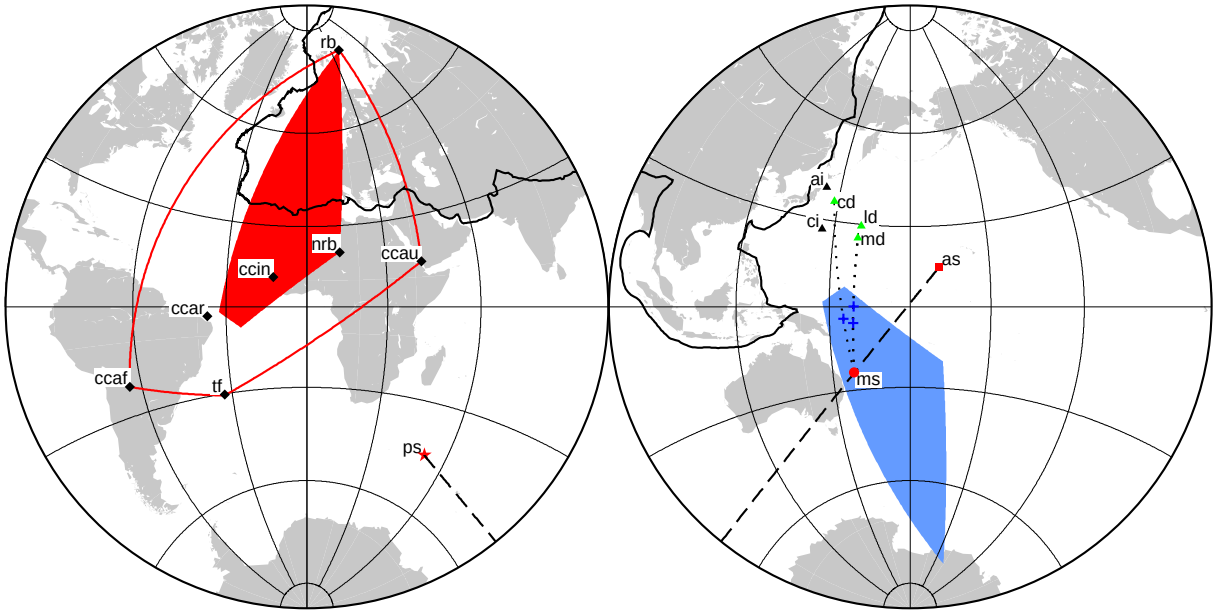

Figure 3.2: Representation of torque orientations of the various model forces for example mantle flow model (based on tomographic model *ngrand* (Grand, 2002), v-ρ scaling factor 0.2 and viscosity profile (Mitrovica and Forte, 2004)). Positive ends of torque vectors are represented by their intersection with the globe in an upper hemisphere stereographic projection. Black diamonds: edge forces. Red: mantle shear; Black striped line is a great-circle segment connecting passive (star) and active (square) shear torques; it crosses the total shear torque (circle) which is the sum of the two. Triangles: LBFs; green: dynamic models, black: isostatically compensated models slightly modified after WR10 (ai: crustal Airy isostatic model, ci: isostatic crust2.0 model). Blue crosses: sum of mantle shear and LBF torques, located on connecting great-circles segments (dotted lines) . Red/blue zone represents physically acceptable range for the sum torque of all boundary forces and its antipodal area, respectively. Crosses in the blue zone represent force sets that enable torque balance of the Eurasian plate. For abbreviations see Table 3.1

Torque orientations ${}_i\overline{T}'_E$ for the various edge forces are displayed in Figure 3.2. Geometrical properties of vector sums state that, for positive magnitudes ${}_iF_E$, the orientation of the total edge force torque (first term in equation 3.1) lies within the area

enclosed by great-circles connecting the individual torques (WR10, red line in Fig. 3.2). The location inside this area depends on the relative magnitude of the different edge forces, and is further confined by physical restrictions therein. Based on the larger contact area per meter boundary we require: 1) continental collision boundaries to have a larger resistance per meter boundary than transform fault boundaries and, 2) continental collision resistance to be strongest on the contact segment with the Indian plate. This restricts the orientation of the total edge force torque to the red area in Figure 3.2. Inversely, it implies that all orientations inside the red area can result from realistic edge force distributions along the plates boundary. Because the system is under-determined (7 unknown edge force magnitudes, 3 degrees of freedom), each specific torque orientation inside the red zone can result from different combinations of individual edge forces. Our approach does not require that we solve for magnitudes of individual edge force types.

3.2.3 Implications for mantle flow

To mechanically balance Eurasia, LBFs and mantle tractions must counterbalance the total torque due to edge forces (eq. 3.1). The orientation of the edge force torque is confined to the red zone of Figure 3.2 so that the orientation of the sum torque of mantle shear and LBFs should be located inside the anti-podal blue zone. This constraint is relatively tight so that it allows us to evaluate mantle flow models for their ability to generate torques that can balance the Eurasian plate.

Table 3.1: Abbreviation for model forces as used in figures

ms	mantle shear
as	active shear
ps	passive shear
cd	LBF model *Crust2.0*
md	LBF model *Mantle*
ld	LBF model *Lithodens*
cc af/ar/in/au	continental collision Africa/Arabia/India/Australia
cctot	total continental collision in case of equal forcing along entire continental boundary
ccin+ar	continental collision in case of equal forcing on Arabian and Indian boundary
tf	transform fault resistance
rb	force at trench roll-back margin
nrb	force at trench non-roll-back margins

3.3 Mantle flow dependent forcing on Eurasia

3.3.1 Mantle tractions

We calculate global mantle flow in a radially varying viscous mantle following the semi-analytical, propagator matrix approach in a spherical shell (Hager and O'Connell, 1981). We use the graphical user interface SEATREE (Milner et al., 2009), which contains a modified implementation by Becker et al. (2006) based on Steinberger (2000). Mantle buoyancy fields are deduced from tomographic or subduction history models that have been expanded in spherical harmonics up to degree 31, corresponding to a wavelength of $1300\ km$. Since we are interested in mantle tractions actually felt by the Eurasian plate, we impose observed plate motions as boundary conditions. Because our mantle flow models do not contain lateral viscosity variations, no toroidal flow is excited and no net rotation of the lithosphere with respect to the mantle can be sustained (O'Connell et al., 1991). Any net rotation imposed on the lithosphere then simply results in a net rotation of the entire mantle with respect to the core, accommodated along the free-slip core-mantle interface. As a consequence, our modelled tractions at the base of the lithosphere reflect plate motions in a no-net-rotation reference frame. In section3.8, we discuss to possible implications of net rotation of the lithosphere and show that it is not likely to significantly affect our conclusions.

We compute tractions at the base of a uniform $100\ km$ thick lithosphere for various mantle flow models, based on a variety of mantle buoyancy fields and (radial) viscosity profiles. The tractions from the mantle flow models are applied to a separate spherical thin shell lithospheric model for Eurasia (Fig. 3.1), on which we perform the torque calculations. The model domain is discretized using triangular elements of 50 to $100\ km$ side length, which was tested to be dense enough that results are insensitive to further grid refinement.

To illustrate the methodology, we present resulting tractions for an example mantle flow model, which is representative for the family of models that we consider. In the subsequent torque analysis (sections 3.4 and 3.5), we will present results for a broader range of models obtained with alternative choices regarding viscosity and mantle buoyancy, and discuss the consequences for torque balance of the Eurasian plate.

Our example model's buoyancy field is derived from tomographic S-wave model *ngrand* (Grand, 2002). Seismic velocities are converted to densities assuming a constant velocity-density scaling ($v - \rho$ scaling) of 0.2, which is around mid-way in the range suggested based on a thermal origin of wavespeed anomalies (Steinberger and Calderwood, 2006;

Simmons et al., 2009). In the uppermost $250\ km$ of the mantle beneath the continents, buoyancy variations due to temperature are probably largely cancelled by compositional variations (Goes and van der Lee, 2002). Following previous studies (Lithgow-Bertelloni and Silver, 1998; Becker and O'Connell, 2001; Steinberger et al., 2001) we therefore remove the top $250\ km$ of forcing. The flow field and corresponding tractions are calculated using the radial viscosity profile of Mitrovica and Forte (2004).

Resulting tractions at the base of the lithosphere are shown in Figure 3.3. For linear flow laws as assumed in this study, total tractions can be viewed as the sum of two contributions (Ricard and Vigny, 1989; Lithgow-Bertelloni and Silver, 1998; Steinberger et al., 2001): 1) convective tractions due to flow driven by buoyancy forces inside the mantle under fixed plates (which we will refer to as 'active tractions'; Figure 3.3a), and 2) tractions from flow driven by motions of plates over a other passive underlying mantle ('passive tractions'; Figure 3.3b.). Passive tractions on Eurasia are dominated by the resistance to absolute motion of the plate itself. Active tractions are typically of shorter wavelength. They are governed by up-wellings and associated outward flow at mid-oceanic ridges (with strongest amplitude near the Iceland hotspot) and down-wellings and associated inward flow at subduction and collision zones. For the assumed mantle flow parameters, active tractions strongly dominate over passive ones, with magnitudes on average three times higher. Consequently, total mantle tractions (Fig. 3.3c) do not visibly show the imprint of absolute plate motion. However, we note that relative magnitudes of passive and active tractions strongly depend on mantle buoyancy magnitude and viscosity (see sections 3.4.2 and 3.4.3).

3.3.2 Lithospheric body forces including dynamic topography

LBFs arise from lateral variations in geopotential energy (GPE) of the lithosphere caused by topography and density structure variations (Artyushkov, 1973; Fleitout and Froidevaux, 1982; Molnar and Lyon-Cean, 1988). They can be assessed when the density structure of the lithosphere is known. In the oceanic realm, cooling of the lithosphere causes the relatively well constrained ridge push (Lister, 1975). In continental interiors and on passive margins, LBFs are more uncertain because the vertical density distribution of the lithosphere is less well constrained.

Normal mantle tractions cause uplift or subsidence of the entire lithosphere and thus affect LBFs. Focusing on long wavelength (neglecting flexure), we can assume pressure equilibrium at the base of the lithosphere between overburden pressure and dynamic pressure from the underlying mantle. Lateral variations in observed topography then arise from three contributions: 1) variations in crustal thickness and/or density, 2) variations in lithospheric mantle thickness and/or density and 3) variations in normal

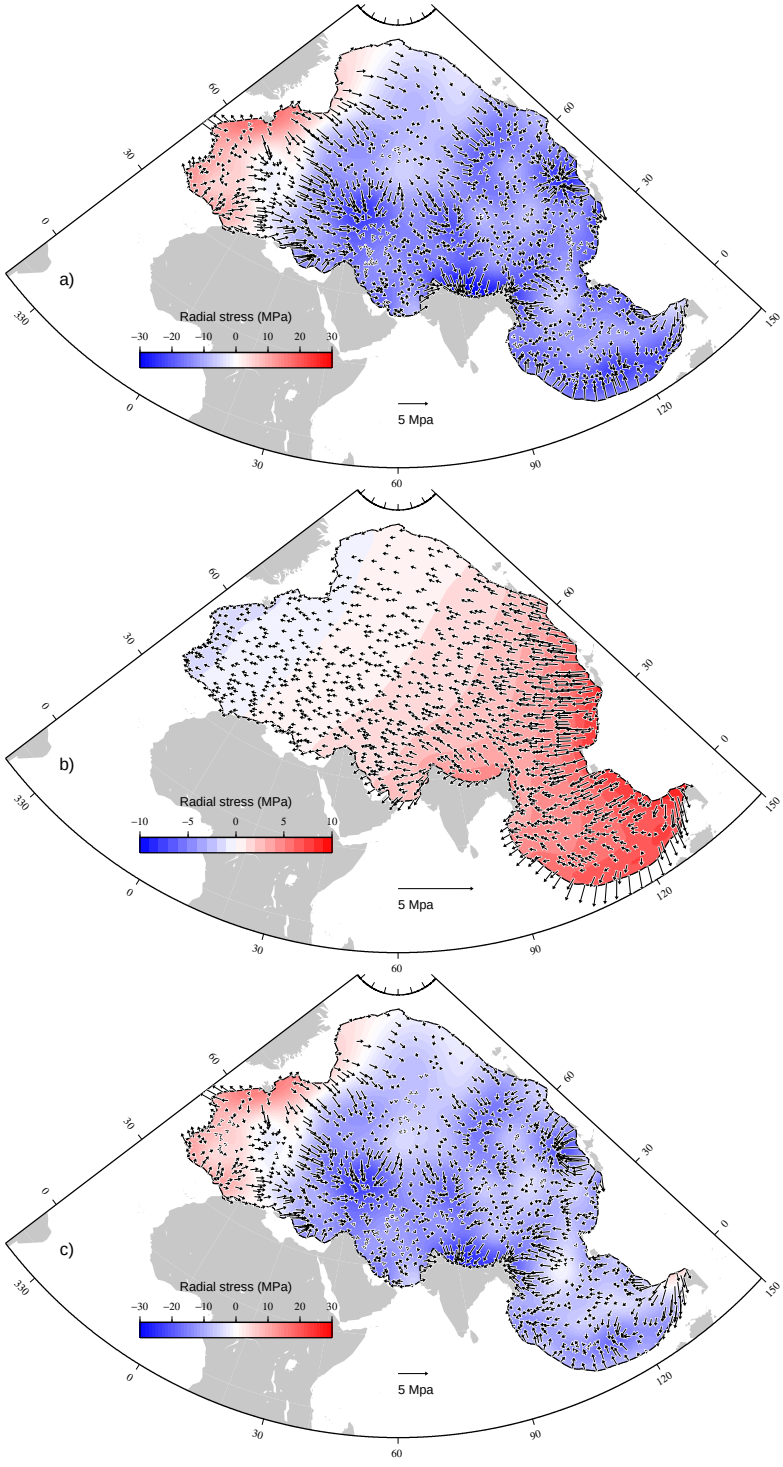

Figure 3.3: Mantle tractions at the base of the Eurasian plate from global mantle flow model with density forcing deduced from tomographic model *ngrand*, viscosity profile of Mitrovica and Forte (2004) and imposed NNR plate velocities. Arrows represents shear stress, contour-colours radial stress, upward is positive. a) active tractions due to mantle buoyancies, b) passive tractions due to motion of the plates over the mantle, c) total tractions

stress from the underlying mantle.

A number of studies have estimated topography resulting from the different contributions with the aim to reconcile results with observed topography, and showed that large wavelength deviations from isostatic equilibrium could indeed be matched to dynamic topography estimates from mantle flow models (Forte and Perry, 2000; Conrad et al., 2004; Forte et al., 2010). However, uncertainties in observations of lithospheric structure and mantle flow modelling are such that topography estimates are consistent only to first order and generally do not add up to observed topography (Simmons et al., 2007; Panasyuk and Hager, 2000). This hampers the combination of crustal and lithospheric structure observations into one lithospheric density model with mantle flow modelling results, while remaining consistent with observed topography. Studies combining the calculation of LBFs with mantle dynamics have adopted different approaches to circumvent this problem. While some have neglected the contribution from dynamic topography (Becker and O'Connell, 2001; Flesch et al., 2007), most have modelled LBFs focusing on part of the available information. One possibility is to model LBFs using the observed crustal structure, and assume that deviations from isostatic equilibrium of the model are a result of the dynamic mantle (Lithgow-Bertelloni and Silver, 1998; Ghosh et al., 2008, 2009; Iaffaldano and Bunge, 2009). Computed LBFs then include a dynamic component, but one that does not generally correlate with normal tractions from mantle flow modelling. Another possibility is to apply pressure variations from mantle flow modelling in combination with observed crustal thickness, and to adapt either crustal densities (Lithgow-Bertelloni and Silver, 1998) or lithospheric mantle densities (Steinberger et al., 2001) in order to match the observed topography.

As we aim to evaluate mantle forcing on the lithosphere based on torque balance, it is important to assess the uncertainty in the torque generated by LBFs on the Eurasian plate. We aim to cover the uncertainty range in lithospheric density structure by computing three different models. Each of the models assumes that the main uncertainty in defining the density structure of the lithosphere lies in a different unit, being either the crust, the lithospheric mantle or dynamic mantle pressure at the base of the lithosphere. Figure 3.4 illustrates the main elements of the three models. In order to remain consistent with the use of radially stratified mantle flow models, all three models assume a constant base of the lithosphere, taken to be $100km$. A short description of the models is given below, together with the presentation of the resulting GPE and force fields. We refer to appendix A for computational details.

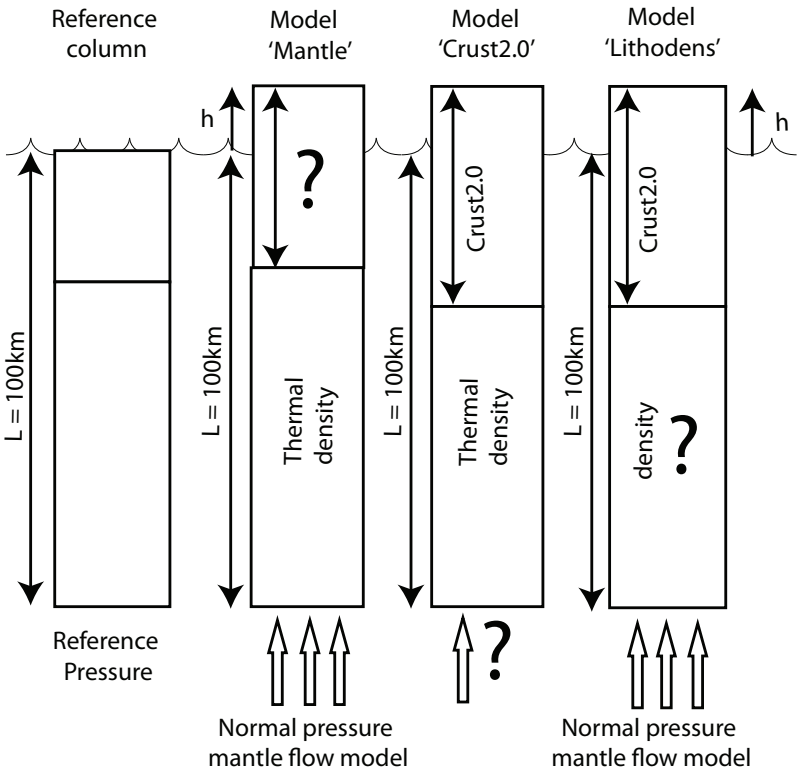

Figure 3.4: Topographic columns illustrating assumptions made in various LBF models. The question mark in each model represents the quantity that is calculated in order for the height of the column to match observed topography, being crustal thickness, normal mantle pressure and lithospheric density for models *Mantle*, *Crust2.0* and *Lithodens*, respectively.

Model *Mantle*

Model *Mantle* is based on dynamic topography deduced from normal mantle tractions at the base of the lithosphere from mantle flow modelling. On the continents and continental margins we assume that the part of the actual topography (ETOPO1 (Amante and Eakins, 2009)) that is not dynamically supported is isostatically compensated within the crust. We assume a constant crustal density and a temperature dependent lithospheric density and compute crustal thicknesses that result in the observed topography. In the oceans, lithospheric structure and bathymetry is based on secular cooling and added to the dynamic topography component.

GPE and force distributions for model *Mantle* depend on the normal component of mantle tractions and therefore vary as a function of mantle flow model. Results for our example mantle flow model are shown in Figure 3.5a. GPE varies both as a result of strong topography (Tibetan plateau) and mantle tractions (high at Iceland and low in eastern Europe, see Fig. 3.3c). Variations due to both sources show approximately the same amplitude, indicating that radial pressure and crustal thickness variations have comparable influence on the force field.

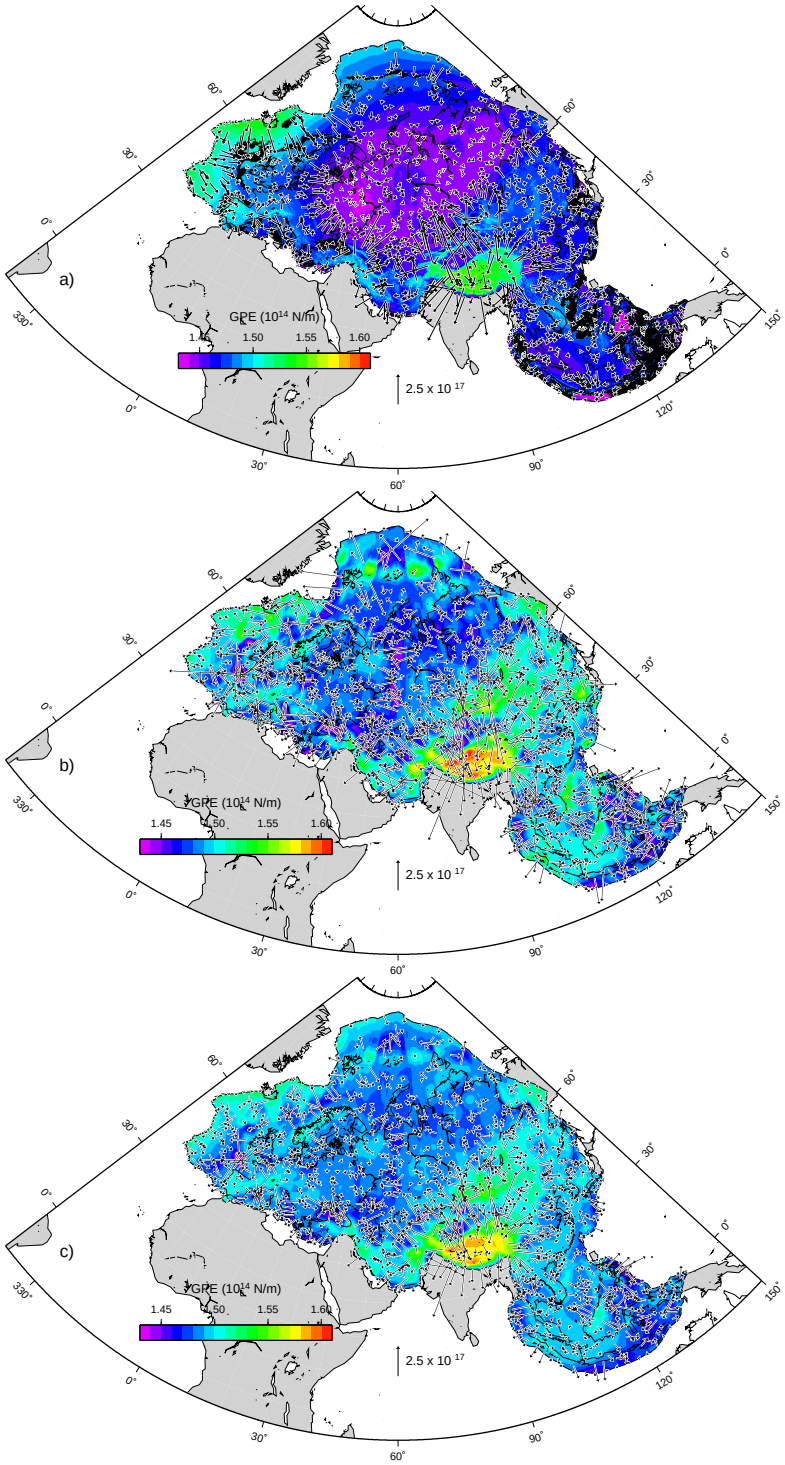

Figure 3.5: Force distribution (arrows) and GPE (contoured values) for the three LBF models including dynamic topography (see Fig.3.4: a) Model *Mantle*, b) Model *Crust2.0*, c) Model *Lithodens*. (Tomographic model *ngrand*, constant $v - \rho$-scaling 0.2, viscosity profile *MF*).

Model *Crust2.0*

Our second model is based on crustal thicknesses and densities of seismological model Crust2.0 (Bassin et al., 2000) and assumes that deviations from isostatic equilibrium are dynamically supported at the base of the lithosphere (Fig. 3.4). This model is comparable to models presented by Lithgow-Bertelloni and Silver (1998); Ghosh et al. (2008, 2009). As in model *Mantle*, the lithospheric mantle density is temperature dependent (linear geotherm). In order to evaluate the compatibility of this model with mantle flow we compare the lithostatic pressures at the base of the lithosphere with normal stresses from mantle flow models (see appendix, Fig. 3. 18). Although major features can be recognized in both models (e.g. the Iceland hotspot and a large ring like depression over central Eurasia), we find that differences are significant. This confirms the need to investigate a range of models for the structure of the lithosphere, based on the different available datasets.
The resulting force distribution for model *Crust2.0*(Fig. 3.5b) shows an outward pattern around the main topographical expression of Eurasia, the Tibetan Plateau, in agreement with observed gravitational collapse of elevated topography. However, whereas model *Mantle* shows lower forcing outside the main mountain areas, the *Crust2.0* model induces significant horizontal forces in regions lacking topography variations, caused by crustal structure variations that are not expressed in the topography. GPE variations occur on length scales which are considerable smaller than in the mantle flow based model *Mantle*, and the resulting force pattern is more chaotic.

Model *Lithodens*

In the third model, we combine crustal thickness and density from *Crust2.0* with normal mantle tractions from mantle flow modelling and assume that uncertainty in the factors governing topography is entirely concentrated in the lithospheric mantle. We calculate averaged densities of the lithospheric mantle so that observed topography is matched (Fig. 3.4). This model is meant to capture the effects of variations in properties of the lithospheric mantle and is in essence comparable to the treatment of LBFs presented by Steinberger et al. (2001). Both lithospheric thickness and density are known to vary laterally but remain uncertain (Artemieva, 2006, 2003). Interpretation of seismic observations is ambiguous due to the combination of thermal and compositional effects (Forte and Perry, 2000). Together, lithospheric thickness and density determine the total weight of the lithospheric mantle, which is the relevant factor towards topography. Again, in order to remain consistent with the use of radially stratified mantle flow models, we model variations in this weight by laterally varying lithospheric mantle density while keeping the depth of the lithosphere fixed to $100\ km$. This simplified

weight distribution will affect resulting LBFs, and should be seen as a first order approximation towards a more realistic model accounting for variable lithospheric thicknesses. Calculated densities range from 3050 to over 3500 kg/m^3 (appendix Fig. 3. 19) exceeding, as expected, the realistic range in parts of the domain. Because they give an indication of the mass of the lithospheric mantle high densities can also indicate a thick lithospheric mantle. Qualitative comparison of calculated densities with lithospheric thicknesses presented by Artemieva (2006) shows that "heavy" lithospheric mantle in Siberia and Scandinavia does correspond with regions of thick lithosphere. The low weight of lithospheric mantle underneath the Tibetan plateau, however, does not correlate with thin lithospheric mantle.
GPE and force distributions for model *Lithodens* depend on the mantle flow model and we again present results for our example model. The resulting GPE field (Fig. 3.5c) resembles that of model *Crust2.0*. However, lateral variations are attenuated, mainly in southeast Asia and in the Atlantic. Generated forces are therefore considerably less chaotic.

3.4 Torque balance analysis

We now proceed to evaluate whether our independent estimates of the various forces are consistent in that they balance the Eurasian plate. We will show that this depends on the assumed mantle flow model. In this section, we concentrate on mantle flow models based on tomographic model *ngrand*. First, we illustrate the torque balance analysis methodology by presenting results for our example mantle flow model. Subsequently, we investigate how torque results are affected by uncertainties in the conversion of seismic wavespeed anomalies to density perturbations ($v - \rho$ scaling) and the (radial) viscosity profile, and analyse how this affects the ability of mantle tractions to balance lithospheric forces on the Eurasian plate. In section 3.5 we subsequently analyse mantle flow models based on other mantle anomaly models.

3.4.1 Example mantle flow model

Shear resulting from active and passive mantle flow yields torques represented by the red star and square, respectively, in Fig. 3.2. The total mantle shear torque (red dot) is the sum of the two separate contributions and therefore lies on the connecting great-circle. Its location is closer to the active shear torque which is of higher magnitude than the passive shear torque. Torques resulting from the three LBF models (LBF torques, green triangles in Fig. 3.2) have quite similar orientations despite the differences in force pattern (Fig. 3.5). As concluded by WR10 for the case of isostatic models, the differences seen in force pattern occur on a small length scale compared to the plate

size and cancel out upon integration. Torques for the isostatic models presented by WR10 are included for completeness in Fig. 3.2 (slightly altered due to update in some modelling parameters, black triangles).
To mechanically balance edge forces on Eurasia (equation 3.1), mantle shear and LBFs must together produce a torque that is oriented inside the blue zone of Fig. 3.2 (see section 3.2). This turns out to be the case for all three LBF models (blue crosses in Fig. 3.2). Tractions generated by our example mantle flow model thus balance lithospheric forces on Eurasia, indicating that independent estimates of edge forces and mantle tractions can indeed be reconciled into a total force set governing the dynamics of Eurasia. We proceed to evaluate the sensitivity of mantle flow models regarding their ability to balance Eurasia on the assumed mantle flow parameters.

3.4.2 Effect of $v - \rho$ scaling factor

Conversion of seismic wavespeed to density based on mineral physics laws is not straightforward as compositional and thermal effects are difficult to separate. Compositional effects are thought to be concentrated in the top part of the mantle, where cratonic roots are chemically distinct from the surrounding mantle (Jordan, 1978; Forte and Perry, 2000), and in the lowermost part of the mantle (Karato and Karki, 2001; Steinberger and Holme, 2008). It is therefore quite common in mantle flow modelling to assume a thermal origin for all anomalies and to use linear conversion between wavespeed anomalies and densities. Most studies thereby remove density forcing in the top 200 to 300 km of the mantle to exclude the effect of cratonic roots (Lithgow-Bertelloni and Silver, 1998; Becker and O'Connell, 2001; Steinberger et al., 2001), where buoyancy variations due to temperature probably are largely cancelled by compositional variations (Forte and Perry, 2000; Goes and van der Lee, 2002). With the assumption of a thermal origin of all anomalies, $v - \rho$ scaling factors for S-wavespeeds have been estimated to lie between 0.10 and 0.30 (Karato and Karki, 2001; Steinberger and Calderwood, 2006; Simmons et al., 2009).
As a first order approximation, we investigate the influence of uncertainties in $v - \rho$ scaling on mantle tractions and resulting torques by assuming a constant scaling factor for the entire mantle, but removing forcing in the top $250\ km$. Active tractions magnitudes scale linearly with $v-\rho$ scaling factor, whereas passive tractions are independent of mantle forcing and thus of $v-\rho$ scaling. As a consequence, the relative contributions of active and passive shear to total mantle shear depends on the assumed $v-\rho$ scaling. This is expressed in the orientation of the mantle shear torque, which location varies along the great-circle connecting the active and passive shear torques as a function of their relative magnitudes (Fig. 3.6). Mantle shear torque orientations for $v - \rho$ scaling

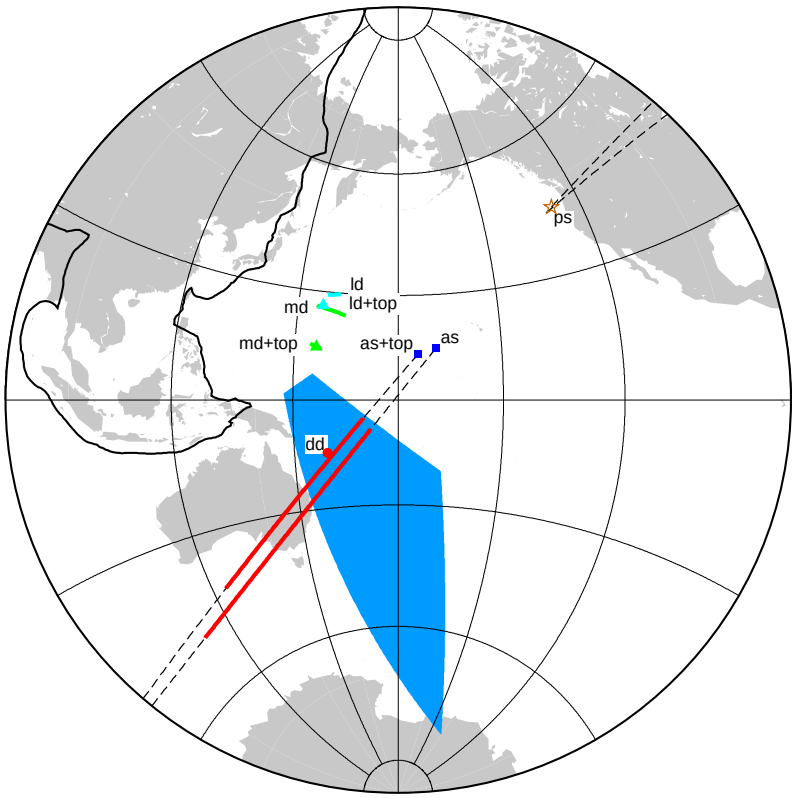

Figure 3.6: Sensitivity of mantle shear and LBF torque orientations to v-ρ scaling for tomographic model *ngrand* and viscosity profile *MF*. Closed/open symbols represent the positive/negative end of torque vectors. For key see Table 3.1. $+top$ stands for models including density forcing in top $250\ km$. Lines gives torque orientation ranges for constant v-ρ scaling factor range of $0.10 - 0.30$. Red dot, green/light blue triangles show results for depth dependent (dd) scaling factor (Simmons et al., 2009).

factors ranging between 0.10 and 0.30 form a $60°$ great-circle segment.

In order to evaluate the simplified $v - \rho$ scaling adopted above, we compare results with torques obtained with: 1) anomalies in the top 250 km of the tomographic model included and treated as fully thermal, 2) the use of the 1-D profile of Simmons et al. (2009) (Fig. 3.7a), which has been developed through simultaneous inversion of tomographic and geodynamic models. This profile allows for variations of $v - \rho$ scaling factor with depth, as would be expected in case of a depth-dependent compositional component in wavespeed anomalies. We find torque orientations of active shear are slightly altered when the top 250 km of forcing is added to the mantle buoyancy field driving the flow. Total mantle shear torques for the assumed $v - \rho$ scaling factor then range form a segment along a slightly different great-circle, parallel to results for models without forcing in the top part of the mantle (Fig. 3.6). Results obtained with the depth-dependent scaling factor of Simmons et al. (2009) are in good agreement with the constant scaling factor results (red dot in Fig. 3.6). In accordance with Bull et al. (2010), the pattern of mantle flow thus seems relatively independent of $v - \rho$ scaling. Overall, variations in mantle shear torque orientation perpendicular to the great-circle trend are largely inferior to variations parallel to it, and are thus dominated by the influence of $v - \rho$ scaling on the relative magnitude of passive versus active shear. This effect is well

captured by assuming a constant $v - \rho$ scaling factor and varying its magnitude.

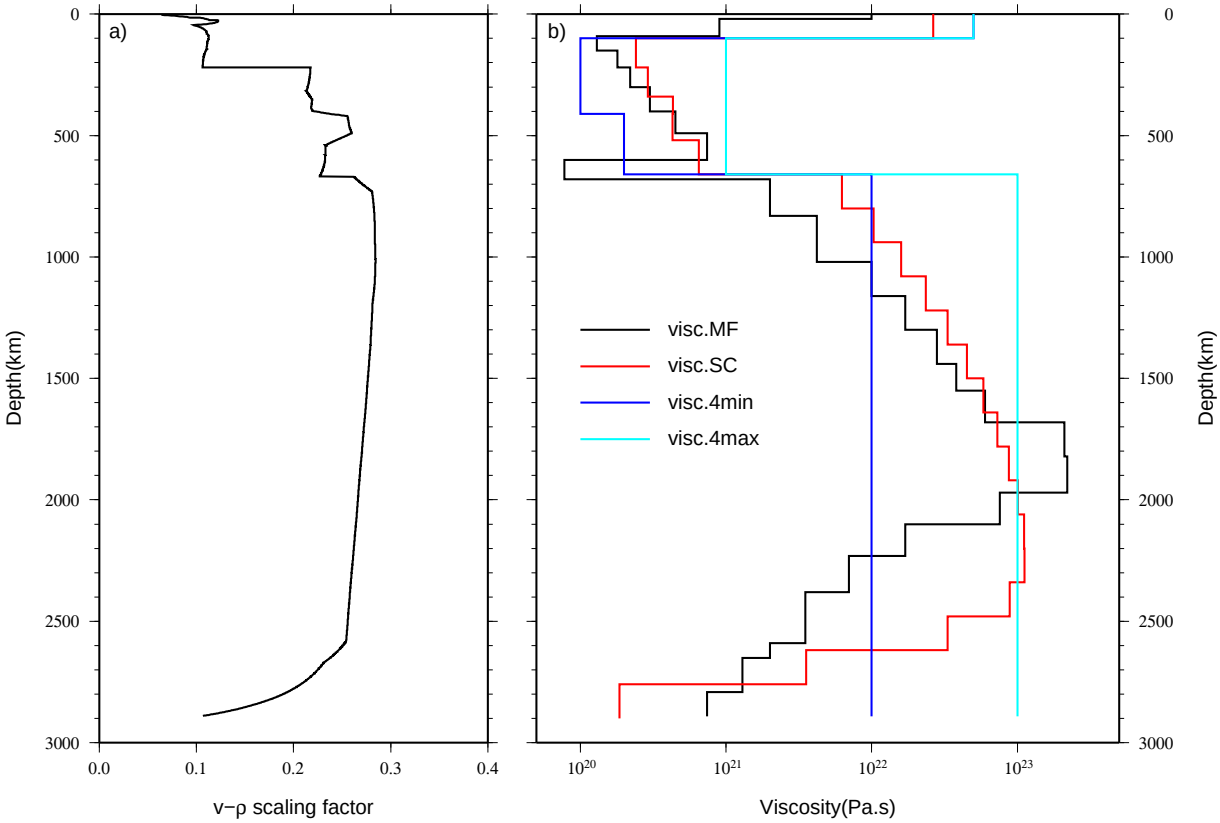

Figure 3.7: a) Depth-dependent v-ρ scaling factor (Simmons et al., 2009). b) Viscosity profiles used in this study. Key: $visc.MF$ (Mitrovica and Forte, 2004), $visc.SC$ preferred profile (Steinberger and Calderwood, 2006), $visc.4min$ and $visc.4max$ represent minimum and maximum values adopted in 4-layer models, inferred from Steinberger and Calderwood (2006).

LBFs for models *Mantle* and *Lithodens* depend on the normal component of mantle tractions and are thus affected by the assumed $v - \rho$ scaling. Torque results prove equally sensitive to the magnitude of $v - \rho$ scaling factor as to whether or not the top 250 km is included in the forcing (Fig. 3.6). This is in accordance with Simmons et al. (2009), who showed dynamic topography to be particularly sensitive to lateral variations in $v - \rho$ scaling factor for this top part of the earth due to compositional effects. Sensitivity of the LBF torque to $v - \rho$ scaling, however, is strongly inferior to that of the mantle shear torque, and is therefore unlikely to significantly influence the ability of a mantle flow model to balance Eurasia.

The dependence of torque results on $v-\rho$ scaling has consequences for the possibility of torque balance on Eurasia, which is only fulfilled for a particular range of $v - \rho$ scaling factors. We find similar $v-\rho$ scaling solution ranges for models in- or excluding forcing in the top 250 km (Fig. 3.8). We also find that results do not significantly depend on

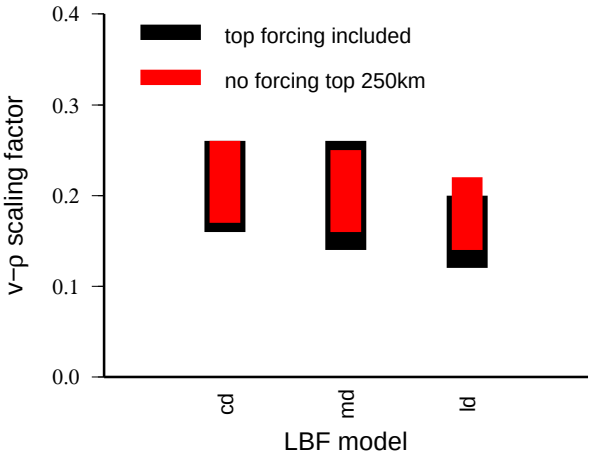

Figure 3.8: V-ρ scaling factor range producing mantle tractions that can balance the Eurasian plate as a function of LBF model (tomographic model *ngrand*, viscosity profile *MF*). LBF models: see Table 3.1

the LBF model. Our results indicate that the simplification of a constant scaling factor is warranted for the purposes of this study, and that sensitivity to the top 250 km of forcing is limited. In our subsequent analysis we therefore represent the uncertainty in $v - \rho$ scaling by varying the magnitude of a constant scaling factor and excluding the top 250 km of forcing.

3.4.3 Effect of viscosity

Viscosity is an important parameter governing mantle flow, but still carries large uncertainties, both radially and laterally. In this study, we restrict ourselves to radially symmetric viscosity profiles, which allow for mantle flow calculations using a semi-analytic approach (see section 3.8 for a discussion of possible implications of this assumption). We investigate the effect of mantle viscosity on torque results by working with two types of viscosity profiles. We use 4-layer models, consisting of a lithosphere, upper-mantle, transition zone and lower-mantle, to systematically study the effect of variations in mantle viscosity. Dark and light blue lines in Figure 3.7b represent the minimum and maximum values assumed for the different layers, which are inferred from Steinberger and Calderwood (2006). Furthermore, we use two radial viscosity profiles that were developed using geodynamic modelling and were shown to reproduce surface observables: profile *MF* (Mitrovica and Forte, 2004), which we have used so far, and profile *SC* (Steinberger and Calderwood, 2006) (Fig. 3.7b).

Viscosity affects the flow response to buoyancy forces and to imposed plate motion differently and therefore influences the relative weight of active versus passive tractions generated by mantle flow (Behn et al., 2004; Naliboff et al., 2009). Active tractions result from Stokes flow and are therefore sensitive to viscosity distribution but not to the absolute viscosity value. Passive tractions, on the other hand, can be approximated by Couette flow, and depend on the absolute magnitude of viscosity. Shear torque re-

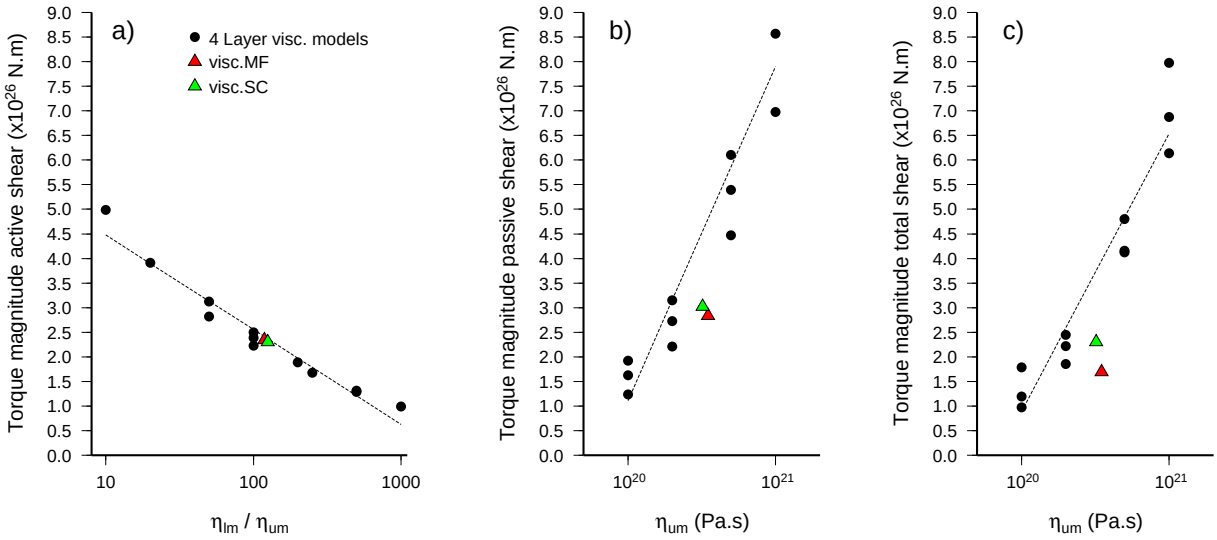

Figure 3.9: Dependence of torque magnitudes of a) active shear, b) passive shear and c) total mantle shear on (average) viscosity of relevant layer (lm: lower mantle, um: upper mantle) for all considered viscosity profiles (see Fig. 3.7b). Scatter along trends show second order sensitivity to the viscosity of the remaining layers. Results are shown for tomographic model *ngrand* and v-ρ scaling of 0.20.

sults obtained with the 4-layer viscosity models reflect these relations: the magnitude of the active shear torque is sensitive to the ratio of lower- and upper-mantle viscosity (Fig. 3.9a), whereas passive shear magnitudes are sensitive to upper-mantle viscosities (Fig.3.9b). Scatter along the trends show second order sensitivity to the viscosity of the transition zone. Passive shear magnitudes show a stronger dependence on viscosity than active shear so that the magnitude of the total mantle shear torque can approximately be related to the value of upper-mantle viscosity alone (Fig. 3.9c).

Torque orientations for passive and active shear (brown stars/blue squares in Fig. 3.10) vary slightly and moderately, respectively, as a function of viscosity profile, indicating that the pattern of mantle traction is also somewhat sensitive to viscosity. Orientations for total mantle shear torques vary strongly (red lines for $v - \rho$ scaling factor range $0.10 - 0.30$), reflecting the differences in ratio of passive and active shear torque magnitudes between models. The yellow zone in Figure 3.10 is a schematic representation of the possible orientation of the total mantle shear torque for the 4-layer viscosity models. Its elongated form following the great-circle trend connecting active and passive shear torques indicates that the dependence of mantle shear torque orientation on viscosity is dominated by the relative weight of the two contribution rather than by the pattern of the tractions. Results for the two more elaborate viscosity profiles *MF* and *SC* (thick lines in Fig. 3.10) are similar to the trend of the yellow zone and confirm this finding.

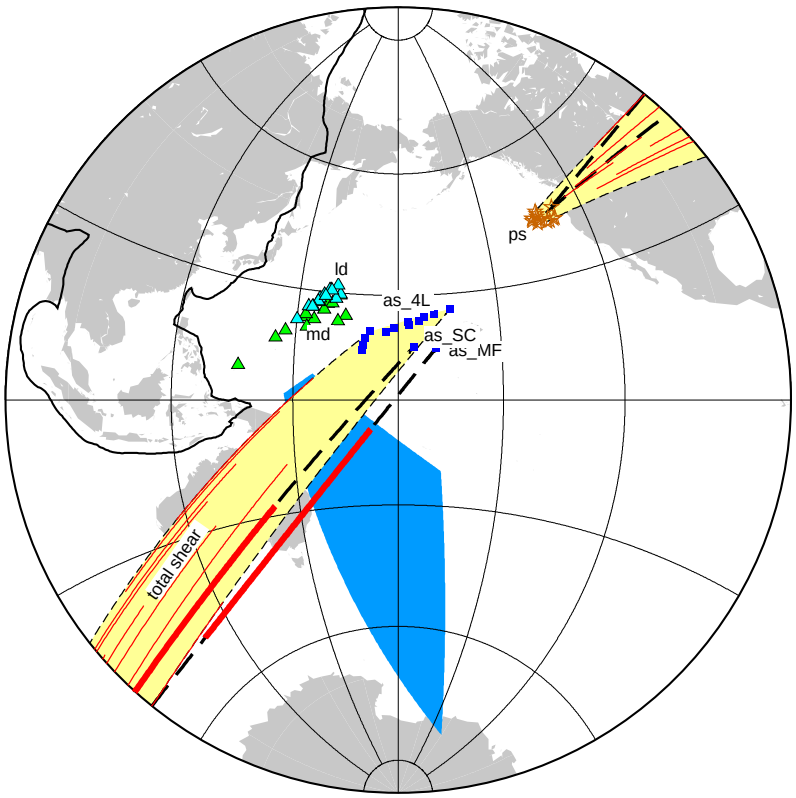

Figure 3.10: Sensitivity of mantle shear torque orientation to mantle viscosity structure for models based on tomographic model *ngrand*. Brown stars: negative end of passive shear (ps), dark blue squares: active shear (as), red lines: total shear torque orientations for v-ρ scaling factors $0.10-0.30$, green/light blue triangles: LBF model *Mantle* (md)/*Lithodens*(ld). 4-layer viscosity profiles produce shear torque that fall into the yellow elongated zone. Key: $4L$: 4-layer viscosity profiles, MF: viscosity profile (Mitrovica and Forte, 2004), SC: viscosity profile (Steinberger and Calderwood, 2006)

LBF torque orientations for model *Mantle* and *Lithodens* are somewhat sensitive to mantle viscosity (green and blue triangles respectively in Fig. 3.10 for $v-\rho$ scaling factor of 0.30), but do not show the strong dependence displayed by the mantle shear torque. The effect of viscosity on the ability of mantle flow models to balance the Eurasian plate is therefore mostly expressed through its influence on the torque magnitudes of passive and active shear. Because this effect is similar to that of $v-\rho$ scaling (see section 3.4.2) they can counterbalance each other. For every viscosity model a range of $v-\rho$ scaling factors can be identified that allows for torque balance on Eurasia. We find that this range, which we will refer to as the torque balance solution range (*TBSR*), varies with the product of upper- and lower-mantle viscosity (Fig. 3.11). Results for the 4-layer viscosity profiles (black, yellow and red stripes, depending on the LBF model used in the torque balance calculations) form a well defined linear trend. Because all models are derived from the same tomographic model, $v-\rho$ scaling factors yield a direct measure of the magnitude of the buoyancy forces that drive active mantle flow. Figure 3.11 then visualizes a trade-off relation between viscosity and the magnitude of mantle buoyancy forces. The more viscous the mantle, the higher buoyancy forcing is required in order to balance Eurasia. A more viscous upper-mantle increases passive shear, thus requiring stronger active flow to counteract its effect. A more viscous lower

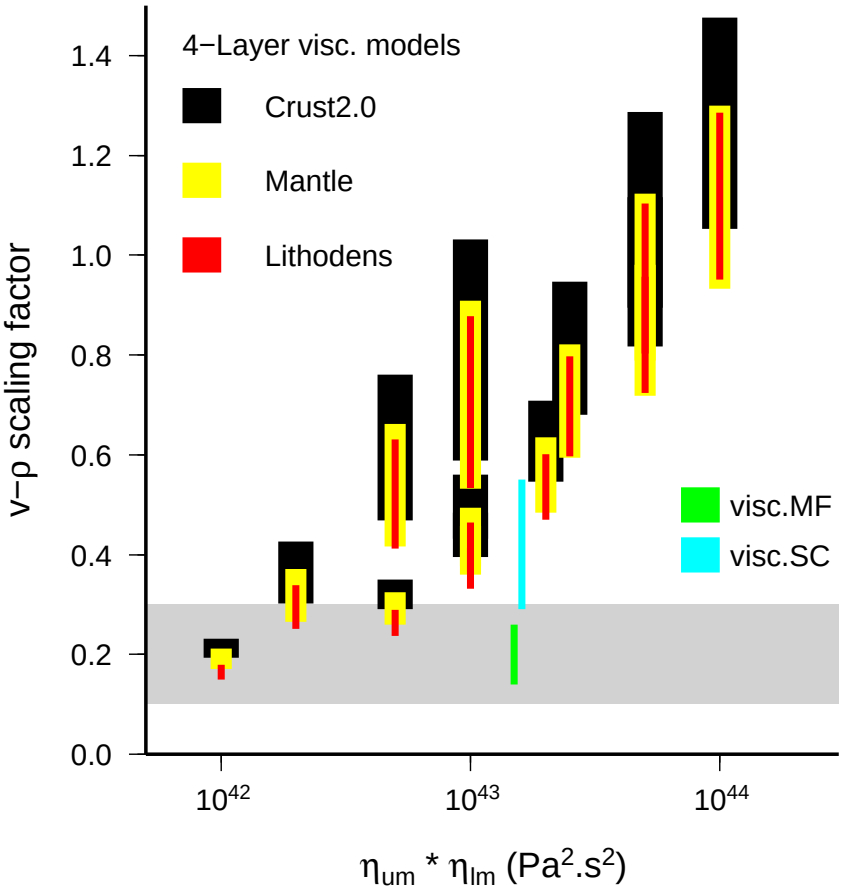

Figure 3.11: Torque balance solution range (TBSR) as a function of viscosity profile. For 4-layer viscosity models results obtained using the three LBF models are presented separately; for viscosity profiles *MF* and *SC* the total range encompassing results for the three LBF models is given. Results are shown for tomographic model *ngrand*. Realistic v-ρ scaling is indicated by gray range.

mantle is more difficult to bring into motion and requires higher forcing in order to generate the same amount of flow. Torque balance of Eurasia thus puts a strong constraint on the combination of mantle viscosity and the magnitude of mantle buoyancy forces.

TBSR results show a similar trend for the three LBF models. Overall, slightly weaker mantle buoyancy forcing is required in case of LBF models *Mantle* and *Lithodens* than for model *Crust2.0* (Fig. 3.11). These models include radial traction components from mantle flow models and the downhill forces caused by dynamic topography effectively amplify forcing due to active shear. The sensitivity of *TBSR* results to the LBF model, however, is strongly inferior to the sensitivity to viscosity. Our conclusions regarding the ability of mantle flow models to balance Eurasia are therefore not affected by the choice of LBF model, and we conclude our results are independent of uncertainties regarding compensation of topography at depth. In our further analysis, we will therefore present *TBSR* results that encompass the ranges for the three individual LBF models.

TBSR results for viscosity profiles *SC* and *MF* deviate from the trend of the 4-layer vis-

cosity models (Fig. 3.11). Although their averaged upper- and lower-mantle viscosities are relatively high, weak mantle buoyancy forcing is required for torque balance. Figure 3.9 shows that active shear torque magnitudes for models *SC* and *FM* fit perfectly with the four layer profiles trend, but passive shear torque magnitudes deviate significantly. Passive shear depends on the viscosity of the mantle just below the moving plates and is not well represented by average upper-mantle viscosities. Low asthenosphere viscosities in profile *MF*, and to some extent in profile *SC*, reduce passive shear relative to 4-layer profiles with corresponding average upper-mantle viscosities. As a result, torque balance is achieved for lower active shear magnitudes, and thus lower $v - \rho$ scaling factors. Although 4-layer viscosity profiles give similar representation of active mantle flow than more elaborate depth-dependent viscosity profiles flow response to plate motion differs. Details of the viscosity profile in the uppermost mantle therefore have significant influence on the ability of a mantle flow model to balance the Eurasian plate and need to be considered.

Overall, $v - \rho$ scaling factors that balance Eurasia fall above the range proposed by mineral-physics (gray band in Fig. 3.11) for most of the viscosity range. We find that for mantle flow models based on tomographic model *ngrand* only weak rheologies produce flow that can be reconciled with Eurasian lithospheric-dynamics. Partly, this can be attributed to the absence of a low viscosity asthenosphere in the 4-layer viscosity profiles. We will, however, show in the next section that this result also agrees with the low averaged anomaly magnitudes of tomographic model *ngrand* relative to other models.

3.5 Results as a function of mantle anomaly model

Tomographic studies have derived mantle velocity anomalies using different kinds of seismic measurements and techniques (review article: (Romanowicz, 2003)). Although these models show considerable correlation on wavelength longer than $5000\ km$, they differ in their smaller scale features (Becker and Boschi, 2002). Geodynamic density models derived from history of subduction are an alternative to tomographic models (Lithgow-Bertelloni and Richards, 1998). These models lack contributions from upwelling material but have been shown to successfully reproduce plate motion (Becker and O'Connell, 2001; Steiner and Conrad, 2007).

Here, we evaluate mantle anomaly models on their ability to produce flow that can balance the Eurasian plate. We analyse how mantle shear and LBF torques depend on the mantle anomaly model used to infer buoyancy forcing and investigate which mantle flow models meet the lithosphere-dynamics constraint outlined in section 3.2. We incorporate our previous findings regarding the influence of $v-\rho$ scaling and viscosity.

We consider six S-wave tomographic models (*S20RTS* (Ritsema and van Heijst, 2000), *ng* (Grand, 2002), *tx* (Simmons et al., 2007), *saw* (Megnin and Romanowicz, 2000), *wmani* (Kustowski et al., 2008) and *sb2l18* (Masters et al., 2000)), three P-wave tomographic models (*kvdh* (Li et al., 2008), *vox* (Boschi et al., 2007) and *bdp* (Antolik et al., 2001)) and two geodynamic density models inferred from subduction history (*lrr98d* (Lithgow-Bertelloni and Richards, 1998) and *stb00d* (Steinberger, 2000)). Tomographic models are converted to densities using a range of constant $v - \rho$ scaling factors and excluding forcing in the top $250\ km$ (section 3.4.2). We will refer to resulting mantle shear torques by the name of the model used for density forcing. In accordance with our finding that details of viscosity distribution are significant (section 3.4.3), we confine ourselves to viscosity profiles *MF* and *SC*.

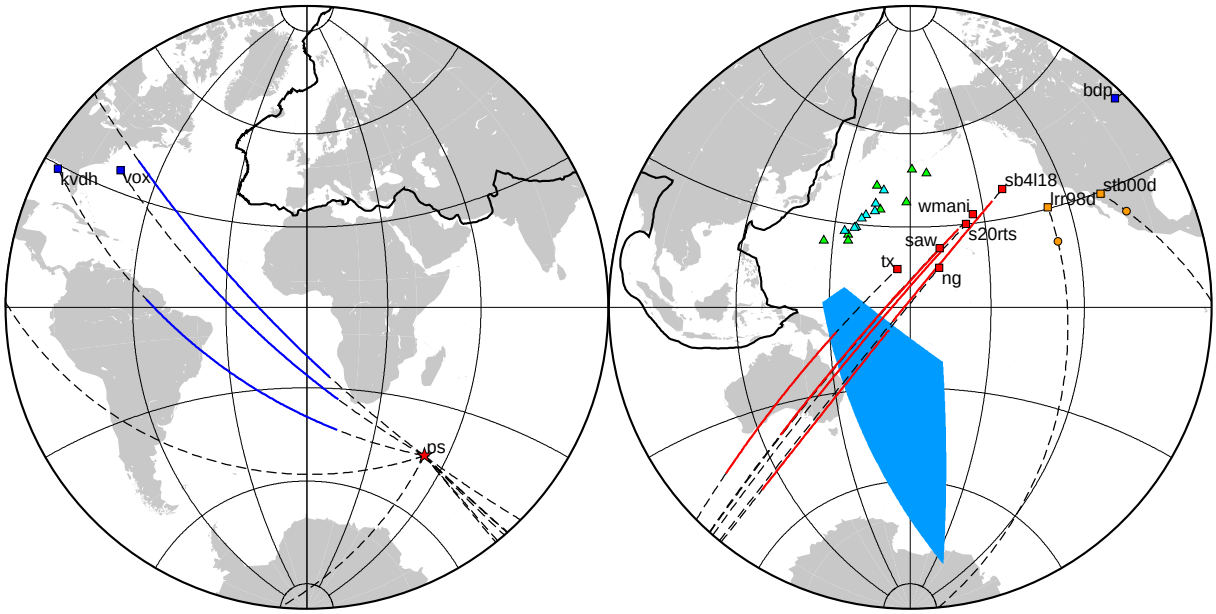

Figure 3.12: Torque orientations as a function of mantle anomaly model driving mantle flow for viscosity profile *MF*. Red/dark blue/orange: S-wave tomography/ P-wave tomography/ subduction-history models. Star: passive shear, squares: active shear, line/circles: total shear for constant v-p scaling factor of 0.10-0.30 (S-wave), 0.20-0.60 (P-wave) or no scaling (subduction-history). Green/light blue triangles: LBF model *Mantle/Lithodens*. For key mantle anomaly models see text.

Resulting torque orientations for viscosity profile *MF* are shown in Figure 3.12. Results for viscosity profile *SC* show the same characteristics. Active shear torques on Eurasia differ considerably for the various models and group by origin type. This agrees with conclusions from Becker and Boschi (2002), who analysed various tomographic and subduction-history models and concluded that both S- and P-wave models show a higher level of correlation with members of their own type than with each other.

Torque orientations for the subduction-history models compare significantly better to S-wave than P-wave models.

Total mantle shear torque orientations for each tomographic model are a linear combination of the corresponding active shear torque with the (model independent) passive shear torque, and vary along the connecting great-circles as a function of $v - \rho$ scaling (section 3.4.2). Subduction-history models directly describe density anomalies and should not require scaling. Results for S-wave tomographic models form a narrow band along the great-circle trend (Fig. 3.12), similar to results as a function of viscosity (section 3.4.3). This reflects differences in anomaly magnitude of the various models; models generating stronger active tractions produce total shear torques that lie further away from the passive shear torque. The spread perpendicular to the great-circle is relatively small, indicating that uncertainties in shear pattern are of second order, at least for the long wavelengths to which torques are sensitive.

LBF torques for models *Mantle* and *Lithodens* (green/light blue triangles in Fig. 3.12) align along an elongated zone. The torque distribution as a function of mantle anomaly model shows similarity to that of the active shear torque. As highs in dynamic topography correspond to up-wellings, around which flow is outwardly directed, and lows to down-wellings, with inward directed flow, downhill forces due to dynamic topography tend to follow the same pattern as mantle shear.

Combining the above results with torques for edge forces (section 3.2.2), we can assess the total torque on the Eurasian plate as a function of mantle anomaly model, and evaluate for which models torque balance is achieved. We find that mantle flow models driven by P-wave anomalies can not balance the Eurasian plate, regardless of the magnitude of buoyancy anomalies (and thus of $v - \rho$ scaling factor) or assumed viscosity profile. Our findings are similar to Becker and O'Connell (2001), who found that P-wave models lead to bad predictions of plate velocities, unless combined with additional buoyancy forcing from upper-mantle slabs. The failure of P-wave models could be due to a lack of radial resolution in the upper-mantle, causing seismically fast structures to mostly correlate with cratonic roots smeared out to great depth (Becker and Boschi, 2002; Becker and O'Connell, 2001). Additionally, our assumption of a constant scaling factor based on thermal origin of wavespeed anomalies is likely to be inappropriate for P-waves, which are particularly sensitive to compositional anomalies (Karato and Karki, 2001).

The possibility of torque balance on Eurasia with mantle tractions driven by S-wave anomalies depends on viscosity and $v - \rho$ scaling factor. For each S-wave tomographic model, torque balance of Eurasia is possible for a particular combination of viscosity and $v - \rho$ scaling (Fig. 3.13a). Models with viscosity profile *SC*, which contains a stiffer

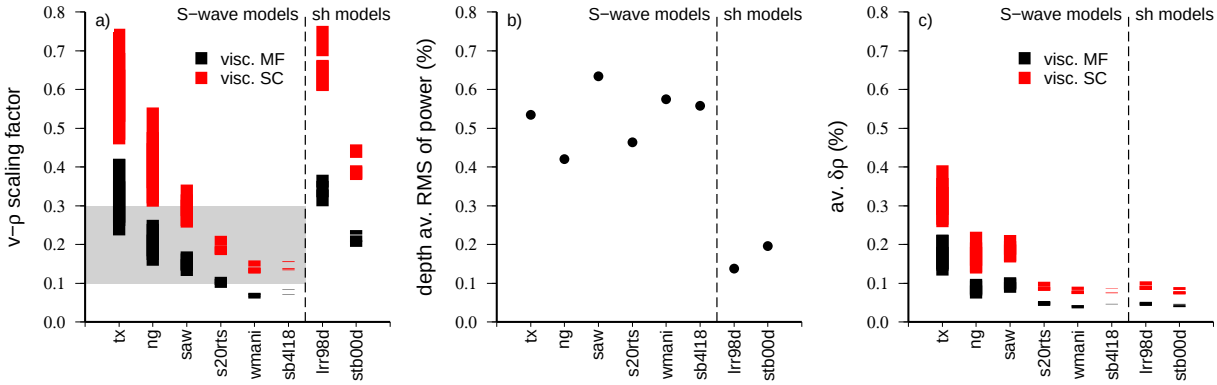

Figure 3.13: V-ρ scaling factor range (a) and buoyancy range (c) allowing for torque balance of Eurasia as a function of S-wave tomography model (presented ranges encompass results for the three LBF models). Subduction-history models (sh models) are included on the right hand side of the graphs, the vertical bar in (a) in this case represents down-scaling factors. Depth averaged RMS of power of the various mantle anomaly models is given in (b). For key mantle anomaly and viscosity models see text.

asthenosphere, require higher $v - \rho$ scaling factors than models with viscosity profile *MF*. The pattern as function of mantle anomaly model, however, is similar for both viscosity distributions. We find that all considered S-wave models can balance Eurasia in combination with $v - \rho$ scaling magnitudes that fit estimates from mineral physics (grey range in Fig. 3.13a) for at least one of the two viscosity profiles.

Subduction-history models *lrr98d* and *stb00d* both generate active shear that is too dominant to fulfil the torque balance constraint. Assuming uncertainties in anomaly amplitudes are stronger than uncertainties in anomaly pattern, we have solved for a uniform scaling factor that down-scales anomaly magnitudes in order to allow for torque balance. Results are presented alongside $v - \rho$ scaling factors of S-wave models in Figure 3.13a.

The trade-off illustrated by Figure 3.13a between mantle anomaly model and $v - \rho$ scaling factor suggests that the main uncertainty due to mantle anomaly models arises from uncertainty in the magnitude of anomalies rather than in their pattern. This makes sense because tomography anomaly amplitudes are strongly affected by choices made regarding damping in the inversion. In order to assess whether this is truly the case, we compare the average anomaly magnitude of the different mantle anomaly models. Following Becker and Boschi (2002), we quantify the average magnitude of a tomographic/subduction-history model by the depth averaged root mean square (RMS) power of the spherical harmonic coefficients (Fig. 3.13b, for more detail see Becker and Boschi (2002)). Multiplication of the depth average RMS power with the applied $v-\rho$ scaling factor then yields the average driving density anomaly (compared to PREM) for that specific mantle flow model.

Results for average density anomaly providing torque balance as a function of anomaly models are given in Figure 3.13c. We find that differences between models are indeed reduced after individual scaling from velocity to density. However, differences still persist. Model *tx* especially requires stronger density anomalies to balance Eurasia than other models on average. Because the effect of magnitude differences between models has been removed, remaining differences are caused by their specific patterns. Therefore, although uncertainty in mantle buoyancy pattern has a small effect on torque balance compared to uncertainty in buoyancy magnitude, we find it can not be dismissed. Trade-off between mantle anomaly model and $v - \rho$ scaling and/or viscosity is only partial. This implies that the choice for a specific anomaly model remains relevant for mantle flow calculations, not only on regional but also on plate-scale quantities.

In summary, we find that the mantle flow models based on S-wave tomographic models balance the Eurasian plate for realistic viscosity profiles and $v - \rho$ scaling. The subduction history models drive mantle flow that is too strong to fulfil the torque balance constraint, and can only balance Eurasia if down-scaled. Mantle flow driven by a buoyancy field derived from the P-wave models produces tractions that do not balance the Eurasian plate, regardless of viscosity or $v - \rho$ scaling.

3.6 Nature of lithosphere-mantle coupling

The magnitude of active versus passive shear stresses at the base of the lithosphere indicates whether lithosphere-mantle coupling is dominated by drive from the mantle or from the plates. This ratio is not well constrained through mantle modelling alone, because it varies significantly depending on the assumed mantle buoyancy forcing and viscosity field. Figure 3.14 shows that for the S-wave anomaly based models considered in this study (all based on physically realistic $v - \rho$ scaling and viscosity values) torque ratios of passive and active shear range between 0.25 and 2.7. Models thus vary between situations in which lithosphere-mantle interaction under Eurasia is governed almost entirely by plate motion or almost entirely by direct forcing from active mantle convection.

In the previous section, we have shown how uncertainties in mantle buoyancy and viscosity affect the ability of mantle flow to balance the Eurasian plate though their effect on the relative magnitudes of active and passive shear stresses. Models that successfully balance Eurasia can therefore provide insight into the nature of lithosphere-mantle coupling. We find that successful models are all characterized by active/passive torque magnitude ratios between 0.54 and 1.2 (bright coloured selection in Fig. 3.14). The torque balance constraint thus considerably confines the relative importance of

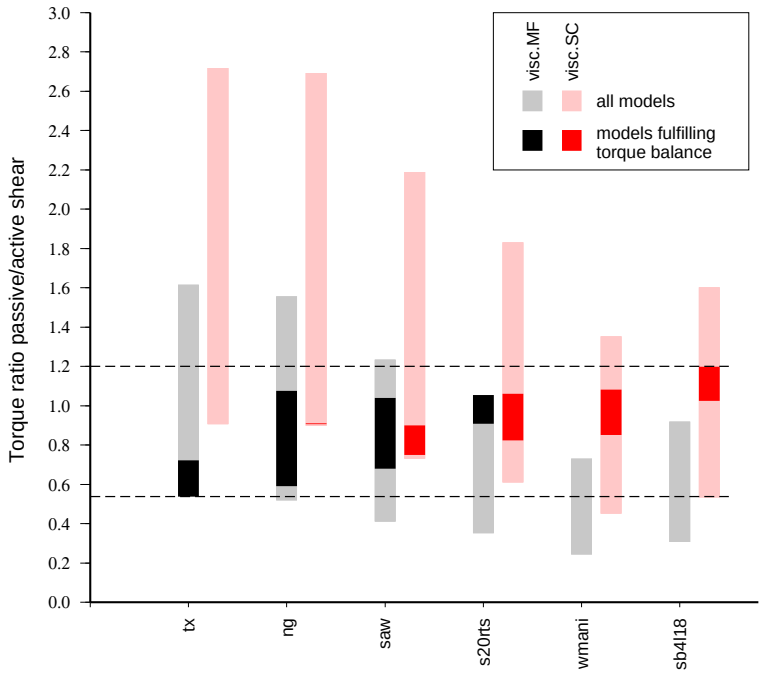

Figure 3.14: Torque magnitude ratio of passive and active shear for mantle flow models driven by S-wave anomalies. Shaded ranges shows values for all considered models (for physically realistic $v - \rho$ scaling factor range of 0.10 to 0.30 and viscosity profiles *MF* and *SC*). Results for models fulfilling the torque balance constraint are shown in bright colours and constrain the passive/active shear ratio to values between 0.54 and 1.2. For key mantle anomaly an viscosity models see text.

plate driven versus mantle buoyancy driven shear stresses under the Eurasian plate. Balance occurs only if the contribution of passive shear to the dynamics of Eurasia is comparable to that of active shear. Because the active and passive shear torques are not anti-podal (Fig. 3.12) their comparable magnitudes do not mean they entirely balance each other. The magnitudes of the total mantle shear torques (passive + active) are about half that of the two separate components, and require significant contributions from LBFs and edge force in order to be balanced (section 3.7.1).

Our comparison of passive and active shear magnitudes is based on torques, which are integrated values over the area of the Eurasian plate. Because the pattern of active shear is of considerably smaller wavelength than that of passive shear (Fig. 3.3), we find that locally, active shear stresses may be three to four times larger than passive shear stresses. Therefore, tractions at the base of the lithosphere are dominated by active mantle flow on a local scale, although tractions arising from resistance to plate motion are of the same importance on the plate scale.

Although Eurasian torque balance considerably confines the relative magnitudes of plate driven and mantle buoyancy driven shear stresses, some uncertainty remains because results depend on the tomographic model driving the flow (Fig. 3.14). As shown in section 3.5, buoyancy magnitude differences between models can be compensated by adapting $v - \rho$ scaling, but differences in the pattern of anomalies remain relevant. As a result, some scatter arises in the orientations of the active shear torques of the various models (Fig. 3.12). Models which active shear torques are located farther east

require a relatively stronger passive shear component to balance Eurasia.
Our results indicate that the contribution to the dynamics of Eurasia of passive, plate motion driven, shear stresses is comparable to that of active, mantle buoyancy driven, shear. Active tractions are expected to be of similar magnitudes globe wide. Passive tractions, however, are mostly governed by the absolute velocity of the topping plate. Because Eurasia is a relatively slowly moving plate, we expect passive shear stresses under faster moving plates to be considerably stronger and therefore to dominate over active shear stresses. This could explain how the dynamics of certain plates could be successfully described including an approximation of mantle tractions as a uniform shear against the direction of absolute plate motion (Cloetingh and Wortel, 1986; Wortel et al., 1991; Copley et al., 2010).

3.7 Which forces drive Eurasia?

3.7.1 Relative importance of mantle shear, lithospheric body forces and edge forces

Our analysis provides a range of mechanically consistent sets of forces acting on the Eurasian plate. This forms a strong physical basis to evaluate the role of different tectonic forces for the dynamics of Eurasia. We consider force sets including the different combinations of mantle flow and LBF models that have been shown to allow for torque balance (section 3.5). Each combination thereby requires a specific balancing torque contribution from edge forces (one specific orientation located inside the red zone of Fig. 3.2). We note that because the system is under-determined (7 unknown edge force magnitudes, 3 degrees of freedom), a specific edge force torque can result from different force distributions along the plate's boundary, which we do not specifically solve for.
We analyse the relative importance of mantle shear, LBFs and edge forces on Eurasia's dynamics by comparing the torque magnitudes of the individual force types with their scalar sum (the vector sum of the torques is implicitly zero because they form a balanced set). We find that results are very similar for all models: the edge force torque is consistently the strongest (Fig. 3.15). Edge forces account for almost half of the total torque magnitudes, regardless of the assumed mantle flow and LBF models. This is caused by the torque's orientations (Fig. 3.2 and Fig. 3.12). For all models, orientations of mantle shear and LBF torques are considerably closer to each other than to the total edge force torque. Therefore their contributions add up constructively: $|\overline{T_{ms}}|+|\overline{T_{LBF}}| \sim |\overline{T_{ms}}+\overline{T_{LBF}}|$ and balancing edge forces hence contribute almost half of the total. The important role we find for edge forces in the dynamics of Eurasia agrees

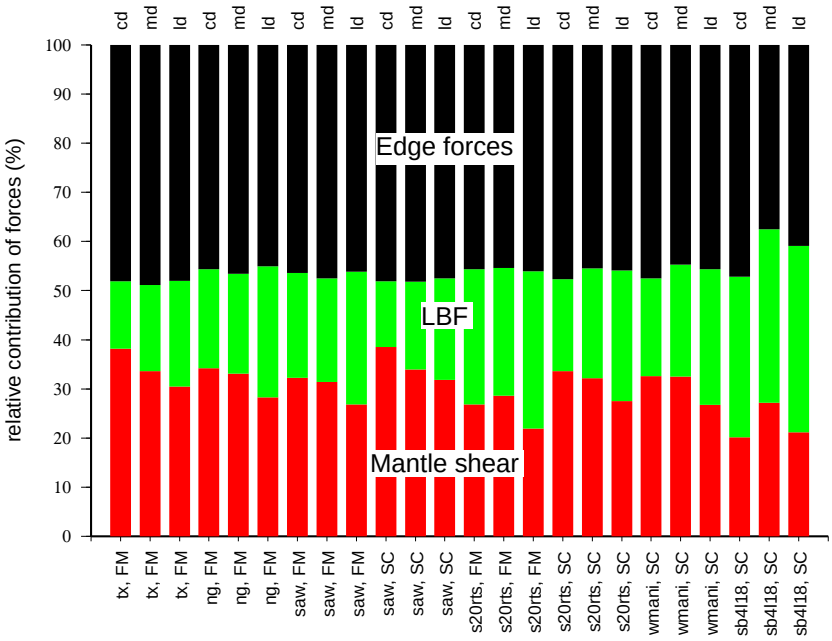

Figure 3.15: Relative magnitudes of mantle shear, LBF and edge forces torques for balancing forcing models (zero net torque), expressed as a percentage of their scalar sum. The lower horizontal axis specifies mantle flow model (Tomographic model, viscosity profile, for key see text), upper axis specifies LBF model (key see Table 3.1).

with results presented by Bird et al. (2008), who found that net edge force torques (referred to as side strength) are comparable to or stronger than mantle shear and LBF torques on most plates with large surface areas. The largest contribution to Eurasia's dynamics is thus provided by forces that are transmitted across plate boundaries.

The relative importance of mantle shear and LBFs is less well resolved because it depends on the assumed mantle flow and LBF models (Fig. 3.15). On average, the mantle shear torque is somewhat stronger, but we find mantle shear versus LBF torque magnitude distributions ranging from 75/25 % to 35/65 %. We note that forcing from mantle buoyancy forces underneath the lithosphere is represented in both terms: shear stresses contribute directly to the mantle shear torque whereas normal stresses affect LBFs. Generally, force models including dynamic topography directly from mantle flow modelling (based on LBF models *Mantle* and *Lithodens*) have a relatively stronger LBF contribution than models that don't (based on LBF model *Crust2.0*). As mentioned earlier, radial traction components in these models cause downhill forces that effectively amplify forcing due to active shear, thus requiring lower mantle buoyancy forcing (and thus mantle shear) to balance the plate (Fig. 3.11). Our results encompass results found by different mantle convection based studies. Neglecting dynamic topography, Becker and O'Connell (2001) found plates are driven for 70% by mantle buoyancy forces and 30% by lithospheric body forces, similar to earlier findings by Lithgow-Bertelloni and Richards (1998). Ghosh et al. (2008) pointed out that viscosity influences the relative strength of mantle shear and LBFs and found best matches to strain rate orientations for fifty-fifty forcing.

Overall, our analysis emphasizes the role of plate interaction in the mechanical balance of tectonic plates. Although our results regarding the relative weight of mantle shear and LBF are comparable to results from mantle convection based studies, we find an additional and dominant net-contribution from edge forces is required to balance Eurasia. Implicitly imposing a zero net torque contribution from edge forces, common in global models that solve for plate velocities, may be inappropriate.

3.7.2 Eurasian plate motion

The absolute motion of a plate is governed by the sum torque of the driving forces acting on it. With no significant slab pull and an averaged mantle shear not aligning with absolute plate motion (Warners-Ruckstuhl et al., 2010), identification of a main driving force for the Eurasian plate is not straightforward. To assess which forces contribute to drive the plate, we compare our torque results with the orientation of the Euler pole of absolute plate-motion. The sum torque of driving forces should parallel this Euler pole in order to drive Eurasia in the correct direction. Because our rheology lacks radial viscosity variations, net rotations of the lithosphere with respect to the mantle can not be excited (O'Connell et al., 1991) and the no-net-rotation reference frame (Argus and Gordon, 1991) is appropriate (for implications see section 3.8).

A summary of our results for the orientation of the various model forces is displayed together with the Euler pole of absolute motion of Eurasia in Figure 3.16. Ellipses represent the uncertainty range of the mantle flow dependent forces. Only models that allow for torque balance are represented. The orientation of the Euler pole is not matched by one single torque and we can not identify a single dominant driving force for Eurasia. Although the orientation of the active shear torque, which is the most prominent expression of mantle buoyancy forces, is consistent with that of a plate driving force, it does not explain observed plate motion on its own. As expected, passive shear is clearly a resistive force, with a torque orientation almost anti-podal to absolute motion.

Gravitational forces acting directly on the Eurasian plate are the most obvious driving forces. The sum torque of LBFs (including ridge push) and active shear is confined to orientations within the black shaded area in Figure 3.16. Models based on realistic $v - \rho$ scaling values (within the range suggested by mineral physics of $0.10 - 0.30$) are restricted to the black area. The zones do not coincide with the Euler pole illustrating that the two forces do not collaborate to drive Eurasia in the observed direction. An additional force must therefore play a role. The plate's motion resulting from active shear and LBFs can be deviated towards the observed direction by a torque with an orientation inside the red shaded area of Figure 3.16. The figure illustrates that such a

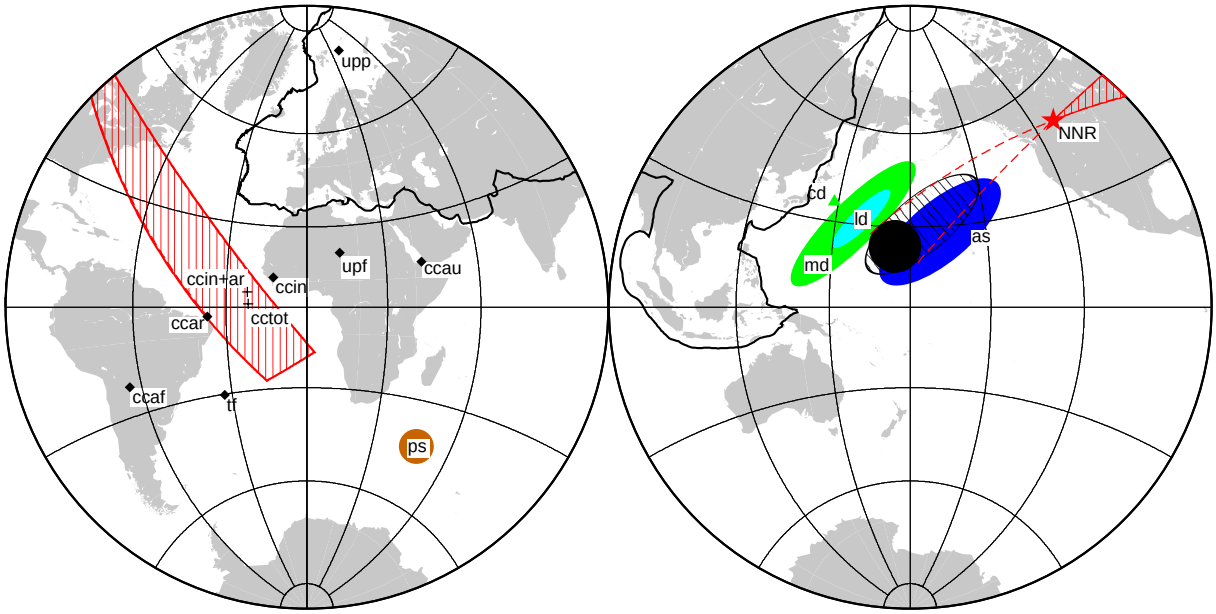

Figure 3.16: Analysis of plate driving forces. Torque orientations of the forces acting on the Eurasian plate are compared to the Euler pole of absolute motion (Argus and Gordon, 1991) (red star). Ellipses indicate uncertainty to mantle flow parameters for models that fulfil the torque balance constraint. Sum torques of active shear and LBFs generally fall into the shaded black ellipse, realistic models are confined to the black area. Red shaded area confines orientation of torques that can deviate the motion generated by active shear and LBFs towards the observed NNR motion. Continental collision on Eurasia's southern boundary complies. For key model forces see Table 3.1.

torque arises from collision forces at Eurasia's southern boundary. We find either uniform collision forcing along the southern continental boundary, or a force distribution generating a similar torque but allowing for stronger collision along the Indian boundary, can push the plate towards its observed trajectory. This important role for edge forces in governing the absolute motion of Eurasia agrees with results presented by Iaffaldano and Bunge (2009), who found in a global analysis that a considerable part of total plate motion changes during the last $10\ Myrs$ could be explained by changes in force transmission across plate boundaries.

The observed direction of motion is only achieved for certain magnitudes of collision forces and thus provides a constraint on this magnitude. Depending on the mantle flow and LBF model we find that an average continental collision force of 2.7 to $5.0 \times 10^{12}\ N/m$ is required to match the observed motion direction, which is the equivalent of 27 to $50\ MPa$ stress along a $100\ km$ thick boundary. Assuming contact area and forces to be twice as large on the collisional segment with India as on the rest of the boundary, we find force magnitudes of 4 to 6 and 2 to $3 \times 10^{12}\ N/m$, respectively, corresponding to stresses of 20 to $30\ MPa$. Those values agree with findings by Copley

et al. (2010), who analysed the forces governing the dynamics of the Indian plate and found collision forces on the contact with the Eurasian plate of 5 to $6\times10^{12}\ N/m$. Becker and Faccenna (2011) recently proposed that strong active mantle tractions related to an active up-welling push the Arabian and Indian plates northwards. This could provide the engine behind the large collisional forces that we find are crutial to the dynamics of the Eurasian plate.

3.8 Main uncertainties

Finally, we consider the uncertainties that arise from assumptions made in the assessment of edge forces, LBFs and mantle tractions, and discuss how they may affect our conclusions.

3.8.1 Edge forces

The confinement of the orientation of the total edge force torque (red area in Fig. 3.2, which we will refer to as solution area) is crucial for the resulting constraint on mantle forcing. We therefore evaluate how uncertainties in the modelling of edge forces may affect the orientation of the total edge force torque.

Our plate scale model is based on a simplified representation of the shape and nature of Eurasia's plate boundaries. For each plate boundary type, we work with a net force that represents the sum of force contributions by processes at and beyond the domain boundaries. We solve for the average magnitude of this net force using torque balance. The direction of this net force varies with the location along the plate boundary. In our model, this direction is imposed based on the underlying force contribution that is deemed to be the most important. Different perspectives/choices are possible, and a main uncertainty thus arises from the direction of forcing imposed in the model. Below, we therefore evaluate changes in the solution area for the net edge force torque by assessing the sensitivity to alternative choices for all plate boundary types.

Roll-back margins

Roll-back margins are expected to be dominated by an outward pull perpendicular to the boundary from the retreating plate, but likely experience resistance at the plate contact anti-parallel to the direction of relative plate motion. In case of oblique subduction, which is common along Eurasia's boundaries, considerable resistance rotates the net forcing direction. Introducing resistance at roll-back margins in our model shifts the roll-back torque orientation southward; in the extreme case of equal driving and resistive forcing magnitudes the torque shifts to a position close to the non-roll-back margins torque (Fig. 3.2). This effectively narrows the solution area of the total edge

force. Because balance of mantle tractions and LBFs consistently requires an edge force torque oriented in the most southern part of the solution area, uncertainty in the direction of forcing at roll-back margins is not likely to affect our conclusions.

Continental collision and non-roll-back margins

Stress transmission along plate boundaries may differ between shear and normal components, potentially rotating resisting forces at collisional boundaries compared to our model that assumes them to be equal. We investigated the extreme case that only normal forces are transmitted through the plate contact. We found that, due to the geometry of the southern boundary of Eurasia in relation to the direction of absolute motion, the effect of variations in collision forcing is minimal after integration. The total continental collision torque (assuming equal forcing per meter boundary on the entire continental collision boundary) is shifted 10° westward, only.

Transform boundaries

Transmission of normal stresses along transform boundaries would rotate forcing away from the imposed direction of shear. This force, usually referred to as transform push was neglected in our study. It has been shown not to influence the dynamics of the Juan da Fuca plate (Govers and Meijer, 2001). Adding a normal component at oceanic transform boundaries shifts the transform resistance torque northward, potentially narrowing the edge force torque solution area at its southern boundary. However, its influence on the solution area is limited because continental collision forces also generate torques that lie in its southern part.

Continental boundary with North-America

WR10 tested the sensitivity of the edge force solution area to boundary conditions on the unknown North-America Eurasia boundary segment and found the effect to be without significant consequences. Assuming that forces do not exceed the magnitudes along the remainder of the boundary, the orientation of the total continental collision torque shifts by a maximum of 10° when the North-America Eurasia boundary segment is added to it.

Torques of all edge forces may furthermore be affected by lateral variations in forcing, which are not taken into account in our simple parameterization, but may be considerable (Iaffaldano and Bunge, 2009). We expect the largest lateral variations to occur along the continental collision contact, which accounts for the largest proportion of the boundary and where lateral variations in thickness of the plate contact are probable.

We have therefore aimed to reduce the uncertainty that may arise from lateral forcing variations by allowing for different forcing magnitudes on continental collision segments as a function of the colliding plate. A test in which our different model forces were parameterized based on velocity dependent forcing did not significantly alter the total edge force solution area, providing confidence that our conclusions are not too sensitive to the exact edge force distribution.

Due to the considerable uncertainties in assessing the imposed direction of forcing described above, additional uncertainties in relative plate motion directions (DeMets et al., 1994) or exact plate boundary geometry are of second order and were not considered.

Overall, we conclude that local uncertainties in forcing affect the orientation of the total edge force torque only mildly and should not affect our conclusions regarding lithosphere-mantle coupling.

3.8.2 Lithospheric body forces

By working with three LBF models, based on different assumptions regarding the compensation of topography at depth, we have aimed to cover the uncertainty range in LBFs on the Eurasian plate. We realize this aim may not be fully achieved; especially the treatment of lateral variations in lithospheric mantle properties may have important effects that were not considered (Pascal, 2006). However, although the three models considered produce quite different force fields, their differences occur on small length-scales compared to the plate's size and only mildly affect the resulting torque on Eurasia. This indicates the LBF torque on Eurasia is well constrained.

3.8.3 Mantle flow modelling

Our mantle flow calculations do not include lateral viscosity variations (LVVs). The role of LVVs on mantle flow and tractions at the base of the lithosphere has been extensively investigated in recent years (Becker, 2006; Conrad and Lithgow-Bertelloni, 2006; Ghosh et al., 2010; Moucha et al., 2007); for a review see Becker and Faccenna (2009). Viscosity variations of around one order of magnitude underneath oceanic and continental regions and stiff cratonic roots reaching up to $400\ km$ depth have been shown to have an important effect on mantle dynamics in that they generate net rotation of the lithosphere (Zhong, 2001; Becker, 2006), absent in mantle flow calculations lacking LVVs. Several studies, however, have indicated that the effect of LVVs on the generated flow field may be restricted (Becker, 2006; Moucha et al., 2007). Conrad and Lithgow-Bertelloni (2006) explicitly analysed the effect of LVVs in the uppermost mantle on excited tractions at the base of the lithosphere and found that the direction of

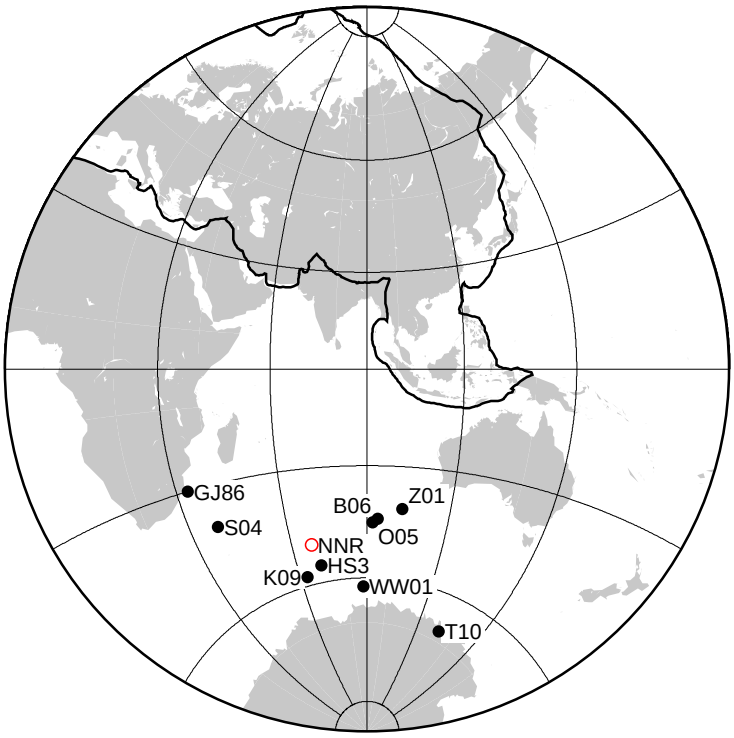

Figure 3.17: Net-rotation Euler poles from various studies as reported by Conrad and Behn (2010) (black dots: GJ86 (Gordon and Jurdy, 1986), HS3 (Gripp and Gordon, 2002), WW01 (Wang and Wang, 2001), Z01 (Zhong, 2001), S04 (Steinberger et al., 2004), O05 (O'Neill et al., 2005), B06 (Becker, 2006), K09 (Kreemer, 2009), T10 (Torsvik et al., 2010)). The red circle represents the negative end of the Euler pole vector of absolute motion of Eurasia in a NNR reference frame (NNR (Argus and Gordon, 1991))

shear varies little, although amplitudes scale with the viscosity increase at continental roots. Becker (2006) concludes that mantle flow models with prescribed plate motions result in similar flow fields in models with and without LVVs if the appropriate net rotation of the lithosphere with respect to the lower-mantle is taken into account, and that LVVs only play a minor role in large-scale features.

Since our analysis concerns plate-scale quantities, the main uncertainty in our modelled mantle tractions likely results from neglecting net rotation of the lithosphere. Lithospheric net rotation has been estimated based on hot-spot tracks (Gordon and Jurdy, 1986; Wang and Wang, 2001; Gripp and Gordon, 2002; Steinberger et al., 2004; O'Neill et al., 2005; Torsvik et al., 2010) , mantle flow modelling (Zhong, 2001; Becker, 2006) and anisotropic constraints (Kreemer, 2009; Conrad and Behn, 2010) and consistently indicates a westward drift of the lithosphere. Although the magnitude of rotation remains uncertain, recent estimates all suggest a relatively slow rotation of 0.1 to $0.2\ ^\circ/Myr$ (Conrad and Behn, 2010; Torsvik et al., 2010). With Eurasia also moving slowly ($0.24^\circ/Myr$ in the NNR reference frame), net rotation can potentially have a considerable effect on passive tractions at the base of the plate.

The Euler pole of lithospheric net rotation is approximately opposite to the pole of absolute motion of Eurasia in a NNR reference frame (Fig. 3.17). Therefore, any net rotation effectively decreases Eurasia's absolute motion without affecting its direction. Because passive tractions mainly result from resistance against motion of the Eurasian

plate itself (see figure 3.3b), we expect net rotation to simply reduce their magnitudes. Balance of the Eurasian plate requires a specific ratio of passive and active tractions (section 3.5), which means that active traction magnitudes required to balance the plate will scale accordingly. Net rotation will thus affect the absolute magnitude of mantle tractions but not their directions nor the relative importance of active versus passive shear. Because net rotation decreases the magnitude of the mantle shear torque it reduces its share in the total dynamics of Eurasia to the advantage of LBFs. The magnitude of the edge force torque is determined by the sum of the mantle shear and LBF torques; hence, its relative contribution is preserved. We conclude that our results regarding the nature of lithosphere-mantle coupling and the relative importance of edge forces to the dynamics of Eurasia are relatively insensitive to net rotation of the lithosphere. Our results for the absolute magnitude of balancing mantle tractions, however, are likely to decrease as a function of net rotation and should be regarded as upper-limits.

3.9 Conclusions

We use mechanical equilibrium of Eurasia to analyse tractions arising from global convective mantle flow models in the light of lithospheric dynamics. We show that current modelling approaches of lithosphere dynamics and mantle flow can successfully be integrated into a new, single-plate scale, combined approach. Results obtained through this combined approach, some new and others confirming earlier results, have the added value of the more complete approach. Our analysis yields a range of mechanically consistent sets of forces acting on the Eurasian plate, which provide insight in the role of the different forces in the dynamics of Eurasia. We conclude that:

1. Of the explored set of mantle anomaly models, mantle flow models based on S-wave tomography produce mantle tractions that meet the torque balance constraint for realistic radial viscosity profiles and $v - \rho$ scaling. Subduction history models drive mantle flow that is too strong to fulfil the torque balance constraint, and can only balance Eurasia if down-scaled. Mantle flow driven by a buoyancy field derived from P-wave anomalies produces tractions that do not balance the Eurasian plate, regardless of viscosity or v-ρ scaling.

2. Torque balance can only be achieved in case torques arising from passive (i.e. plate motion driven) and active (i.e. mantle buoyancy driven) shear are of similar magnitudes. Therefore, we conclude that lithosphere-mantle coupling is equally governed by resistance to plate motion as by active forcing from the underlying mantle. On a local scale, however, tractions at the base of the lithosphere are

dominated by active mantle flow due to their short wavelength character. Although the two shear contributions produces torques of similar magnitudes they do not balance each other.

3. A considerable net torque from edge forces is required to balance total mantle tractions and LBFs. This torque is stronger than the mantle and LBFs torques regardless of considered uncertainties. Hence, the largest contribution to Eurasia's dynamics is provided by forces originating on other plates and transmitted across plate boundaries. This result suggests that implicitly imposing a zero net torque contribution from edge forces, common in global models that solve for plate velocities, is inappropriate.

4. Our torque analysis shows that the largest uncertainties in mantle tractions at the base of the lithosphere arise from differences in flow magnitude rather than pattern between mantle flow models. Anomaly magnitudes in the tomographic/subduction history models, velocity-density scaling and viscosity all influence the relative magnitude of passive versus active tractions under the lithosphere, which is the key factor in fulfilling Eurasian torque balance. However, differences in mantle buoyancy patterns do remain significant and trade-off with $v - \rho$ scaling and/or viscosity is only partial. Our results do not significantly depend on uncertainties regarding compensation of topography with depth.

5. Although mantle flow and LBFs are the main drivers of Eurasia's absolute motion, continental collision at Eurasia's southern boundary significantly contributes by pushing the plate northward. Depending on the assumed mantle flow parameters, averaged collision forces along the southern boundary of 2.7 to 5.0×10^{12} N/m are required to match the observed direction of motion.

Acknowledgments

We thank Gene Humphreys and editor Bruce Buffet for their stimulating remarks which helped improve the manuscript, as well as Thorsten Becker for enlightening discussions and comments on an earlier draft, Nathan Simmons for discussions on velocity-density scaling and Bernhard Steinberger for discussion on mantle tractions in an early stage of this work. This manuscript has also benefited from careful reviews by Lucy Flesh and Greg Houseman as part of the evaluation of KWR's thesis. Figures were produced with the GMT software by Wessel and Smith (1991). Work supported by the Netherlands Organisation for Scientific Research (NWO, Earth and Life Sciences (ALW)), in the context of the EUROMARGINS EUROCORES Programme of the European Science Foundation, project 01-LEC-EMA22F WESTMED.

Appendix A Dynamic models of lithospheric body forces

The net horizontal force F generated by topography variations is the horizontal derivative of the geopotential energy (GPE) P, which is derived from the integrated vertical stress of a lithospheric column (Artyushkov, 1973; Fleitout and Froidevaux, 1982; Molnar and Lyon-Cean, 1988).

$$F_x = \frac{\delta}{\delta x} P \ , \quad F_y = \frac{\delta}{\delta y} P \tag{3}$$

$$P = \int_L^{-h} \left[\int_L^z \rho z' g \, dz' \right] dz \tag{4}$$

Where z is depth ($z = 0$ at sealevel), h is topography, L is the total depth, ρ is density and g is gravitational acceleration. In the case of isostatic equilibrium, L is the compensation depth at which pressure does not vary laterally. In our treatment of LBFs we allow for variations in dynamic support of the lithosphere by the mantle, expressed by pressure differences at depth L. Our results are sensitive to the choice of L, mainly in magnitude. To be consistent with mantle tractions obtained through mantle flow modelling assuming a constant lithospheric thickness of $100\ km$, the logical choice for L is $100\ km$.

We calculate the horizontal forces generated by topography variations using three end-member models for the lithospheric density distribution as a function of depth, on which we elaborate below. In contrast to the isostatically compensated models presented by Warners-Ruckstuhl et al. (2010), we treat the plate as one entity and include oceanic domains into the GPE calculations. In all models oceanic lithospheric thicknesses are deduced from the age of the lithosphere (Müller et al., 2008) and the boundary layer cooling model with constant basal heat flux, after Crough (1975), used in combination with parameter values derived by Wortel and Vlaar (1989).

A.1 Model *Mantle*

In model *mantle* we account for a dynamic contribution to topography generated by mantle convection. We use mantle flow modelling to calculated normal stresses on the base of the lithosphere (Milner et al., 2009).

In continental areas we assume that the part of the actual topography from ETOPO1 (Amante and Eakins, 2009) that is not dynamically supported is isostatically compensated within the crust. The pressure difference between lithospheric columns at the base of the lithosphere is taken to equilibrate normal stresses due to mantle flow (τ_m).

We work with constant crustal density ρ_{cr} and temperature dependent lithospheric mantle density $\rho_m(z)$, assuming a linear geotherm $T(z)$ throughout the lithosphere:

$$\rho_m(z) = \rho_a(1 + \alpha T(z)), \quad T(z) = T_a \frac{z+h}{L+h} \tag{5}$$

$$\rho_{av} = \frac{\rho_{moho} + \rho_a}{2}, \quad \rho_{moho} = \rho_a(1 + \alpha(\frac{T_a h_{cr}}{h+L}) \tag{6}$$

were ρ_a and T_a are the density and temperature of the asthenosphere, α is the thermal expansion coefficient, ρ_{av} is the average density of the lithospheric mantle and ρ_{moho} is the density at sub-Moho depth.
Corresponding crustal thicknesses h_{cr} are calculated by comparison with a reference column of crustal and lithospheric mantle thicknesses h_{cref} and h_{mref} at sea level with zero normal mantle tractions. For regions above sea level:

$$h_{cr} = h_{cref} + h + \frac{h\rho_{cr} + h_{mref}\rho_{avref} - \rho_{av} - \tau_m/g}{\rho_{av} - \rho_{cr}} \tag{7}$$

The GPE of a column above sea level then follows from eq. 4:

$$P/g = \frac{1}{2}\rho_{cr}h_{cr}^2 + \frac{1}{2}\rho_{moho}(L+h-h_{cr})^2 + \rho_{cr}(L+h-h_{cr})h_{cr} - \frac{1}{6}\alpha\rho_a(T_a - \frac{T_a h_{cr}}{h+L})(L+h-h_{cr})^2 \tag{8}$$

A similar equation can be formulated for continental regions below sea level, which we include for depths up to $-1\ km$ in order to exclude trenches where flexure is dominant and our assumptions are not appropriate.
In the oceans, lithospheric structure and reference bathymetry is deduced from secular cooling. We assume a constant $6\ km$ crustal layer above the cooling lithosphere. The height of the lithospheric column is subsequently altered by adding the dynamic topography component caused by normal mantle tractions. This means that ocean depth in this model does not necessarily correlate with observed bathymetry. For theoretical bathymetry due to cooling of the lithosphere h_{theor}, ocean depth becomes:

$$h = h_{theor} + \frac{\tau_m}{g(\rho_a - \rho_w)} \tag{9}$$

yielding GPE of an oceanic column of:

$$\begin{aligned} P/g = {} & \frac{1}{2}\rho_w h^2 + \frac{1}{2}\rho_{cr}h_{cr}^2 + \frac{1}{2}\rho_a(1+\alpha T_a)(h_L)^2 + \frac{1}{2}\rho_a(L+h-(h_{cr}+h_L))^2 - \rho_w h(L+h) \\ & + \rho_{cr}h_{cr}(L+h-h_{cr}) + \rho_{av}h_L(L+h-(h_{cr}+h_L)) - \frac{1}{6}\alpha\rho_a T_a(L+h-h_{cr})^2 \end{aligned} \tag{10}$$

Table 3. 2: Values used in LBF calculations

Parameter	Symbol	Value
Crustal density	ρ_c	$2850\ kg/m^3$
Crustal thickness reference column	h_{ref}	$35\ km$
Asthenospheric density	ρ_a	$3250\ kg/m^3$
Temperature asthenosphere	T_a	$1200°C$
Thermal expansion coefficient	α	$4 \times 10^{-5}\ /°C$
Maximum depth of integration	L	$100\ km$
Seawater density	ρ_w	$1000\ kg/m^3$

Forces on the interface between continental and oceanic regions are govern by the choice of reference values for continental lithosphere and oceanic ridges and are excluded from the calculations.

A.2 Model *Crust2.0*

Starting point for this model are seismological estimates of the lithospheric density structure. Topography, crustal thicknesses and densities are taken from model Crust2.0 (Bassin et al., 2000). The density of the lithospheric mantle linearly depends on temperature (eq. 5). Vertical stress integrals are calculated without assuming any kind of compensation. For areas above sealevel GPEs follow from equation 8, continental regions below sealevel yield GPE in a similar manner. Oceanic regions are treated in a way similar to continental regions, meaning actual bathymetry and crustal thicknesses are used. Lithospheric thicknessess are deduced from the theoretical secular cooling model used in model *Mantle* and GPE follows from equation 10, replacing the conventional ridge push force.

Variations in pressure of the total lithospheric column at the base of the lithosphere illustrate deviations from local isostasy (Fig. 3. 18). These variations should reflect normal stresses from the underlying mantle, although we note that lateral load variations on length scales up to $500\ km$ can be supported by flexural strength of the lithosphere. Variations in supporting normal stresses at the base of model *Crust2.0* correlate with crustal thickness variations and occur on small length scale. In order to compare this field with normal stresses from mantle flow modelling (Fig.3.3c, see main text), we apply a low-pass filter with the range corresponding to the mantle flow models ($l_{max} = 31$, wavelength larger than $1300\ m$).

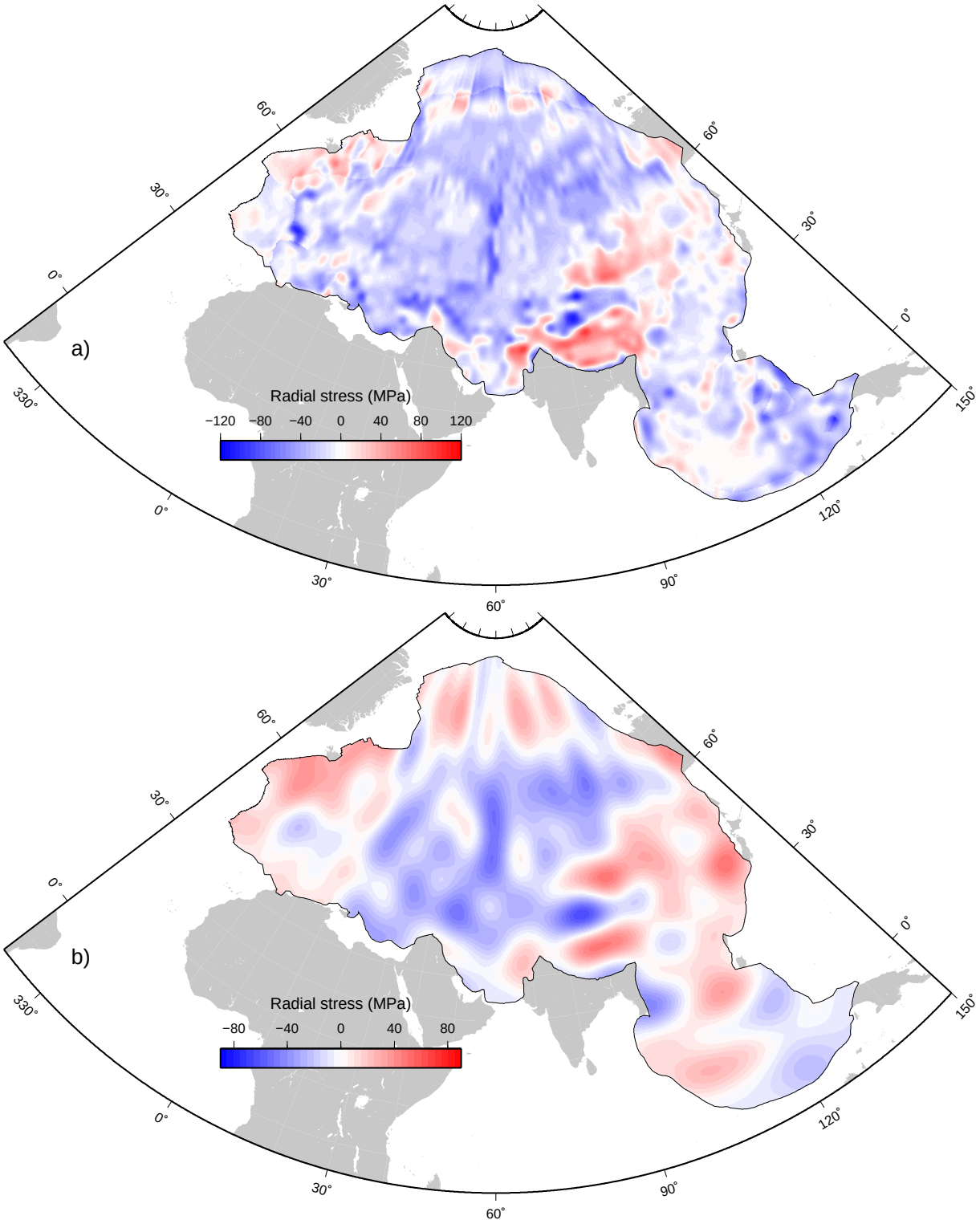

Figure 3. 18: a) Computed radial stress component at the base of the lithosphere that equilibrates model *Crust2.0*. Upward stress is positive. b) Same as a, but filtered for the wavelength range of our mantle flow model results ($l_{max} = 31$). Compare with Fig 3.3.

A.3 Model *Lithodens*

In this model, we combine crustal thickness and density from *Crust2.0* with normal mantle tractions from mantle flow modelling. In essence, this model is similar to model *Crust2.0*. However, averaged densities of the lithospheric mantle are adapted so that pressure overload from the lithospheric column matches variations in normal stresses from mantle flow modelling at its base. Lithospheric columns are compared to a reference lithospheric column at sea level with zero normal mantle tractions. For continents and continental margins we find ρ_m as follow: Above sealevel,

$$\rho_m = \frac{\rho_{cref} h_{cref} + \rho_{avref}(L - h_{cref}) + \tau_m/g - \rho_{cr} h_{cr}}{L + h - h_{cr}} \tag{11}$$

Below sealevel,

$$\rho_m = \frac{\rho_{cref} h_{cref} + \rho_{avref}(L - h_{cref}) + \tau_m/g - \rho_{cr} h_{cr} + \rho_w h}{L + h - h_{cr}} \tag{12}$$

As we now have constant lithospheric densities, GPEs are given by: Above sealevel,

$$P/g = \frac{1}{2}\rho_{cr} h_{cr}^2 + \frac{1}{2}\rho_{moho}(L + h - h_{cr})^2 + \rho_{cr}(L + h - h_{cr}) h_{cr} \tag{13}$$

Below sealevel,

$$P/g = \frac{1}{2}\rho_{cr} h_{cr}^2 + \frac{1}{2}\rho_{moho}(L + h - h_{cr})^2 + \rho_{cr}(L + h - h_{cr}) h_{cr} + \frac{1}{2}\rho_w h^2 - (L + h) h \rho_w \tag{14}$$

Oceanic regions are treated in a way similar to model *Crust2.0*. However, as for the continental regions we now adapt lithospheric densities in order to match pressure at depth L with normal traction components from the mantle flow model:

$$\rho_m = \frac{\rho_{cref} h_{cref} + \rho_{avref}(L - h_{cref}) + \tau_m/g - \rho_{cr} h_{cr} + \rho_w h - (\rho_a(L + h - h_{cr} - h_L)}{h_L} \tag{15}$$

GPE for oceanic regions is then:

$$\begin{aligned} P/g = \frac{1}{2}\rho_w h^2 + \frac{1}{2}\rho_{cr} h_{cr}^2 + \frac{1}{2}\rho_m (h_L)^2 + \frac{1}{2}\rho_a (L + h - (h_{cr} + h_L))^2 - \rho_w h (L + h) \\ + \rho_{cr} h_{cr} (L + h - h_{cr}) + \rho_m h_L (L + h - (h_{cr} + h_L)) \end{aligned} \tag{16}$$

Model densities for the lithospheric mantle are displayed in Figure 3. 19 (see main text for discussion).

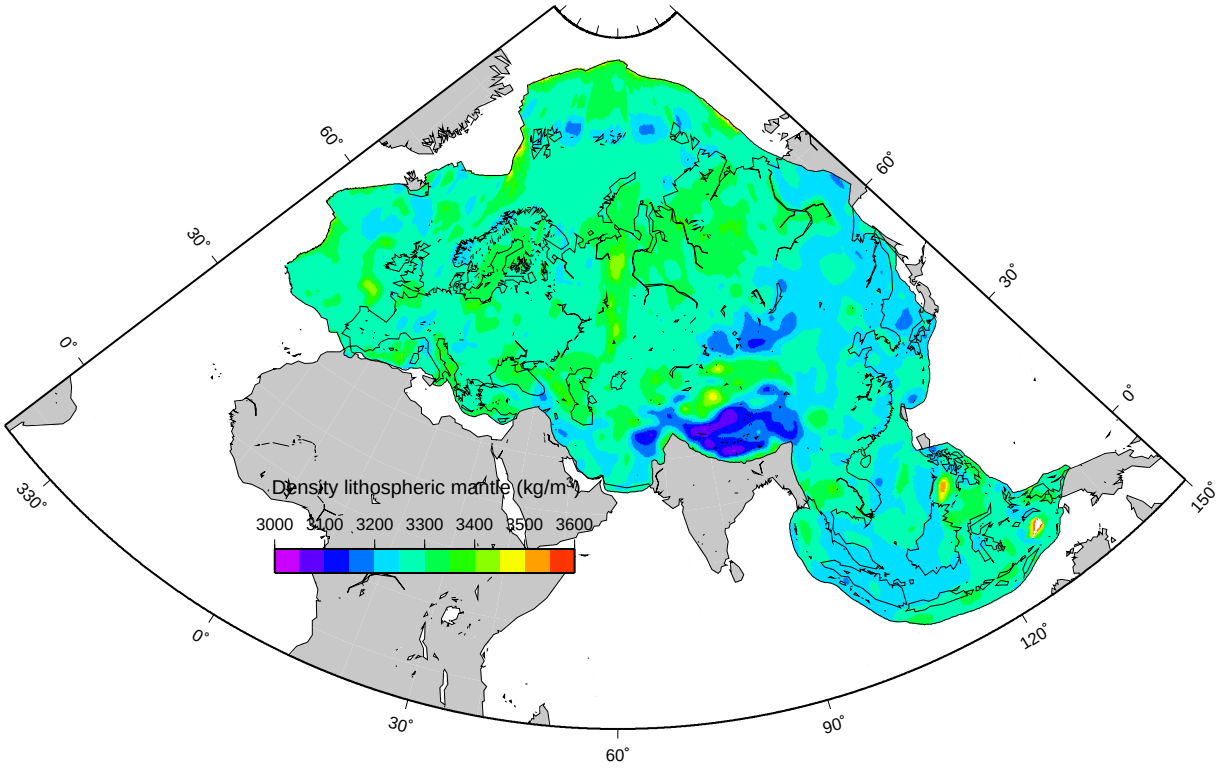

Figure 3. 19: Computed lithospheric mantle densities that equilibrate model *Lithodens*.

Chapter 4

Forces controling the stress field of the Eurasian plate: impact of collision forces

Abstract

For most tectonic plates, lithospheric torque balance models including simplified lithosphere-mantle coupling have successfully reproduced the large-scale stress field. This is not the case for Eurasia, suggesting interaction with the actively convecting mantle plays a major role in its dynamics. Mantle-convection based global studies account for more realistic mantle forcing on the lithosphere, but imply a physically ungrounded zero net contribution to the dynamics of each plate from forces due to plate interaction. In a previous study (Warners-Ruckstuhl et al. (2012), chapter 3 of this thesis), we presented a new, combined lithosphere-mantle modeling approach to the dynamics of tectonic plates and have established the combined importance of tractions from convective mantle flow and edge forces to the dynamics of Eurasia. Here, we extend our analysis and evaluate comprehensive, mechanically balanced, force models on the basis of their ability to reproduce observed stress orientations. We incorporate tractions from convective mantle flow modeling in a lithospheric model in which edge and lithospheric body forces are modeled explicitly and compute resulting stresses in a homogeneous elastic thin shell. For large parts of Eurasia observed stress directions are reproduced within data uncertainty. We find that the large-scale Eurasian stress field is governed by collision forces along the southern plate boundary. Stress observations require collision forces on the India-Eurasia boundary of $6 - 10\ TN/m$. Implication of mechanical equilibrium is that forces on the contacts with the African and Arabian plates amount to $1 - 2\ TN/m$. Uncertainties in the lithospheric density structure and pattern of mantle tractions do affect stress orientations locally but are of second order. Overall, we find that edge forces generate a larger net contribution to the dynamics of Eurasia than mantle shear stresses and lithospheric body forces.

4.1 Introduction

The intra-plate stress field is the result of forces acting on the lithosphere and as such contains valuable information on the dynamics of plate tectonics. The distinct long wavelength character of the observed stress field (Zoback, 1992) suggests a dominant role for plate tectonic forces and transmission of stresses over long distances. A satisfactory model of the forces acting on the lithosphere should therefore explain the dominant features of the stress field. Thus far, no such model has been presented for

the Eurasian plate.

Studies modeling the large-scale stress field commonly follow one of two different approaches. The emphasis is either on the lithosphere, over-simplifying interaction with the underlying mantle by basing it on absolute plate motion (Forsyth and Uyeda, 1975; Wortel et al., 1991; Bird, 1998; Bird et al., 2008), or on the convecting mantle, unwarrantedly implying a zero net torque (integrated forces) on each plate from edge forces due to plate interaction (Steinberger et al., 2001; Lithgow-Bertelloni and Guynn, 2004; Ghosh et al., 2008; Forte et al., 2010; Naliboff et al., 2009). Although the lithosphere-based approach has been quite successful in reproducing the large scale stress field for many tectonic plates (Indo-Australia (Cloetingh and Wortel, 1986; Reynolds et al., 2002), South-America (Meijer et al., 1997; Coblentz and Richardson, 1996), North-America (Richardson and Reding, 1991; Humphreys and Coblentz, 2007), Africa (Coblentz and Sandiford, 1994)), this is not the case for Eurasia (Goes et al., 2000). Global mantle based studies also did not produce particularly good results for the Eurasian part of their models (Steinberger et al., 2001; Lithgow-Bertelloni and Guynn, 2004). The difficulty of capturing the forces acting on the Eurasian plate illustrates that its dynamics can not be approximated by concentrating on either the mantle or the lithosphere, but is governed by a combination of the two (Warners-Ruckstuhl et al., 2010, 2012).

To quantify the forces generating the large-scale stress-field of the Eurasian plate we therefore focus on the lithosphere as well as the underlying mantle. To this end, we merge the strong points of the two classical modeling approaches into a new, combined approach, which we recently presented in Warners-Ruckstuhl et al. (2012) (hereafter referred to as WR2011, chapter 3 of this thesis). This approach incorporates tractions from convective mantle flow modeling in a lithospheric plate-scale model in which edge forces and lithospheric body forces (LBFs) are included explicitly. It has the advantage that all forces acting on the plate are simultaneously included in the torque balance calculations, unlike in mantle-oriented global approaches were, generally, edge forces implicitly generate a zero net torque on each plate (Steinberger et al., 2001; Lithgow-Bertelloni and Guynn, 2004). Combination of lithospheric and mantle modeling was thus far performed at a global scale (Becker and O'Connell, 2001; Conrad and Lithgow-Bertelloni, 2002; Iaffaldano and Bunge, 2009). By focusing on a single plate, our analysis allows for a more detailed resolution of edge forces, which were shown to approximately cancel out globally (Becker and O'Connell, 2001). As will be argued in this study, edge forces play a key role in stressing Eurasia.

Our analysis builds on WR2011, where we analyzed torques arising from edge forces, LBFs and mantle tractions on the Eurasian lithosphere. We concluded that only spe-

cific torque combinations result in mechanical equilibrium and successfully account for Eurasia's absolute motion. Here, we evaluate force distributions corresponding to these successful torques by making use of the stress field. We extend our knowledge regarding the forces acting on Eurasia by 1) solving for the magnitudes of edge forces along Eurasia's boundary and 2) evaluating different LBF and mantle flow models that could not be distinguished on the basis of torques but differ in their distribution of forces.

The initial response of rocks to loading is to deform elastically, resulting in stresses that may subsequently drive permanent deformation processes. We focus on constraining forces governing the lithospheric stress field and restrict ourselves to modeling of the first-step: computing elastic stresses. These elastic stresses represent the potential for permanent deformation. The next step of connecting these stresses to kinematic observations (velocities, strain and rotation rates) requires insight into the rheological properties of the lithosphere and is beyond the scope of this paper. We evaluate our elastic stress models based on present-day stress directions from the World Stress Map project (Heidbach et al., 2008). Although observed stresses have likely been subject to relaxation as a result of permanent deformation, stress directions are not affected by viscous relaxation or slip on a network of randomly oriented faults that isotropically reduces stress magnitudes. Directions of stresses in our models should therefore coincide with observed stresses in most regions. Stress directions are, however, affected by slip on a single major fault. We will therefore test the sensitivity of our results to major faults inside our model domain.

Several previous stress modeling studies have addressed the European part of the Eurasian plate (Grünthal and Stromeyer, 1992; Gölke and Coblentz, 1996; Jarosiński et al., 2006). These studies successfully reproduced observations in western Europe by truncating the plate and imposing a no-slip condition on the chosen boundary. They identified ridge push and African collision as the principal controllers of the first-order stress field. The resulting tractions on the fixed intra-plate boundary should represent the forces on the model domain by the remainder of the Eurasian plate. The problem is that there is no means of verifying their physical correctness and consistency with the nature of plate boundaries on the rest of the plate, i.e., boundary tractions are merely fitting parameters. We avoid this problem by working with the whole Eurasian plate; it is a natural mechanical unit where boundary tractions stem from physical processes. The whole Eurasian plate approach by Hieronymus et al. (2008) in a box-like model geometry focused on the effects of rheology on intra-plate deformation and stress relaxation. The stresses that drive visco-plastic deformation, however, result from an over-simplified force set that is not physically constrained. With this study we aim

at providing a model of the dynamics of Eurasia where no arbitrary forces are implemented, but in stead mechanical equilibrium is used to constrain the total set of forces acting on the plate. Because the stress field is sensitive to the distribution of forces rather than to their integrated value, stress observations allow for a strong test for our force models. This test enables us to resolve the relative importance of mantle versus lithospheric forces to the dynamics of Eurasia.

4.2 Observations

The World Stress Map 2008 data release (WSM) (Heidbach et al., 2008) provides information on the current stress field, obtained from various sources including earthquake focal mechanisms, borehole breakouts and geological field observations of recent and active faulting. The available data concerns stress directions and does not have a depth dependence. We therefore take the data to represent depth-averaged stress directions. The data coverage for Eurasia is highly uneven (Europe, the whole southern boundary, the Tibetan plateau and the Baikal region are densely sampled whereas extensive parts of central Asia lack any indicators). To prevent densely sampled regions entirely controling plate-wide evaluations of model results we average directions of most compressive horizontal principal stress ($S_H max$) over $1^\circ \times 1^\circ$ intervals. We use weight-factors of 3, 2 and 1 for A, B and C quality data of the WSM, respectively (Fig. 4.1). Averaging of the WSM data has the advantage of distributing the weight of the data more evenly over the regions where data are present without interpolation or smoothing, thus preserving local variations in stress orientation. The chosen interval size controls the relative weight of regions with high concentrations of data in average model misfits. We have checked that our conclusions are not affected by this choice.

4.3 Force modeling

4.3.1 Geometry and plate boundaries

The intra-plate stress field is critically sensitive to choices of plate geometry and plate boundary forcing on horizontal length scales exceeding a few hundred kilometers. We perform calculations on the model Eurasian plate introduced by Warners-Ruckstuhl et al. (2010) (Fig. 4.1). This model is based on major plate boundaries (Bird, 2003) on which plate boundary types can readily be identified. The model domain includes several microplates, e.g. in SE Asia, Okinawa, Birma, Aegean and Anatolia. Major internal faults may affect the transmission of stresses and are incorporated in some of our models. They do not affect torque balance calculations because forces across internal faults oppose each other and do not generate a net torque.

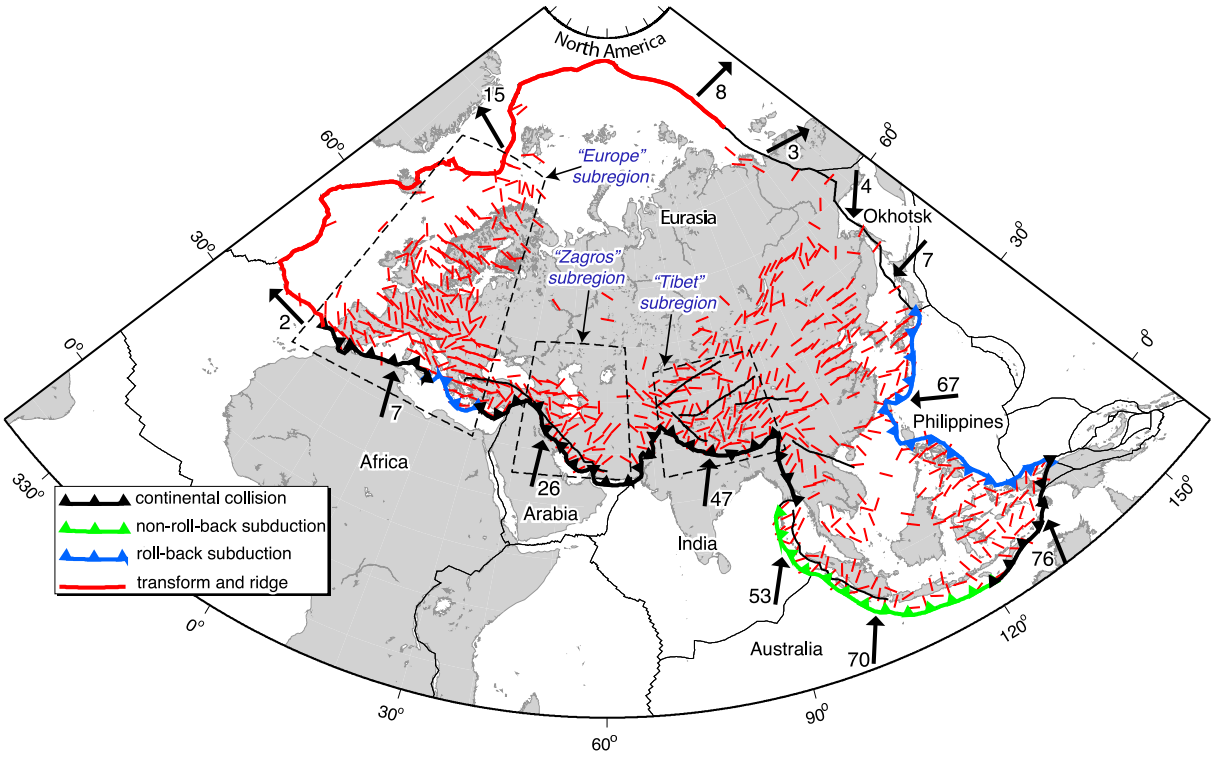

Figure 4.1: Boundary types and internal faults (thin black lines) of our model Eurasian plate. Arrows denote relative motion of adjacent plate with respect to Eurasia according to NUVEL-1a, rate of motion is indicated in mm/yr. Red bars indicate average directions of most compressive horizontal principal stress. Dashed rectangles enclose sub-regions in which we separately evaluate model stresses.

Following Warners-Ruckstuhl et al. (2010), the type of forcing on Eurasia's boundary is based on tectonic setting (Fig.4.1). We distinguish between four edge force types (Fig. 4.1): 1) transform fault resistance on the ridge and transform boundary (red line), 2) continental collision force on the segments colliding with Africa, Arabia, India and Australia (black triangles), 3) forces at trench roll-back margins (including the effect of the narrow section showing slab reversal in Taiwan) (purple triangles) and 4) forces at non-roll-back margins (orange triangles). The boundary between continental North-America and Eurasia (black line) is not classified because the exact boundary is unclear both in location and nature due to negligible relative velocities and the absence of seismicity or recent tectonic features (Chapman and Solomon, 1976).

4.3.2 Model forces

As input for the stress modeling we consider mechanically consistent sets of forces acting on the Eurasian plate consisting of edge forces, LBFs and mantle tractions. Our analysis builds upon previous work [WR2011], in which we presented various models

of LBFs and mantle flow and analyzed their ability to mechanically balance the total edge force torque on the Eurasian plate. In this study, we consider combinations of the successful models, which are shortly described below. We then continue beyond our previous work by specifically solving for the the unconstrained magnitude of edge forces using the torque balance equation (section 4.3.3).

Mantle tractions are calculated using global mantle flow models driven by tomographically derived buoyancy anomalies and topped by moving plates. We use the graphical user interface SEATREE (Milner et al., 2009), which computes Stokes flow in a radially varying viscous mantle through an implementation of a semi-analytic propagator matrix approach (Hager and O'Connell, 1981) by Becker et al. (2006) based on Steinberger (2000). We account for two components of forcing on the lithosphere: direct forcing by shear stresses and indirect forcing by normal stresses that induce dynamic topography and affect LBFs (Hager et al., 1985; Lithgow-Bertelloni and Silver, 1998). We consider mantle flow models that were shown to successfully balance the Eurasian plate [WR2011]. These models are based on S-wave tomographic anomalies and generate tractions on the lithosphere that have comparable contributions from buoyancy forces inside the mantle and from plate motion (for more information see WR2011).

LBFs result from horizontal pressure gradients in the lithosphere caused by lateral variations in topography and density structure inside the lithosphere (Artyushkov, 1973). Normal stresses from the underlying mantle influence LBFs by inducing dynamic topography, which were shown to have an important impact on the stress field (Steinberger et al., 2001; Lithgow-Bertelloni and Guynn, 2004). LBFs can be fully quantified when the density structure of the lithosphere is known. However, uncertainties are significant in continental areas and have a large effect on the LBF distribution in Eurasia [WR2011]. Following WR2011, we therefore consider three LBF models, where the uncertainty in density structure is either projected into the crust, into the lithospheric mantle or into dynamic mantle stresses at the base of the lithosphere. To remain consistent with the use of radially stratified mantle flow models we assume a constant base of the lithosphere, taken to be at $100\ km$ depth. Ridge push, sometimes incorrectly implemented as an edge force, results from lateral variations in the density structure of oceanic lithosphere and is an integral part of all three LBF models. We give a short description of the LBF models and refer to WR2011 for more details. LBF model *Mantle* is based on dynamic topography deduced from mantle flow modeling. The part of the actual topography (ETOPO1 (Amante and Eakins, 2009)) that is not dynamically supported is assumed to be isostatically compensated by variations in crustal thickness. LBF model *Crust2.0* is based on crustal thicknesses and densities of seismological model Crust2.0 (Bassin et al., 2000) and assumes that deviations from isostatic equi-

librium are dynamically supported at the base of the lithosphere. LBF model *Lithodens* combines crustal thickness and density from *Crust2.0* with normal stresses from mantle flow modeling and assumes that remaining lateral topography variations are caused by density variations within the lithospheric mantle.
Edge forces result from mechanical interaction with neighboring plates, and although their directions can be estimated with some confidence, their magnitudes are uncertain. Following Forsyth and Uyeda (1975), we impose edge force orientations and assume a constant magnitude per unit length of boundary for each edge force type, which we solve for by means of the torque balance equation. Edge force types are based on tectonic setting (see section 4.3.1) and represent the averaged contribution of processes at and beyond the boundary domain. These forces may arise from a combination of forcing mechanisms; the force magnitudes solved for through torque balance quantify the net forcing along the boundary segments. Transform fault resistance, continental collision and forces at non-roll-back subduction segments arise from friction at the plate contact and are modeled anti-parallel to the direction of motion relative to the adjacent plate (NUVEL-1a (DeMets et al., 1994)). Forces at subduction roll-back segments are expected to be dominated by suction of the retreating slab and are modeled outward and perpendicular to the trench.

4.3.3 Torque balance solutions

Mantle shear stresses and LBFs are fully quantified and constrain the orientation and magnitude of the total edge force torque through torque balance. Each edge force torque can, however, result from a range of force distributions along the plate's boundary so that the solution to the torque balance equation consists of a range of models. Collision forces along the southern plate boundary were shown to play a dominant role in the dynamics of Eurasia [WR2011] and may considerably vary laterally due to changes in plate contact thickness. As a first step, we therefore explore the torque balance solution range by solving for individual magnitudes of the collision forces on the combined African/Arabian, the Indian and the Australian plate contact while systematically varying the magnitudes of the other edge forces. Thereby: i) we neglect forcing on the ill-constrained continental boundary with the North-American/Okhotsk plate; ii) we vary resistance at oceanic transform boundaries between 0 and $1\ TN/m$, and iii) we assess forcing at roll-back margins between 0 and $0.5\ TN/m$. For all combinations of mantle flow and LBF models torque balance is namely only achieved for low force magnitudes in southeast Asia. Furthermore: iv) we solve for forces at non-roll back margins simultaneously with the force on the Australian collisional boundary because the two forces show a trade-off due to their similar torque orientations. Force

magnitudes on the non-roll back margin are varied between 1 to 0.25 times that of the continental collision boundary. Based on the analysis of the stress fields for the various models we will subsequently refine the edge force distribution (section 4.6.1).

4.4 Stress modeling

4.4.1 General aspects

We compute stress fields in our model Eurasian lithosphere by solving the mechanical equilibrium equations using finite elements in a spherical shell (GTECTON (Govers and Meijer, 2001)). Spatial discretization of the model domain was verified to be dense enough that results are insensitive to further grid refinement. Our model is fully elastic with Youngs modulus of $70\ GPa$ and a Poisson's ratio of 0.25. We solve for vertically averaged stress distribution using a plane stress formulation. Stresses are presented for a uniform model thickness of $100\ km$, i.e. displayed stress magnitudes have not been adapted for variations in effective elastic thickness (Tesauro et al., 2009).

4.4.2 Stress results for reference model

Stress results for the spectrum of mechanically balanced force sets vary considerably. We present results for the model that generates the best fit with observations, which will serve as a reference model for subsequent refinement of the edge force distribution (section 4.6.1). This model contains LBFs from model *Lithodens* and basal tractions from a mantle flow model based on tomographic model *ngrand* (converted to densities using a constant scaling factor of 0.18) and the radial viscosity profile of Mitrovica and Forte (2004). Collision forces along the southern boundary dominate edge forcing (inset of Fig. 4.2). The resulting stress field (Fig. 4.2) shows nearly uni-axial compression in large parts of Europe and western Asia caused by the interaction between collision forces and ridge push. Average stress magnitudes are typically of the order of 50 MPa. The Tibetan plateau is in an overall state of extension because gravitational collapse forces dominate over compressive collision forces. Eastern Asia is characterized by a strike-slip stress regime resulting from negligible edge forces on the eastern plate boundary. Southeast Asia shows low stress levels with considerable lateral variations in both stress regime and orientations. The absence of significant edge forcing causes local gravitational effects and mantle traction distribution to have a dominant imprint. The model adequately reproduces the observed large-scale stress directions within WSM data uncertainties for considerable parts of the plate (Scandinavia, Aegean and southeastern Europe, western Spain, Central and eastern Tibetan plateau, Baikal, China) (Fig. 4.3). Three main regions, however, show important systematic misfits: the west-

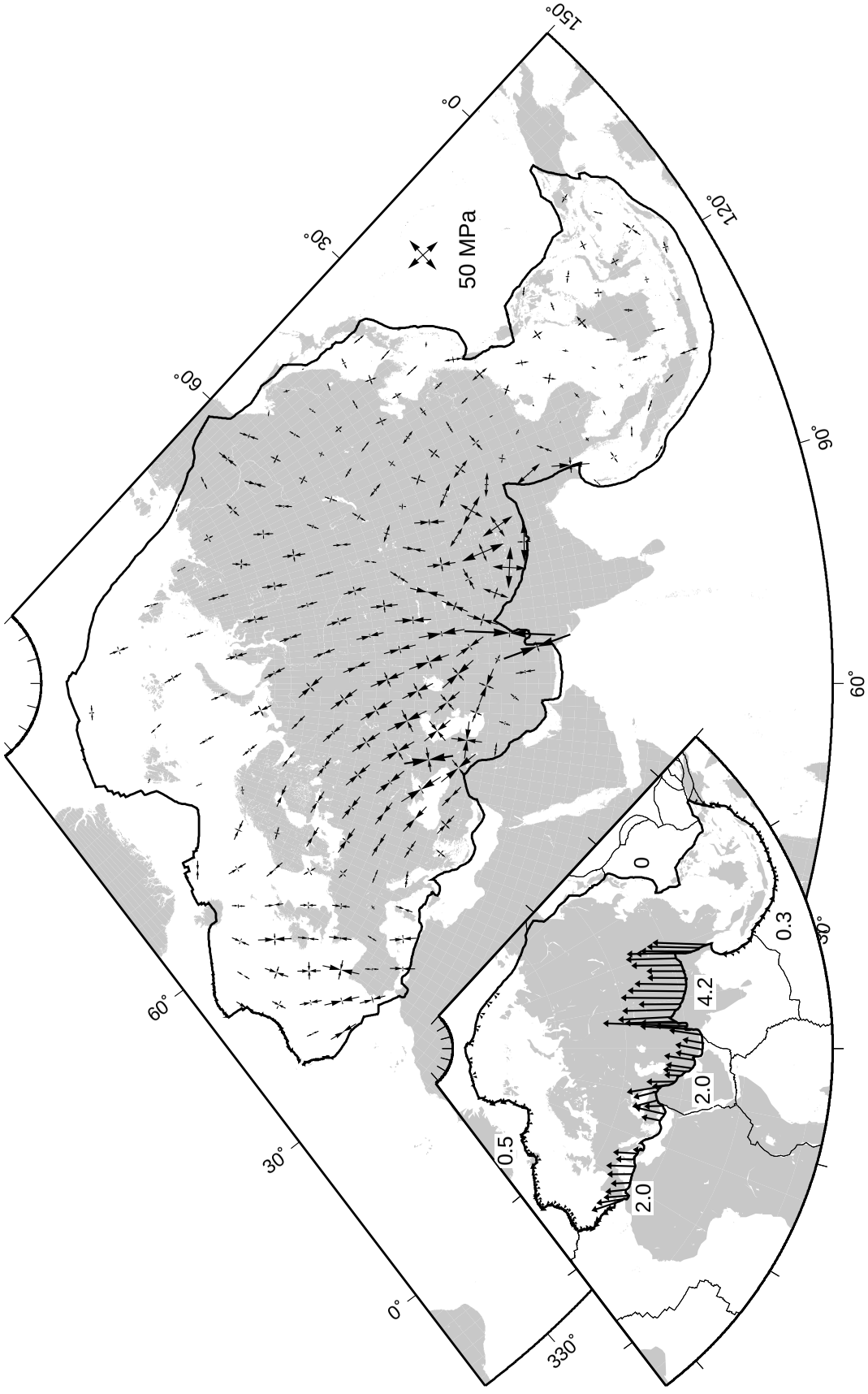

Figure 4.2: Stress field for reference model. Corresponding edge forces are displayed in the inset; numbers are average magnitudes in TN/m.

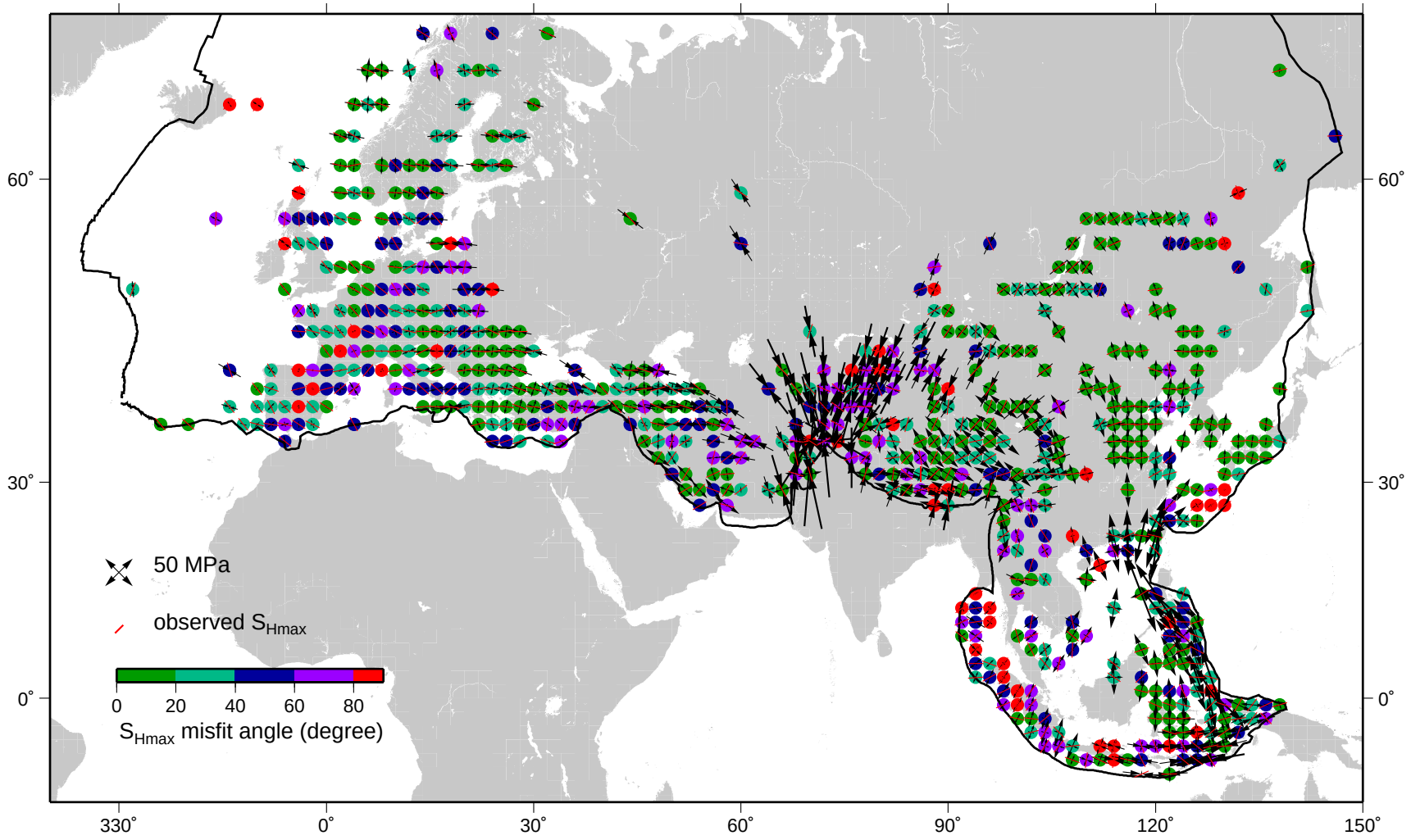

Figure 4.3: Comparison of stress model results (axes) for reference model with observations (red stripes). Colors represent local misfit angles (average misfit angle is 35°).

ern Tibetan plateau, southcentral Europe and the western part of the East-European platform. The average misfit angle over the entire domain is $35°$.

4.5 Sensitivity of the stress field to model forces

We evaluate the sensitivity of the stress field to alternative model force distributions by the change in average misfit angle with observations. All considered force sets are mechanically balanced so that changing one force implicitly evokes changes in other forces. It is therefore not possible to completely isolate the effect of variations in a single force. However, below we analyze the sensitivity of the average misfit angle to each individual force separately; this allows us to identify which forces control the fit with observations.

4.5.1 Edge force distribution

Because the total edge force torque adapts to mechanically balance mantle tractions and LBFs we analyze the sensitivity of the stress field to the distribution of edge forces for a specific combination of mantle flow and LBF model. Model misfit angles as function of the magnitude of the various edge forces show similar characteristics regardless of the choice of mantle flow and LBF model and are presented for that of the reference model (Fig. 4.4). Each graph in Figure 4.4 displays the same models, encompassing the entire edge force solution range to the torque balance equation (see section 4.3.3). Models are only physically realistic if collision forces along the African/Arabian, the Indian and the Australian plate contact are resistive (positive values). Furthermore, resistance should be strongest on the Indian segment, which has the largest vertical plate contact area. Models fulfilling these requirements are indicated by closed circles in Figure 4.4. The reference model, marked by a red cross, is the physically realistic model that generates the best fit with observations.

We find that average misfit angles strongly depend on the magnitude of collision forces (Fig. 4.4a, b and c) but are unsensitive to transform fault resistance or forces at roll-back and non-roll-back margins (Fig. 4.4d, e and f, respectively). Force magnitudes on the collisional boundaries with Africa/Arabia, India and Australia strongly correlate: increased forcing on the Indian boundary requires weaker forcing on the other two segments to maintain mechanical equilibrium. Physically realistic models constrain forcing on the Indian boundary to magnitudes between $3.1TN/m$ and $4.4TN/m$ (grey band in Fig. 4.4b). Interestingly, physically unrealistic models, with an outward driving force on the Australian collisional boundary (negative values in Fig. 4.4c) but allowing for higher Indian collision forces, generate the lowest misfit angles. We therefore conclude that the stress field is predominantly sensitive to the magnitude of colli-

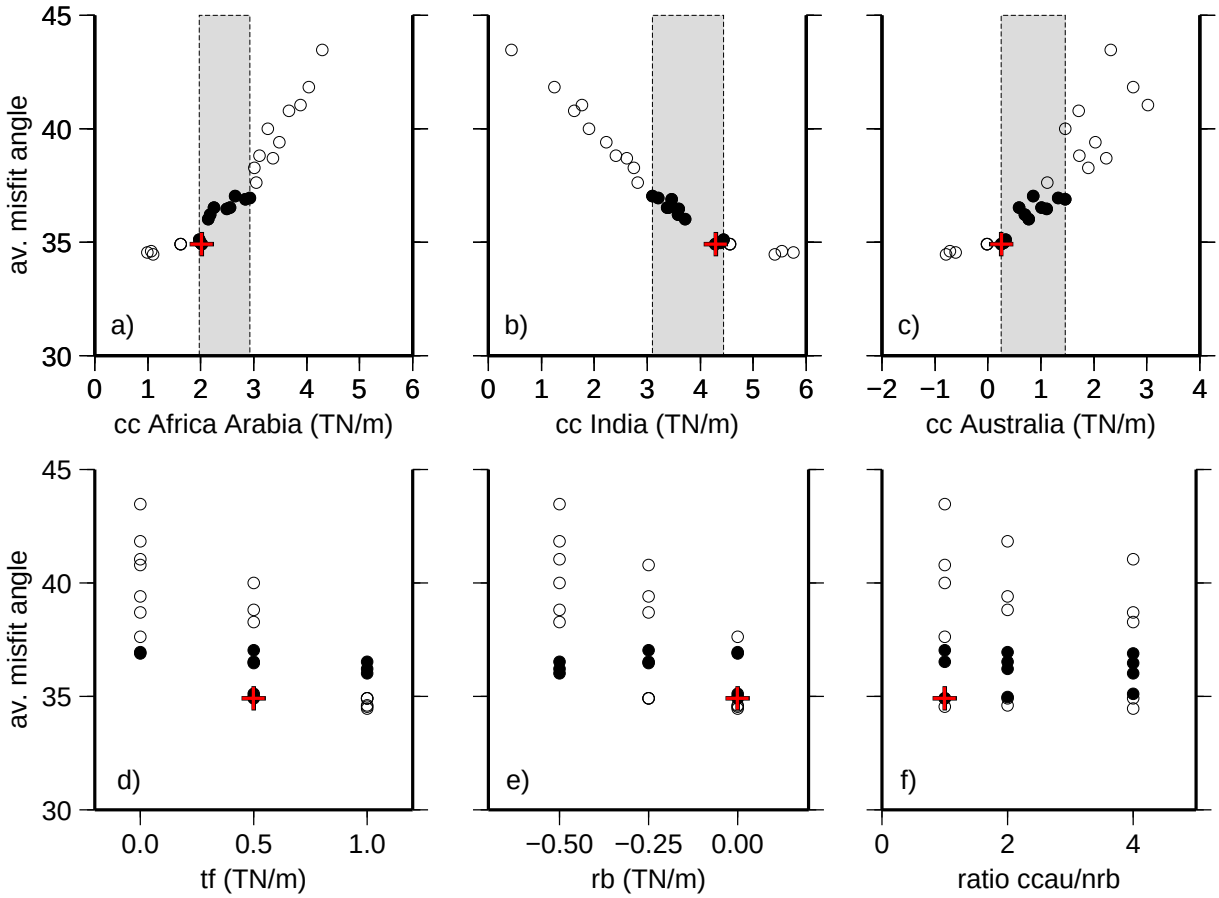

Figure 4.4: Dependence of the misfit in stress directions for the whole Eurasian plate on the magnitude of a) collision forces on the African and Arabian plate contact, b) collision forces on the Indian plate contact, c) collision forces on the Australian plate contact, d) transform fault resistance (tf), e) outward pull at roll-back margins (rb) and f) the ratio of collision forces at the continental versus oceanic Australian boundary (ration ccau/nrb). Results are shown for LBF model *Lithodens* and mantle tractions based on tomographic model *ngrand*. Closed circles represent physically realistic force sets. These models restrict collision force magnitudes to values enclosed by the grey bands. Reference model is indicated by red cross.

sion forces along the Indian boundary. Stress observations are best matched for forcing exceeding $4\ TN/m$ (Fig. 4.4f).

4.5.2 Mantle flow model

Here, we investigate whether the distribution of mantle tractions affects regional stresses. Uncertainties in mantle tractions arise from 1) the distribution of tomographic anomalies from which we infer buoyancy forces, 2) scaling between velocity and density anomalies ($v - \rho$ scaling) and 3) mantle viscosity. We previously showed that the magnitude of mantle tractions is affected by all three parameters and controls the ability of

a mantle flow model to successfully balance the Eurasian plate [WR2011]. The pattern of mantle tractions, however, depends mainly on the choice of tomographic model. We therefore consider mantle tractions deduced from a range of S-wave tomographic models and confine their magnitudes to values enabling torque balance by adapting $v - \rho$ scaling and viscosity magnitudes within the uncertainty bounds indicated by mineral physics (for more information see WR2011). We show results for the three tomographic models that produce the best fit to observations (*ngrand* (Grand, 2002), *s20rts* (Ritsema and van Heijst, 2000) and *saw* (Megnin and Romanowicz, 2000)). Because edge force solutions to the torque balance equation vary considerably as a function of $v-\rho$ scaling magnitude we consider, for each model, the entire range for which torque balance is possible. Since we found in the previous section that the magnitude of the Indian collision force controls stress field orientations, we evaluate mantle flow models as function of this collision force (Fig. 4.5).

For all three tomographic models we find that misfit angles depend on the magnitude of mantle buoyancy forces (expressed through the magnitude of $v - \rho$ scaling): models with the weakest forcing (triangles in Fig. 4.5) give the best results whereas models with the largest forcing (diamonds in Fig. 4.5) give the worst. This sensitivity is controlled by collision forces adapting to the total mantle traction torque rather than by local changes in stresses at the bottom of the plate. Strong tractions from active mantle flow imply relatively low Indian collisional forces, resulting in large-scale stresses that do not fit observations.

On the plate scale, all three tomographic models achieve similar minimum misfit angles (Fig. 4.5a). This agrees with Steinberger et al. (2001), who found that modeled stress orientations are relatively insensitive to the choice of global mantle flow model. To asses if stress orientations are affected locally we consider average misfit angles for the subregions Europe, Zagros and the Tibetan plateau (Fig. 4.5b, c and d, respectively; subregions are indicated by dashed rectangles in Fig. 4.1). We find that in Europe, where stress magnitudes are low (Fig.4.2), stress directions do depend on the pattern of mantle tractions (Fig. 4.5b); mantle tractions based on tomographic model *s20rts* locally give best results. This model, however, generates very poor ($> 50^\circ$) fit of stress orientations in the Zagros subregion for physically realistic models (Fig. 4.5c, closed symbols). Generally, we find that the indirect effect of mantle tractions on the stress field, caused by edge forces adapting to the zero torque constraint, dominates over the direct effect of their precise distribution. Although the stress field is locally sensitive to the mantle flow model, stress field analysis does therefore not lead to a more refined selection of mantle flow models than the one made by WR2011 on the basis of their net forcing on Eurasia.

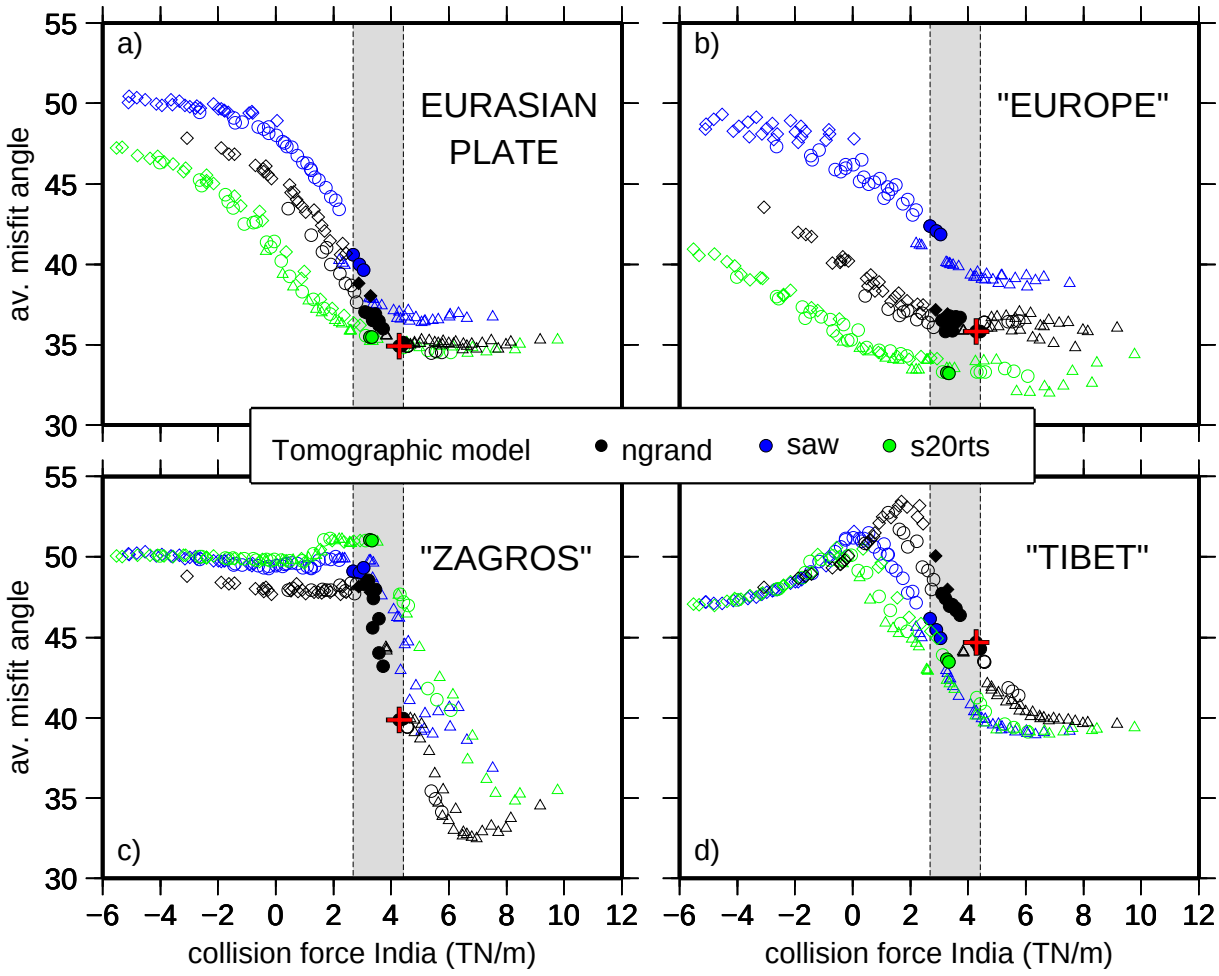

Figure 4.5: Dependence of average misfit angle on mantle flow model (see text for tomographic model references) as function of the magnitude of collision forces on the Indian plate contact. Symbols indicate $v - \rho$ scaling factor. Triangles, circles and diamonds respectively represent magnitudes of either 0.16, 0.18 and 0.20 (ngrand), 0.12, 0.14 and 0.16 (saw) or 0.17, 0.18 and 0.19 (s20rts). Results are given for: a) the whole Eurasian plate, b) Europe subregions, c) Zagros subregion and d) Tibet subregion. Grey band indicates magnitude range for physically realistic models (models represented by closed symbols). Reference model is indicated by red cross. LBFs are from model *Lithodens*.

4.5.3 Lithospheric density structure

We evaluate the three LBF models presented in section 4.3.2 based on their ability to reproduce observed stress orientations. Again, we consider average misfit angles for the whole Eurasian plate and the subregions Europe, Zagros and Tibet as a function of the Indian collision force (Fig. 4.6a, b, c and d, respectively). Results are shown for mantle flow model *ngrand* but have comparable trends for the other models.

We find misfit angles for the three LBF models are similar when averaged over the entire plate (Fig. 4.6a) but differ significantly for the different sub-regions. Stresses in Eu-

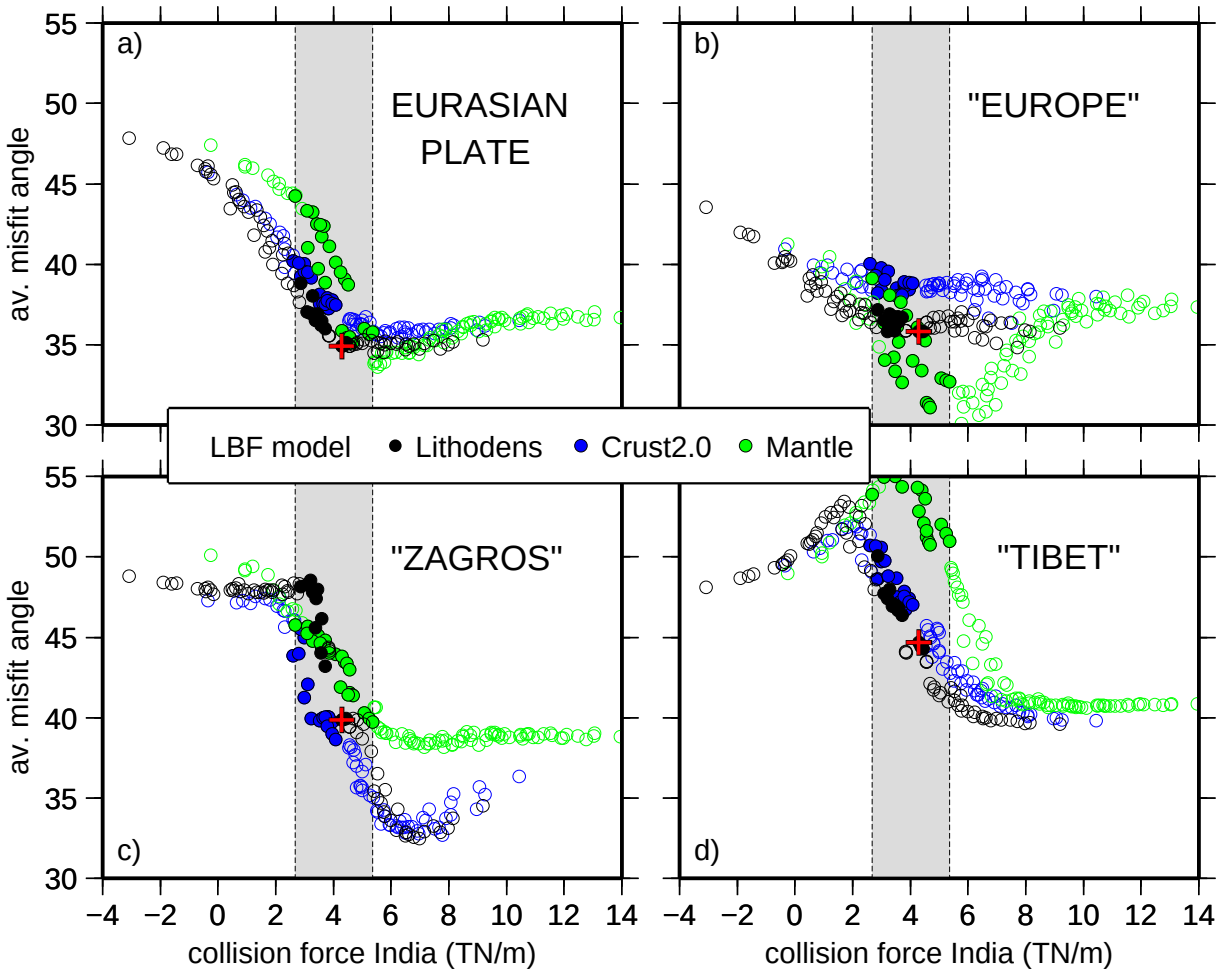

Figure 4.6: Dependence of average misfit angle on LBF model as function of the magnitude of collision forces on the Indian plate contact. Results are given for: a) the whole Eurasian plate, b) Europe subregions, c) Zagros subregion and d) Tibet subregion. Grey band indicates magnitude range for physically realistic models (models represented by closed circles). Reference model is indicated by red cross. Mantle tractions are derived from tomographic model *ngrand* with viscosity profile Mitrovica and Forte (2004) and $v - \rho$ scaling magnitudes of 0.16, 0.18 or 0.20

rope are best matched for LBF model *Mantle* (Fig. 4.6b), which ignores observed crustal structure. This result is surprising since the crustal structure here is well-constrained. Our interpretation of this discrepancy is that deep seated mantle density anomalies that are emphasized by model *Mantle* have a stronger imprint on the European stress field than shallow crustal structures. Model *Lithodens*, which is based on both observed crustal structure and deep seated anomalies, apparently does not generate a sufficient mantle contribution to LBFs to counterbalance the imprint of the crustal structure. This is likely caused by the mapping of variations in lithospheric mantle properties into a lithosphere with constant thickness. Lithospheric thickness variations, which are large

in Europe (Artemieva, 2003), potentially strongly influence LBFs (Pascal, 2006).
In contrast to Europe, incorporation of observed crustal thickness variations is essential for the representation of stress orientations in the Zagros and Tibet subregions. Model *Lithodens* gives best results (Fig. 4.6c and d). Overall, we conclude that the large-scale stress field allows to evaluate different models for compensation of topography at depth. We find that both the observed crustal thickness and variations in properties of the underlying mantle are essential to reproduce observations. Despite the shortcoming of model *Lithodens* in Europe this model therefore has our preference.

4.5.4 Overall findings

Although the large-scale Eurasian stress field is affected by the distribution of mantle tractions and LBFs, its sensitivity to the magnitude of Indian collision forces is dominant. Independently of the LBF and mantle flow model, stress observations in Tibet are best matched by physically unrealistic models with Indian collision forces of $6\ TN/m$ and stronger (Fig. 4.5d and 4.6d, open symbols represent unrealistic models). These magnitudes are required to achieve the correct level of compensation for extensional LBFs from the Tibetan plateau. Within the bounds of our first-order distribution of edge forces, such magnitudes on the Indian plate contact can only be counterbalanced by unrealistic outward forcing on other collisional boundaries. We therefore proceed to reevaluate assumptions made regarding the distribution of edge forces.

4.6 Model refinements

4.6.1 Edge force distribution

Because the total edge force torque is constrained through mechanical equilibrium by LBFs and mantle tractions, larger collision forces on the Indian contact require compensating forces elsewhere on the plate boundary. We consider three variations on the first-order distribution of edge forces adopted thus far:
1) A considerable uncertainty in the assessment of edge forces lies in the treatment of the unknown continental boundary with the North-American plate. Thus far, prompted by the lack of seismic activity, we let this boundary free. However, some level of forcing may be present without finding an expression in the old and strong lithosphere that characterizes the region surrounding this boundary. We consider forcing on this boundary in the direction of relative motion. Due to the vicinity of the Euler pole, forces are directed in a fan-like pattern, outward on its northeastern part and inward on its southwestern part.
2) India's collision with Eurasia is highly oblique on the Pakistan and Birma segments

of the boundary between the two plates (Fig. 4.1). Transmission of stress on what can be considered a continental transform boundary is likely reduced with respect to the central part of the plate contact. We therefore separate the oblique segments of the Indian boundary from the central part and independently solve for the magnitude of forcing.
3) We allow for variations in force magnitude between the African and the Arabian collisional plate boundary.
Overall, we find that the above modifications of the edge force distributions do not affect the relation between plate-wide averaged misfit angle and the magnitude of collision forces on the southern plate boundary. They do, however, lead to physically realistic models with higher forcing on the Indian segment than models constrained to our first-order assumptions. Increased collisional forcing on the Arabian boundary compared to that of Africa does slightly improve stress results in Europe. Stresses matches deteriorate in the Zagros, however, so that plate average misfit remains comparable. Added forcing on the North-American continental plate boundary and decreased forcing on the oblique boundaries with India do not influence the match with observations, partly because of the absence of nearby stress data.
Figure 4.7 shows the edge force distribution and resulting stress field for our preferred model, which matches observations best. Indian collision forces are more than doubled compared to our reference model, improving the data fit for the Tibet subregions by 6°. Collision forces now exceed gravitational collapse forces, resulting in a fan-like pattern of S_{Hmax} directions. Stress amplitudes in the northeastern part of the plate are considerably increased due to the combination of strong collision forces and forcing on the North-American boundary. Stress orientations in this part of the plate remain unchanged and fit observations well (Fig. 4.8). Stresses in Europe are slightly rotated due to the different forcing on the African and Arabian collision zones, marginally improving the match with observations. Misfits remain considerable in central Europe, and might be caused by the negligence of local lithospheric thickness variations in the treatment of LBFs (section 4.5.1). Edge forcing on the southeast Asian boundaries is entirely absent so that stresses are governed by LBFs and mantle tractions.
Although the average S_{Hmax} orientation misfit is only slightly reduced compared to the reference model and remains considerable at 34°, refinement of the edge force distribution allows for considerably better representation of stresses in the Tibetan plateau. Two regions show systematic misfit in all our models: the western part of the East-European platform and the Tien Shan region. Both regions are characterized by rotated stress directions with regard to surrounding regions, which are not reproduced by our models. In both regions major lateral lithospheric discontinuities might affect

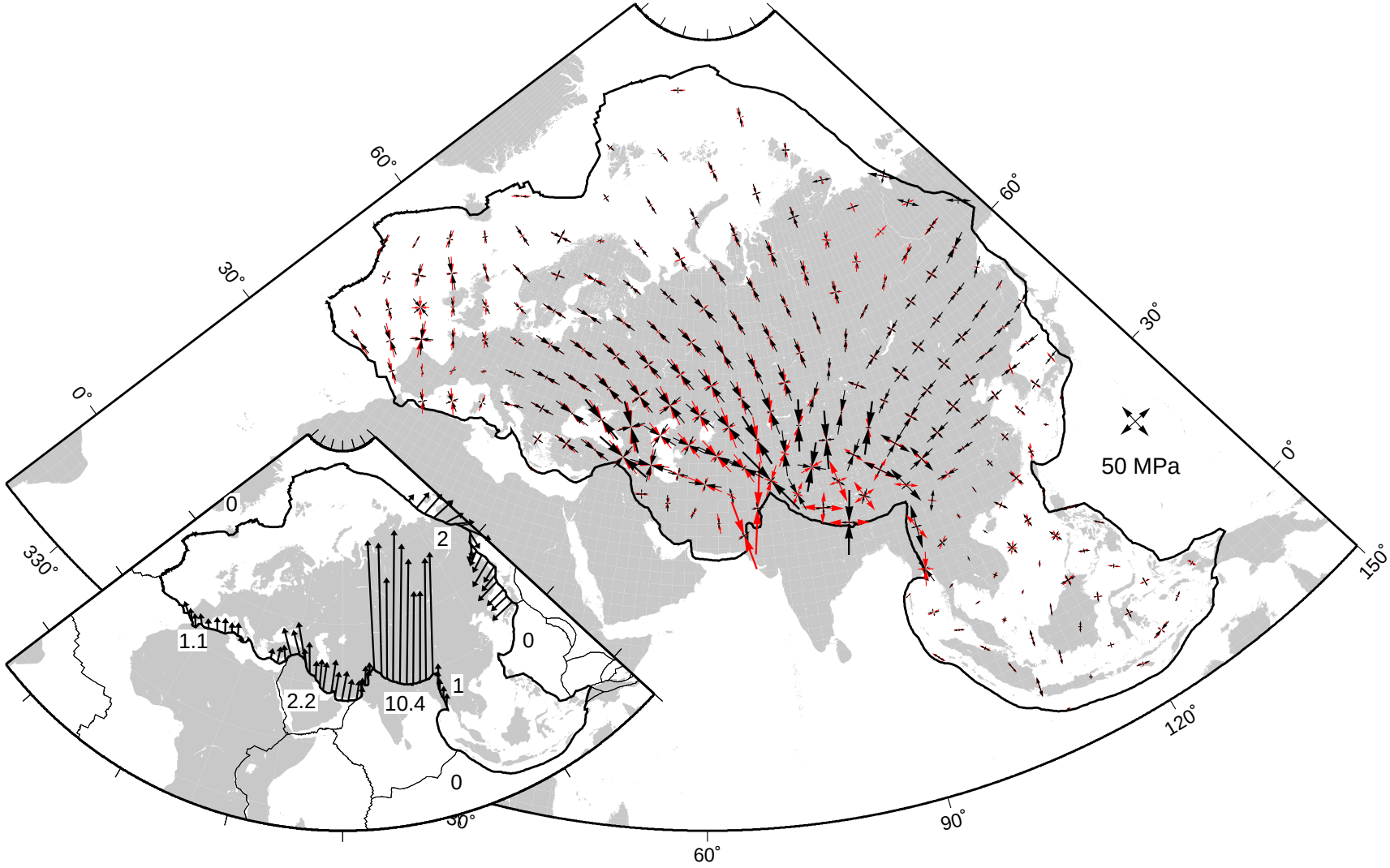

Figure 4.7: Stress field for preferred model (black axes) compared to reference model (red axes). Corresponding edge forces are displayed in the inset; numbers are average magnitudes in TN/m.

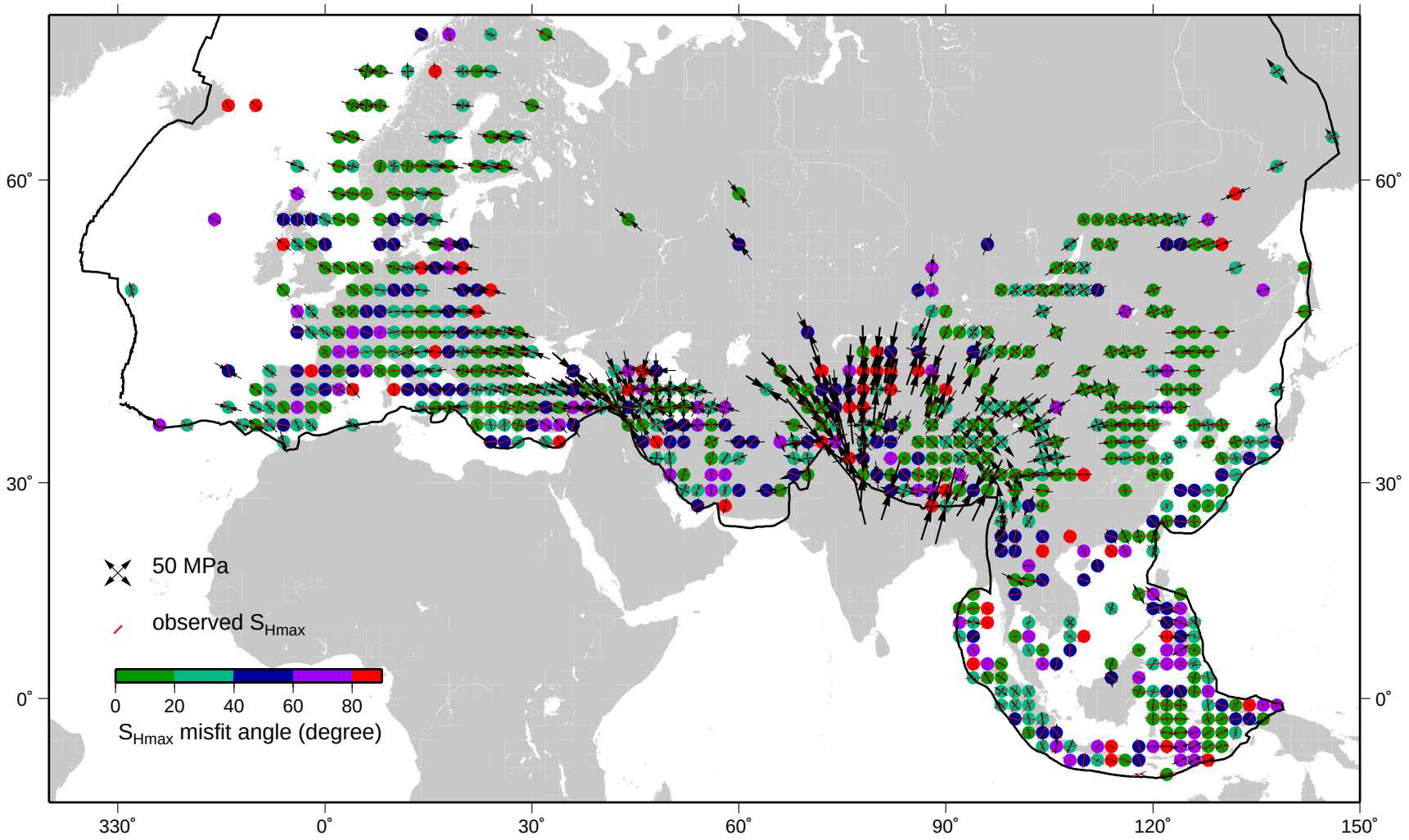

Figure 4.8: Comparison of stress model results (stress axes) for preferred model with observations (red stripes). Colors represent local misfit angles (average misfit angle is 34°).

local stress orientations.

Our analysis suggests strong variations in forcing magnitude on Eurasia's southern collisional boundary, with forces of around $1 - 2\ TN/m$ on the African boundary increasing to $10\ TN/m$ on the boundary with India. Stronger forcing on the Indian plate contact is expected as a result of an increase in both the thickness of the collisional boundary and the speed of the approaching plate. Our result for the magnitude of forcing on the Indian boundary is comparable to that found by England and Houseman (1989) based on a comparison of the calculated and estimated strain rate in Tibet(6 to $11\ TN/m$). It is, however, higher than suggested by Copley et al. (2010) for the Indian plate based on a comparison of the plate's dynamics before and after collision with Eurasia (5 to $6\ TN/m$). This may be explained in case any slab pull still acts on the Indian plate. The outward pull on the Indian plate then reduces the net resistive force on India, resulting in asymmetric forcing on the India-Eurasia plate contact.

Earlier we found that collision forces on the southern boundary substantially deviate its absolute motion [WR2011]. The amount of push required to match the observed direction of absolute motion constrains the total amount of collision forces and can arise from either equal forcing of 2.7 to $5.0\ TN/m$ along the entire southern collisional boundary or from any force distribution that integrates to the same torque. Collision forces of our preferred model average to $4.0\ TN$ per meter collisional boundary and generate a torque of similar orientation as a model with a homogeneous force distribution. Our preferred model thus successfully reproduces Eurasia's absolute direction of motion.

4.6.2 Effect of internal faults

We investigate how our results are affected by anisotropic transmission of stresses by incorporating major geological strike-slip features into our model. Based on strain rates (Kreemer et al., 2003), we include seven internal faults (North-Anatolia, main-recent-Zagros, Karakorum, Altyn Tagh, Kunlun, Red River and great-Sumatra faults) and one shear zone (Tien Shan). Each individual feature is approximated by a single fault in our model (black lines inside our model plate in Fig. 4.1). We use a slippery node technique (Melosh and Williams, 1989) that allows for fault parallel slip. As an extreme end-member case we neglect fault friction, allowing us to asses the maximum possible effect of the faults on the modeled stress field. The finite length and local changes in orientation of the faults do, however, introduce mechanical resistance.

Figure 4.9 shows the stress field resulting from our preferred force model (Fig. 4.7) for a model with and without faults. As expected, S_{Hmax} orientations rotate towards strike normal directions in the vicinity of a fault. However, the lateral extent of stress field

rotations is small compared to the scale of our domain and plate-wide averaged misfit angles are not significantly affected.

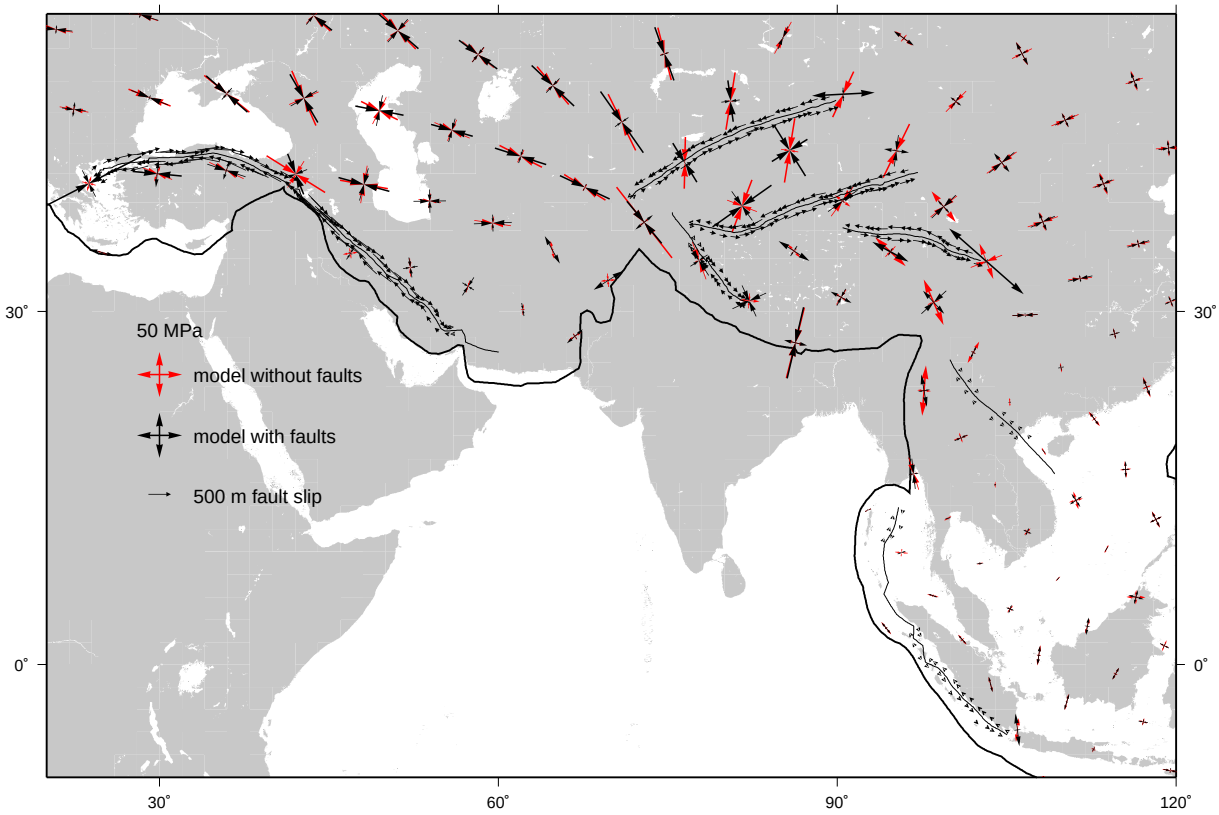

Figure 4.9: Effect of faults on modeled stress field. Stress fields are given for models with equal forcing (preferred model) with (black axes) and without (red axes) faults. Model slip directions are indicated by black arrows.

An interesting result is the predicted sense of shear on faults, which provides an additional test for the applied force field. We find that slip directions are generally well reproduced (right lateral: North-Anatolia fault, main-recent-Zagros fault, Karakoram faults, Red-River fault, great-Sumatra fault, left lateral: Altyn Tagh fault, Kunlun fault, Tien Shan shear zone). We do, however, not resolve slip on the great-Sumatran fault and Red-River fault due to the negligible edge forcing in southeast Asia. Models with larger resistive forces on the Java/Sumatra subduction zone (around $2\ TN/m$) show increased right-lateral slip over the entire length of these two faults, suggesting that actual forcing on the boundary in southeast Asia may be higher than inferred from our models.

4.7 Discussion

In this study, we concentrate on reproducing the large-scale stress field by means of a comprehensive analysis of the forces acting on the Eurasian plate. We find that with an appropriate set of forces the large-scale stress field is satisfactorily reproduced for large parts of the plate when adopting a simple homogeneous elastic rheology. Our approach significantly differs from that of Hieronymus et al. (2008), who modeled the large-scale Eurasian stress field based on a simplified force set and concentrated on the effects of rheology. Their conclusion that strong variations in lithospheric strength are required to prevent stresses caused by Indian collision from propagating throughout the plate is in contrast with our results. Their findings could, however, be an expression of shortcomings in their force set.

We systematically find that force models that best reproduce the stress field on the plate scale have negligible edge forces in southeast Asia. Although higher forcing slightly improves the local match with observations, this affects the remainder of the edge force distribution and deteriorates the match with observations elsewhere. The low contribution of edge forces in southeast Asia to the torque balance of Eurasia possibly reflects a low degree of force transmission to the rest of the plate.

Torque balance solutions for the magnitudes of edge forces depend on the net torque generated by LBFs and mantle shear stresses and are thus sensitive to uncertainties in their modeling. We have aimed to asses the uncertainty in LBFs and mantle tractions by considering various models and find that they result in edge force solutions with comparable main characteristics. Further improvements in the modeling of LBFs and mantle tractions involves incorporation of lateral variations in lithospheric thickness and mantle viscosity. As outlined in WR2011, these model refinements probably affect model forces (and thus stresses) locally but are not expected to considerably influence plate-scale quantities (Becker, 2006). Therefore, they are unlikely to affect our conclusions regarding the distribution of edge forces on Eurasia's boundary.

Our analysis provides a total set of forces acting on the Eurasian plate and thus enables us to evaluate the importance of the different forces to its dynamics. Following WR2011, we quantify the relative importance of mantle shear, LBFs and edge forces by comparing the magnitudes of the torque generated by the individual force types with their scalar sum (the vector sum of the torques is implicitly zero because they form a balanced set). In our preferred force model, edge forces contribute 47% of the total torque magnitude, against 28% for mantle shear stresses and 25% for LBFs. Edge force thus play a dominant role in the dynamics of Eurasia. The important role we find for edge forces agrees with Bird et al. (2008), who found that net edge force torques are

comparable or stronger than mantle shear and LBF torques on most plates with large surface areas.

4.8 Conclusions

Using lithospheric stress field data, we analyzed the forces acting on the Eurasian plate. Building on our earlier work we obtain a model for the force distribution which a) combines edge forces, lithospheric body forces and tractions from global mantle flow models; b) is in mechanical equilibrium; c) drives the Eurasian plate in a direction in agreement with the direction of absolute motion; d) accounts for the large scale stress field in the Eurasian plate.
Concerning the role of the various types of forces and the sensitivity of Eurasia's large scale stress field to aspects of the force distribution we conclude:

1. Collision forces along the southern plate boundary govern the large-scale Eurasian stress field. Stress observations require collision forces on the India-Eurasia boundary of $6 - 10\, TN/m$. Implication of mechanical equilibrium is that forces on the African and Arabian plate contacts amount to $1 - 2\, TN/m$.

2. The stress field is susceptible to uncertainties in the lithospheric density structure, albeit less strongly so than to uncertainties in the magnitude of collision forces. Europe, where stress levels are relatively low, is most sensitive. Taking into account the effects of dynamic topography and variations in lithospheric mantle structure significantly improves the fit between model stresses and observations.

3. Stress analysis does not lead to discrimination of mantle flow models further than has been done previously by Warners-Ruckstuhl et al. (2012) based on the constraint of torque balance on the Eurasian plate.

4. Torque balance systematically results in low forcing in southeast Asia. This may reflect a low degree of force transmission to the rest of the Eurasian plate.

5. Edge forces generate a larger net contribution to the dynamics of Eurasia than mantle shear stresses and lithospheric body forces.

Acknowledgments

Figures were produced with the GMT software by Wessel and Smith (1991). Work supported in part by the Netherlands Organisation for Scientific Research (NWO, Earth and Life Sciences (ALW)), in the context of the EUROMARGINS EUROCORES Programme of the European Science Foundation, project 01-LEC-EMA22F WESTMED.

Bibliography

Amante, C. and Eakins, B. W. (2009). ETOPO1 1 arc-minute global relief model: Procedures, data sources and analysis. *NOAA Technical Memorandum NESDIS NGDC-24*, page 19.

Antolik, M., Ekstrom, G., and Dziewonski, A. M. (2001). Global event location with full and sparse data sets using three-dimensional models of mantle P-wave velocity. *Pure Appl. Geophys.*, 158:291–317.

Argus, D. F. and Gordon, R. G. (1991). No-net-rotation model of current plate velocities incorporating plate motion model NUVEL-1. *Geophys. Res. Lett.*, 18:2039–2042.

Artemieva, I. M. (2003). Lithospheric structure, composition, and thermal regime of the east European craton: implications for the subsidence of the Russian platform. *Earth Planet. Sci. Lett.*, 213:431–446.

Artemieva, I. M. (2006). Global $1^\circ \times 1^\circ$ thermal model TC1 for the continental lithosphere: Implications for lithosphere secular evolution. *Tectonophysics*, 216:245–277.

Artyushkov, E. V. (1973). Stresses in the lithosphere caused by crustal thickness inhomogeneities. *J. Geophys. Res.*, 78:7675–7708.

Bassin, C., Laske, G., and Masters, G. (2000). The current limits of resolution for surface wave tomography in North America. *EOS, Trans. AGU*, 81.

Becker, T. W. (2006). On the effect of temperature and strain-rate dependent viscosity on global mantle flow, net rotation and plate-driving forces. *Geophys. J. Int.*, 167:943–957.

Becker, T. W. and Boschi, L. (2002). A comparison of tomographic and geodynamic mantle models. *Geochem. Geophys. Geosyst.*, 3:2001GC000168.

Becker, T. W., Conrad, C., Lithgow-Bertelloni, C., O'Connell, R., O'Neill, C., Richards, M., Steinberger, B., and Zhong, S. (2006). Global spectral flow code development and benchmark plan, http://geosys.usc.edu/projects/seatree.

Becker, T. W. and Faccenna, C. (2009). A review on the role of subduction dynamics for regional and global plate motion. *Subduction Zone Geodynamics*, pages 3–34.

Becker, T. W. and Faccenna, C. (2011). Mantle conveyor beneath the Tethyan collisional belt. *Earth Planet. Sci. Lett.*, 310(3):453–461.

Becker, T. W. and O'Connell, R. J. (2001). Predicting plate velocities with mantle circulation models. *Geochem. Geophys. Geosyst.*, 2:2001GC000171.

Behn, M. D., Conrad, C. P., and Silver, P. G. (2004). Detection of upper mantle flow associated with the african superplume. *Earth Planet. Sci. Lett.*, 224(3-4):259–274.

Bird, P. (1998). Testing hypothesis on plate-driving mechanisms with global lithosphere models including topography, thermal structure and faults. *J. Geophys. Res.*, 103:10115–10129.

Bird, P. (2003). An updated digital model of plate boundaries. *Geochem. Geophys. Geosyst.*, 4:doi:10.1029/2001GC000252.

Bird, P., Liu, Z., and Rucker, W. K. (2008). Stresses that drive the plates from below: Definitions, computational path, model optimization and error analysis. *J. Geophys. Res.*, 113:doi:10.1029/2007JB005460.

Boschi, L., Becker, T. W., and Steinberger, B. (2007). Mantle plumes: Dynamic models and seismic images. *Geochem. Geophys. Geosyst.*, 8:2007GC001733.

Bull, A. L., McNarama, A. K., Becker, T. W., and Ritsema, J. (2010). Global scale model of the mantle flow field predicted by synthetic tomography models. *Phys. Earth Planet. Int.*, 182:129–138.

Chapman, M. E. and Solomon, S. C. (1976). North American-Eurasian boundary in north east Asia. *J. Geophys. Res.*, 81:921–930.

Chapple, W. M. and Tullis, T. E. (1977). Evaluation of the forces that drive the plates. *J. Geophys. Res.*, 82:1967–1984.

Cloetingh, S. and Wortel, R. (1986). Stress in the Indo-Australian plate. *Tectonophysics*, 132(1-3):49–67.

Coblentz, D. D. and Richardson, R. M. (1996). Analysis of the south American intraplate stress field. *J. Geophys. Res.*, 101(B4):8643–8657.

Coblentz, D. D. and Sandiford, M. (1994). Tectonic stresses in the African plate: constraints on the ambient lithospheric stress state. *Geology*, 22:831–834.

Conrad, C. P. and Behn, M. D. (2010). Constraints on lithosphere net rotation and asthenospheric viscosity from global mantle flow models and seismic anisotropy. *Geochem. Geophys. Geosyst.*, 11:doi:10.1029/2009GC002970.

Conrad, C. P. and Lithgow-Bertelloni, C. (2002). How mantle slabs drive plate tectonics. *Science*, 298:207–209.

Conrad, C. P. and Lithgow-Bertelloni, C. (2004). The temporal evolution of plate driving forces: Importance of slab suction versus slab pull during the cenozoic. *J. Geophys. Res.*, 109:doi:10.1029/2004JB002991.

Conrad, C. P. and Lithgow-Bertelloni, C. (2006). Influence of continental roots and asthenosphere on plate-mantle coupling. *Geophys. Res. Lett.*, 33(5):doi:10.1029/2005GL025621.

Conrad, C. P., Lithgow-Bertelloni, C., and Louden, K. E. (2004). Iceland, the faralon slab, and dynamic topography of the north atlantic. *Geology*, 32:177–180.

Copley, A., Avouac, J. P., and Royer, J. Y. (2010). India-Asia collision and the Cenozoic slowdown of the Indian plate: Implications for the forces driving plate motions. *J. Geophys. Res.*, 115:doi:10.1029/2009JB006634.

Crough, S. T. (1975). Thermal model of oceanic lithosphere. *Nature*, 256:388–390.

DeMets, C., Gordon, R. G., Argus, D. F., and Stein, S. (1994). Effect of recent revisions to the geomagnetic reversal time scale on estimates of current plate motion. *Geophys. Res. Lett.*, 21:2191–2194.

Duncan, R. A. and Richards, M. A. (1991). Hotspots, mantle plumes, flood basalts, and true polar wander. *Rev. Geophys.*, 29:31–50.

England, P. and Houseman, G. (1989). Extension during continental convergence, with application to the Tibetan plateau. *J. Geophys. Res.*, 94:17561–17579.

Fleitout, L. and Froidevaux, C. (1982). Tectonics and topography for a lithosphere containing density hertrogeneities. *Tectonics*, 1:21–56.

Flesch, L. M., Holt, W. E., Haines, A. J., Wen, L., and Shen-Tu, B. (2007). The dynamics of western North America: Stress magnitudes and the relative role of gravitational potential energy, plate interaction at the boundary and basal tractions. *Geophys. J. Int.*, 169(3):866–896.

Forsyth, D. W. and Uyeda, S. (1975). On the relative importance of the driving forces of plate motion. *Geophys. J. R. Astr. Soc.*, 43:163–200.

Forte, A. M., Moucha, R., Simmons, N. A., Grand, S. P., and Mitrovica, J. X. (2010). Deep-mantle contributions to the surface dynamics of the North American continent. *Tectonophysics*, 481:3–15.

Forte, A. M. and Perry, C. H. K. (2000). Geodynamic evidence for a chemically depleted continental tectosphere. *Science*, 290:doi:10.1126/science.290.5498.1940.

Ghosh, A., Becker, T. W., and Zhong, S. J. (2010). Effects of lateral viscosity variations on the geoid. *Geophys. Res. Lett.*, 37:doi: 10.1029/2009GL040426.

Ghosh, A., Holt, W. E., and Flesch, L. M. (2009). Contribution of gravitational potential energy differences to the global stress field. *Geophys. J. Int.*, 179:787–812.

Ghosh, A., Holt, W. E., Wen, L., Haines, A. J., and Flesch, L. M. (2008). Joint modeling of lithosphere and mantle dynamics elucidating lithosphere-mantle coupling. *Geophys. Res. Lett.*, 35:doi: 10.10292008GL034365.

Goes, S., Loohuis, J. J. P., Wortel, M. J. R., and Govers, R. (2000). The effect of plate stresses and shallow mantle temperatures on tectonics of noth western Europe. *Global Planet. Change*, 27:23–38.

Goes, S. and van der Lee, S. (2002). Thermal structure of the North American uppermost mantle inferred from seismic tomography. *J. Geophys. Res.*, 107:doi:10.1029/22000JB000049.

Gölke, M. and Coblentz, D. D. (1996). Origins of the European stress field. *Tectonophysics*, 266:11–24.

Gordon, R. G. and Jurdy, D. M. (1986). Cenozoic global plate motions. *J. Geophys. Res.*, 91:12389–12406.

Govers, R. and Meijer, P. T. (2001). On the dynamics of the Juan de Fuca plate. *Earth Planet. Sci. Lett.*, 189:115–131.

Grand, S. P. (2002). Mantle shear wave tomography and the fate of subducted slabs. *Phil. Trans. R. Soc. London*, 360:2475–2491.

Gripp, A. E. and Gordon, R. G. (2002). Young tracks of hotspots and current plate velocities. *Geophys. J. Int.*, 150:321–361.

Grünthal, G. and Stromeyer, D. (1992). The recent crustal stress field in central Europe: trajectories and finite element modeling. *J. Geophys. Res.*, 97:11805–11820.

Hager, B. H., Clayton, R. W., Richards, M. A., Comer, R. P., and Dziewonski, A. M. (1985). Lower mantle heterogeneity, dynamic topography and the geoid. *Nature*, 113:541–545.

Hager, B. H. and O'Connell, R. J. (1981). A simple global model of plate dynamics and mantle convection. *J. Geophys. Res.*, 86:4843–4867.

Harper, J. F. (1975). On the driving forces of plate tectonics. *Geophys. J. R. Astr. Soc.*, 40(3):465–474.

Heidbach, O., Tingay, M., Barth, A., Reinecker, J., Kurfe, D., and Müller, B. (2008). The world stress map database release 2008. *www.world-stress-map.org*, page doi:10.1594/GFZ.WSM.Rel2008.

Hieronymus, C. F., Goes, S., Sargent, M., and Morra, G. (2008). A dynamical model for generating Eurasian lithospheric stress and strain rate fields: Effect of rheology and cratons. *J. Geophys. Res.*, 113:doi:10.1029/2007JB004953.

Humphreys, E. D. and Coblentz, D. D. (2007). North American dynamics and western US tectonics. *Rev. Geophys.*, 45:8755–1209.

Iaffaldano, G. and Bunge, H. P. (2009). Relating rapid plate-motion variations to plate-boundary forces in global coupled models of the mantle/lithosphere system: Effects of topography and friction. *Tectonophysics*, 474:393–404.

Jacoby, W. R. (1970). Instability in the upper mantle and global plate movements. *J. Geophys. Res.*, 75:5671–5680.

Jarosiński, M., Beekman, F., Bada, G., and Cloetingh, S. (2006). Redistribution of recent collision push and ridges push in central Europe: insights from fem modelling. *Geophys. J. Int.*, 167:860–880.

Jordan, T. H. (1978). Composition and development of the continental tectosphere. *Nature*, 274:544–548.

Karato, S. I. and Karki, B. B. (2001). Origin of lateral variation of seismic wave velocities and density in the deep mantle. *J. Geophys. Res.*, 106:21771–21783.

Kreemer, C. (2009). Absolute plate motions constrained by shear wave splitting orientations with implications for hot spot motions and mantle flow. *J. Geophys. Res.*, 114:doi:10.1029/2009JB006416.

Kreemer, C., Holt, W. E., and Haines, A. J. (2003). An integrated global model of present-day plate motions and plate boundary deformation. *Geophys. J. Int.*, 154:8–34.

Kustowski, B., Ekstrom, G., and Dziewonski, A. M. (2008). Anisotropic shear-wave velocity structure of the earth's mantle: A global model. *J. Geophys. Res.*, 113:doi:10.1029/2007JB005169.

Li, C., van der Hilst, R. D., Engdahl, E. R., and Burdick, S. (2008). A new global model for P wave speed variations in Earths mantle. *Geochem. Geophys. Geosyst.*, 9(5):2007GC001806.

Lister, C. R. B. (1975). Gravitational drive on oceanic plates coused by thermal contraction. *Nature*, 257:663–665.

Lithgow-Bertelloni, C. and Guynn, J. H. (2004). Origin of the lithospheric stress field. *J. Geophys. Res.*, 109:doi:10.1029/2003JB002467.

Lithgow-Bertelloni, C. and Richards, M. A. (1998). The dynamics of Cenozoic and Mesozoic plate motions. *Rev. Geophys.*, 36:27–78.

Lithgow-Bertelloni, C. and Silver, P. G. (1998). Dynamic topography, plate driving forces and the African superswell. *Nature*, 395:269–272.

Liu, Z. and Bird, P. (2002). North America plate is driven westward by lower mantle flow. *Geophys. Res. Lett.*, 29:2002GL016002.

Masters, G., Laske, G., Bolton, H., and Dziewonski, A. (2000). The relative behavior of shear velocity, bulk sound speed, and compressional velocity in the mantle: Implications for chemical and thermal structure. *AGU Monograph*, 117.

Megnin, C. and Romanowicz, B. (2000). The shear velocity structure of the mantle from the inversion of body, surface and higher modes waveforms. *Geophys. J. Int.*, 143:709–728.

Meijer, P. T., Govers, R., and Wortel, M. J. R. (1997). Forces controlling the present-day state of stress in the Andes. *Earth Planet. Sci. Lett.*, 148:157–170.

Meijer, P. T. and Wortel, M. J. R. (1992). The dynamics of motion of the South American plate. *J. Geophys. Res.*, 97:11915–11931.

Melosh, H. J. and Williams, C. A. (1989). Mechanics of graben formation in crustal rocks: A finite element analysis. *J. Geophys. Res.*, 94(B10):13961–13973.

Milner, K., Becker, T. W., Boschi, L., Sain, J., Schorlemmer, D., and H., W. (2009). The solid earth research and teaching environment: a new software framework to share research tools in the classroom and across disciplines. *EOS, Trans. AGU*, 90:12.

Mitrovica, J. X. and Forte, A. M. (2004). A new inference of mantle viscosity based upon joint inversion of convection and glacial isostatic adjustment data. *Earth Planet. Sci. Lett.*, 225:177–189.

Molnar, P. and Lyon-Cean, H. (1988). Some simple physical aspects of the support, structure, and evolution of mountain belts. *Spec. Pap. Geol. Soc. Am.*, 218:179–207.

Moucha, R., Forte, A. M., Mitrovica, J. X., and Daradich, A. (2007). Lateral variations in mantle rheology: implications for convection related surface observables and inferred viscosity models. *Geophys. J. Int.*, 169(1):113–135.

Müller, R., Sdrolias, M., Gaina, C., and Roest, W. R. (2008). Age, spreading rates, and spreading asymmetry of the world's ocean crust. *Geochem. Geophys. Geosyst.*, 9:2007GC001743.

Müller, R. D., Roest, W. R., Royer, J. Y., Gahagan, L. M., and Sclater, J. G. (1997). Digital isochrons of the world's ocean floor. *J. Geophys. Res.*, 102:3211–3214.

Müller, R. D., Royer, J., and Lawer, L. A. (1993). Revised plate motion relative to the hotspot from combined atlantic and indian ocean hotspot tracks. *Geology*, 21:275–278.

Naliboff, J. B., Conrad, C. P., and Lithgow-Bertelloni, C. (2009). Modification of the lithospheric stress field by lateral variations in plate-mantle coupling. *Geophys. Res. Lett.*, 36:doi:10.1029/2009GL040484.

O'Connell, R. J., Gable, C. W., and Hager, B. H. (1991). Toroidal- poloidal partitioning of lithospheric plate motions. In *Sea-Level and Mantle Rheology*, pages 535–551. Kluwer Acad.

O'Neill, C., Müller, R. D., and Steinberger, B. (2005). On the uncertainties in hot spot reconstructions and the significance of moving hot spot reference frames. *Geochem. Geophys. Geosyst.*, 6:doi:10.1029/2004GC000784.

Panasyuk, S. V. and Hager, B. H. (2000). Models of isostatic and dynamic topography, geoi anomalies, and their uncertainties. *J. Geophys. Res.*, 105:28199–28209.

Pascal, C. (2006). On the role of heat flow, lithosphere thickness and lithosphere density on gravitational potential stresses. *Tectonophysics*, 425(1-4):83–99.

Reynolds, S. D., Coblentz, D. D., and Hillis, R. R. (2002). Tectonic forces controlling the regional intraplate stress field in continental Australia: Results from new finite element modeling. *J. Geophys. Res.*, 107(B7):2131.

Ricard, Y. and Vigny, C. (1989). Mantle dynamics with induced plate tectonics. *J. Geophys. Res.*, 94(B12):17543.

Richardson, R. M. (1992). Ridge forces, absolute plate motion and the intraplate stress field. *J. Geophys. Res.*, 97:11739–11748.

Richardson, R. M. and Reding, L. M. (1991). North American plate dynamics. *J. Geophys. Res.*, 96:12201–12223.

Richardson, R. M., Solomon, S. C., and Sleep, N. H. (1979). Tectonic stress in the plates. *Rev. Geophys.*, 17:981–1019.

Ritsema, J. and van Heijst, H. J. (2000). Seismic imaging of structural heterogeneity in earth's mantle: Evidence for large-scale mantle flow. *Sci. Prog.*, 83:243–259.

Romanowicz, B. (2003). Global mantle tomography: progress status in the last 10 years. *Annu. Rev. Earth and Planet. Sci.*, 31(1):303–328.

Schellart, W. P., Stegman, D. R., and Freeman, J. (2008). Global trench migration velocities and slab migration induced upper mantle volume fluxes: Constraints to find an Earth reference frame based on minimizing viscous dissipation. *Earth Sc. Rev.*, 88:118–144.

Schubert, G., Turcotte, D., and Olson, P. (2001). *Mantle convection in the Earth and planets*. Cambridge Univ. Press.

Simmons, N. A., Forte, A. M., and Grand, S. P. (2007). Thermochemical structure and dynamics of the african superplume. *Geophys. Res. Lett.*, 34:doi:10.1029/2006GL028009.

Simmons, N. A., Forte, A. M., and Grand, S. P. (2009). Joint seismic, geodynamic and mineral physical constraints on three-dimensional mantle heterogeneity: Implications for the relative importance of thermal versus compositional heterogeneity. *Geophys. J. Int.*, 177:1284–1304.

Steinberger, B. (2000). Slabs in the lower mantle results of dynamic modelling compared with tomographic images and the geoid. *Phys. Earth Planet. Int.*, 118:241–257.

Steinberger, B. and Calderwood, A. R. (2006). Models of large-scale viscous flow in the earths mantle with constraints from mineral physics and surface observations. *Geophys. J. Int.*, 167:1461–1481.

Steinberger, B. and Holme, R. (2008). Mantle flow models with core-mantle boundary constraints and chemical heterogeneities in the lowermost mantle. *J. Geophys. Res.*, 113:doi:10.1029/2007JB005080.

Steinberger, B., Schmeling, H., and Marquart, G. (2001). Large-scale stress field and topography induced by global mantle circulation. *Earth Planet. Sci. Lett.*, 186:75–91.

Steinberger, B., Sutherland, R., and O'connell, R. J. (2004). Prediction of Emperor-Hawaii seamount locations from a revised model of global plate motion and mantle flow. *Nature*, 430(6996):167–173.

Steiner, S. A. and Conrad, C. P. (2007). Does active upwelling help drive plate motion? *Phys. Earth Planet. Int.*, 161:103–114.

Tesauro, M., Kaban, M. K., and Cloetingh, S. A. P. L. (2009). How rigid is Europe's lithosphere? *Geophys. Res. Lett.*, 36(16):doi:10.1029/2009GL039229.

Torsvik, T. H., Müller, R. D., van der Voo, R., Steinberger, B., and Gaina, C. (2008). Global plate motion frames, toward a unified model. *Rev. Geophys.*, 46:doi:10.1029/2007RG000227.

Torsvik, T. H., Steinberger, B., Gurnis, M., and Gaina, C. (2010). Plate tectonics and net lithosphere rotation over the past 150 my. *Earth Planet. Sci. Lett.*, 291(1-4):106–112.

Wang, S. and Wang, R. (2001). Current plate velocties relative to hotspots: implications for hotspot motion, mantle viscosity and global reference frame. *Earth Planet. Sci. Lett.*, 189:133–140.

Warners-Ruckstuhl, K. N., Govers, R., and Wortel, M. J. R. (2012). Lithosphere-mantle coupling and the dynamics of the Eurasian plate. *Geophys. J. Int.*, in review.

Warners-Ruckstuhl, K. N., Meijer, P. T., Govers, R., and Wortel, M. J. R. (2010). A lithosphere-dynamics constraint on mantle flow: Analysis of the Eurasian plate. *Geophys. Res. Lett.*, 37:doi:10.1029/2010GL044431.

Wortel, M. J. R., Remkes, M. J. N., Govers, R., Cloetingh, S. A. P. L., and Meijer, P. T. (1991). Dynamics of the lithosphere and the intraplate stress field. *Phil. Trans. R. Soc. Lond. A*, 337:111–126.

Wortel, M. J. R. and Vlaar, N. J. (1989). Subduction zone seismicity and the thermo-mechanical evolution of downgoing lithosphere. *Pure Appl. Geophys.*, 128:625–659.

Zhong, S. (2001). Role of ocean-continent contrast and continental keels on plate motion, net rotation of lithosphere, and the geoid. *J. Geophys. Res.*, 106:703–712.

Zoback, M. L. (1992). First-and second-order patterns of stress in the lithosphere: the world stress map project. *J. Geophys. Res.*, 97:11703–11728.

Samenvatting

De sterke 100 à 200 km dikke buitenschil van de aarde, de lithosfeer, is opgedeeldin tektonische platen die schuiven over de onderliggende vervormbare mantel. Dit proefschrift richt zich op een beter begrip van de krachten die deze platen doen bewegen en tegelijk verantwoordelijk zijn voor de grootschalige spanningen die aan de basis staan van aardbevingen. In het bijzonder wordt aandacht geschonken aan de rol van de diepe mantel. Doordat de interne structuur van de aarde in de laatste decenia steeds beter in kaart gebracht is, is de stroming van de mantel steeds beter af te schatten. Het is daardoor mogelijk geworden te kwantificeren in welke mate krachten samenhangend met die stroming doorwerken op de lithosfeer. Deze resultaten geven inzicht in de nog immer onduidelijke aard van de interactie tussen de platen en de onderliggende mantel. In het geval de beweging van de platen voornamelijk het gevolg is van afkoeling, en als gevolg daarvan zinken (subduceren), van de platen zelf, zal de mantel plaatbeweging tegenwerken, waarbij er een wrijvingskracht aan de basis van de platen ontstaat. Wanneer echter de platen vooral door een actief stromende mantel aangedreven worden, zullen de schuifkrachten aan de basis van de platen juist een aandrijvende werking hebben. De daadwerkelijke interactie tussen de platen en de onderliggende mantel bestaat uit het netto effect van de bovengenoemde scenario's en hangt dus nauw samen met de oorsprong van de krachten die de platen in beweging brengen en houden.

In dit proefschrift wordt de interactie tussen de lithosfeer en de diepe mantel in detail bestudeerd aan de hand van een kwantitatieve analyse van het totaal aan krachten werkend op tektonische platen. Ik presenteer een nieuwe aanpak waarbij modellen voor krachten die hun oorsprong hebben in de lithosfeer en in de mantel worden gecombineerd op de schaal van individuele platen. Deze aanpak garandeert een goede resolutie van zowel de krachten die ontstaan door interactie tussen de platen zelf als die tussen de plaat en de mantel. Een groot scala aan modellen wordt stap voor stap geëvalueerd aan de hand van drie uitgangspunten. Het eerste en meest fundamentele uitgangspunt is dat tektonische platen mechanisch in balans zijn. Voor een over het aardoppervlak roterende plaat betekent dit dat er geen netto krachtmoment op mag werken. Vervolgens moet een correcte krachtenset zowel de geobserveerde plaatbeweging ten opzichte van de diepe mantel als het geobserveerde spanningsveld in de plaat kunnen verklaren (zie respectievelijk figuur 1.1 en 1.3 uit de introductie van dit proefschrift).

Hoewel de gepresenteerde aanpak op alle tektonische platen toepasbaar is, richt ik mij in dit proefschrift op de Euraziatische plaat. Vanwege zijn grote omvang, lage snelheid

ten opzichte van de diepe mantel, grote diversiteit aan interactie met andere platen en gebrek aan subducerende oceanische lithosfeer wordt de dynamica van Eurazië niet gedomineerd door een enkele kracht. Daardoor zijn de beweging en het spanningsveld van Eurazië gevoelig voor krachten van verschillende oorsprong en is de plaat ideaal is om een beter inzicht te krijgen in de verhoudingen tussen deze krachten. Een belangrijke vraag hierbij is: Voelt de Euraziatische plaat de stroming van de diepe mantel, en indien dat het geval is, in welke mate? In dit proefschrift presenteer ik een zo compleet mogelijke analyse van de krachten werking op Eurazië. Deze worden onderverdeeld in drie kategorieën: 1) krachten als gevolg van interactie van Eurazië met naburige platen (bijvoorbeeld botsingskrachten tussen Eurazië en het Indiase continent aan de zuidgrens van de plaat), 2) krachten als gevolg van variaties in topografie en bathymetrie (gebergte ketens hebben de neiging te bezwijken onder hun eigen gewicht), 3) krachten aan de basis van de plaat vanuit de onderliggende mantel.
Mijn kwantitatieve model-resultaten leiden tot de volgende conclusies. Krachten vanuit een stromende mantel zijn onmisbaar voor de mechanische balans van de plaat. De voorwaarde van balans impliceert dat de interactie tussen de plaat en de onderliggende mantel in vergelijkbare mate beheerst wordt door weerstand tegen plaatbeweging als door aandrijving door actieve stroming in de mantel. Ook levert deze voorwaarde de mogelijkheid om te discrimineren tussen verschillende type modellen die de structuur van de aardmantel beschrijven: enkel een selectie hiervan drijft stroming aan die past bij een gebalanceerde Euraziatische plaat. Hoewel krachten vanuit de diepe mantel wezenlijk zijn leveren krachten als gevolg van interactie met aangrenzende platen het grootste krachtmoment op Eurazië. Om zowel de plaatbeweging als de spanningen in de plaat te kunnen verklaren dienen botsingskrachten op de grens met de Indiase plaat (verantwoordelijk voor onder andere de vorming van het Himalaya-gebergte) vijf à tien keer zo groot te zijn als die met Afrikaanse- (Alpen) en Arabische (Zagros-gebergte) platen. In concreto betekent dit dat vooral de botsing met India invloed heeft op de beweging van Eurazië. De diepe mantel levert een netto krachtmoment op Eurazië dat in grootte minimaal de helft is van dat van de botsingskrachten op de zuidgrens van de plaat, en vergelijkbaar is met het krachtmoment resulterend uit topografie-gerelateerde krachten.

Acknowledgements

Since I did not append 'stellingen' to my thesis (one line statements that are a Dutch habit), let me start with one here: *the more effort one puts into something, the more one will appreciate the result.* This definitely applies to my PhD. After seven years of reading, modeling, writing, struggling and a lot of learning, I am very happy, and even a bit proud, of the end-result you hold in your hands. The course of my PhD has not been a standard one and was dotted with leaves for sports and injuries. I feel very privileged that I had the possibility to combine my sports career with the work at the university. This has asked supplementary efforts and flexibility from many people, whom I would like to thank dearly.

First and foremost, I had wonderful supervisors, who complemented each other and were always there for me when needed. **Rinus** , you had me sold for tectonophysics since the first course I took with you. I have always been inspired by your passion for understanding the earth. Your (in my eyes) incredible recollection of scientific advances and overview of open-standing questions has guided me when I could not see the track ahead or simply took the wrong one. I would also like to thank you for putting your trust in me (and talk in my favor more than one time) even though research has not always been my main focus. Without it the combination of sports and PhD would not have been possible. Your concern did not end with my sports carrier; I very much appreciate your guidance in figuring out which way I want to go on form here on. **Rob**, your seemingly endless energy and courage in tackling problems was a real example for me during my PhD. Thank you for your infinite help during, above all, all my modeling adventures. Whether the reason for me coming to your room where technical problems or lack of physically understanding of assumptions and/or results, I always left with fresh ideas to tackle the problem. In retrospect I agree that your usual way of not handing over the straight solution has made me learn so much more, so I admit that I am very grateful for that now!

Research leads to nothing if results are not communicated clearly. Writing articles has been a tedious part of the process for me, and the comments of both Rinus and Rob have transformed my sluggish first drafts into (at least I think so...) understandable and readable end-products . Their help has extended from structuring and clarifying the contents all the way to removing dangling participles. Rinus, Rob: I wish I could have spared you a lot of time and effort there, and I really feel grateful for all the time and patience both of you put into it.

Paul, although you may not be an official supervisor of my PhD, you have definitely been an essential consultant. Thank you for your patient help during my master thesis,

which got me acquainted with all the material that has in the end become the basis of this thesis. Furthermore, thank you for your geometrical insight that has turned out to be a key factor in the presentation of my results.
My paranymphs and room mates for the last 3 years, **Steven** and **Ali** made it both a joyful and scientifically stimulating experience to come to office. Guys, this has meant a lot to me! Sharing our mutual frustrations about the slowness of our writing was definitely the best way to come to terms with it and keep on going. I wish you both all the luck in finishing your work, you can do it and it will be worth it!
I have not been around university as much as I would have liked, however, this is not to blame on my colleagues throughout the years. **Edith**, **Thomas**, **Joost**, **Pasha**, **Jelly**, **Shalaley**, **Marsha**, **Jeroen**, **Walter**, **Robin**, and especially former-roommates **Roberta**, **Marzieh** and **Gabi**: thanks for the discussions and 'gezelligheid'! Without my laptop that enabled me to work at home, at Papendal and all over the world I couldn't have kept my research going. **Theo**, **Joop** and **Wienand**, thank you for all your effort (and patience) into helping me with the far to many computer related matters that I do not understand. **Ildiko**, **Margreet** and everyone at **P&O** thank you for your help with all the administrative hassle that went with my alternative employment contract...
It has always been very important to me that my coaches and sports-buddies understood my desire to do something intellectual alongside the sports. **Ronald**, **Peter** (Verlooy), **Peter** (van Wijk), **Peter** (Vergouwen), **Eric**, **Els**, **Yvonne** (van Haperen), **Yvonne** (Wisse), **Remona** en **Babs**: thank you for being interested and make me feel like you though I was brave, instead of a fool. It definitely made it easier to pick up work after heavy training.
Finally, I profoundly thank my family and close friends for understanding my situation, helping me to manage my time and efforts and distracting me now and again. **Mams**, **Nic**, **Yv**, **Maureen**, **Sietske** en **Frenke**, the conversations we had about my difficulty to divide my attention between sports and research were a great mental support. My deepest gratitude goes to my husband, **Chiel**, who has been alongside me all the way: your love, care and kicks in the butt made all the difference!

Curriculum Vitae

2 Nov. 1980	Born in Baden, Switzerland
1992 - 1998	Pre-university education (VWO) O.S.G. Huizermaat, Huizen, The Netherlands
1998 - 2004	Study of Geophysics Universiteit Utrecht, The Netherlands *Cum Laude*
1999 - 2004	Student teaching assistant Universiteit Utrecht, The Netherlands
2000 - 2010	Professional athlete Track & field, Heptathlon
2004 - 2011	PhD candidate Tectonophysics group, Universiteit Utrecht, The Netherlands
from Oct. 2011	Post-Doctoral researcher Tectonophysics group, Universiteit Utrecht, The Netherlands